Studies on the identification of antiviral lipid molecules against dengue virus using lipidomics

（リピドミクスを活用した抗デングウイルス活性を有する脂質分子の同定に関する研究）

Takao Sanaki

Contents

Contents i
Abbreviations ii
Notes vii

General Introduction 1

Chapter I
Development of MS-based analytical systems of lipid molecules
Introduction 8
Materials and methods 10
Results 21
Discussion 34
Summary 37

Chapter II
Inhibition of dengue virus infection by 1-stearoyl-2-arachidonoyl-phosphatidylinositol *in vitro*
Introduction 39
Materials and methods 41
Results 54
Discussion 80
Summary 85

Conclusion 86
Acknowledgement 89
References 90
Summary in Japanese（和文要旨） 106

Abbreviations

AA:	arachidonic acid
ACTB:	β-actin
AGC:	automatic gain control
ATP:	adenosine 5'-triphosphate
AXL:	AXL receptor tyrosine kinase
BSA:	bovine serum albumin
$CaCl_2$:	calcium chloride
CCL:	C-C motif chemokine ligand
CXCL:	C-X-C chemokine ligand
D-PBS:	Dulbecco's PBS
dd-MS^2:	data-dependent tandem mass spectrometry
DENV:	dengue virus
DF:	dengue fever
DHA:	docosahexaenoic acid
DMEM:	Dulbecco's modified Eagle's medium
DS:	dextran sulfate
DSPI:	distearoyl-phosphatidylinositol
EC_{50}:	50% effective concentration
EDTA:	ethylenediaminetetraacetic acid
EET:	epoxyeicosatrienoic acid
ELISA:	enzyme-linked immunosorbent assay
EPA:	eicosapentaenoic acid

ESI: electrospray ionization

FASN: fatty acid synthase

FBS: fetal bovine serum

Gapdh: glyceraldehyde-3-phosphate dehydrogenase

GC: gas chromatography

h: hour

HDoHE: hydroxydocosahexesaenoic acid

HDoPE: hydroxydocosapentaenoic acid

HEPE: hydroxyeicosapentaenoic acid

HETE: hydroxyeicosatetraenoic acid

HETrE: hydroxyeicosatrienoic acid

HILIC: hydrophilic interaction chromatography

HRP: Horseradish peroxidase

i.d.: inner diameter

IFN: interferon

IL: interleukin

ISs: internal standards

IT: injection time

kb: kilobase

LC: liquid chromatography

LOX: lipoxygenase

LPI: lysophosphatidylinositol

LPS: lipopolysaccharide

LTB_4:	leukotriene B_4
MA:	Mead acid
MBOAT7:	membrane-bound O-acyltransferase 7
mDa:	millidalton
MEM:	minimal essential medium
MeOH:	methanol
min:	minute
MOI:	a multiplicity of infection
MRM:	multiple reaction monitoring
ms:	millisecond
MS:	mass spectrometry
MS/MS:	tandem mass spectrometry
NAFLD:	nonalcoholic fatty liver disease
NaCl:	sodium chloride
NH_4Cl:	ammonium chloride
NP:	normal-phase
NS:	nonstructural protein
PA:	phosphatidic acid
PAF:	platelet activating factor
PBS:	phosphate-buffered saline
PC:	phosphatidylcholine
PE:	phosphatidylethanolamine
PG:	phosphatidylglycerol

PGD_2:	prostaglandin D_2
PGE_2:	prostaglandin E_2
PI:	phosphatidylinositol
PI-L:	phosphatidylinositol purified from bovine liver
PI-S:	phosphatidylinositol purified from soy
PIP:	phosphoinositide
PMA:	phorbol 12-myristate 13-acetate
PMAr:	PMA stimulation and resting
POPG:	1-palmitoyl-2-oleoyl-phosphatidylglycerol
ppm:	parts per million
PS:	phosphatidylserine
QqLIT:	hybrid triple quadrupole-linear ion trap
QqQ:	triple quadrupole
QTOF:	quadrupole time-of-flight
RP:	reverse-phase
RPMI:	Roswell Park Memorial Institute
RT-qPCR:	reverse transcriptase-quantitative real-time polymerase chain reaction
s:	second
SA:	1-stearoyl-2-arachidonoyl
SAPA:	1-stearoyl-2-arachidonoyl-phosphatidic acid
SAPC:	1-stearoyl-2-arachidonoyl-phosphatidylcholine
SAPE:	1-stearoyl-2-arachidonoyl-phosphatidylethanolamine
SAPG:	1-stearoyl-2-arachidonoyl-phosphatidylglycerol

SAPI: 1-stearoyl-2-arachidonoyl-phosphatidylinositol

SAPS: 1-stearoyl-2-arachidonoyl-phosphatidylserine

sCD14: soluble CD14

sNS1: secreted nonstructural protein 1

sPLA2: secretory phospholipase A2

SPM: specialized pro-resolving lipid mediator

SREBP: sterol regulatory element binding protein

SRM: selected reaction monitoring

$TCID_{50}$: 50% tissue culture infective dose

TIM-1: T cell immunoglobulin and mucin domain-containing protein 1

TLR: Toll-like receptor

TMB: 3,3′,5,5′-Tetramethylbenzidine

TNF-α: tumor necrosis factor α

TNFSF10: tumor necrosis factor superfamily member 10

Notes

Contents of the present thesis were published in the following articles.

1. **Sanaki T, Inaba Y, Fujiwara T, Yoshioka T, Matsushima K, Minagawa K, Higashino K, Nakano T, and Numata Y.** A hybrid strategy using global analysis of oxidized fatty acids and bioconversion by *Bacillus circulans*. Rapid Commun Mass Spectrom 30, 751–762, 2016.

2. **Sanaki T, Kasai-Yamamoto E, Yoshioka T, Sakai S, Yuyama K, Fujiwara T, Numata Y, and Igarashi Y.** Direct Involvement of Arachidonic Acid in the Development of Ear Edema *via* TRPV3. J Oleo Sci 66, 591–599, 2017.

3. **Sanaki T, Wakabayashi M, Yoshioka T, Yoshida R, Shishido T, Hall WW, Sawa H, and Sato A.** Inhibition of dengue virus infection by 1-stearoyl-2-arachidonoyl-phosphatidylinositol *in vitro*. FASEB J 33, 13866–13881, 2019.

General Introduction

Biological functions of lipid molecules

Lipids, which are categorized to major eight groups: fatty acyls, glycerolipids, glycerophospholipids, sphingolipids, sterol lipids, prenol lipids, saccharolipids, and polyketides (Table 1), have diverse biological function (Figure 1) (1, 2). Glycerophospholipids, sphingolipids and sterol lipids, which are the major components in cell membranes, are related to maintain cell morphology (3, 4). Furthermore, lipid raft, which are rich in sphingomyelin and cholesterol (5), are functional domains that accumulate membrane proteins (6, 7) and have important roles in membrane signal transduction (8, 9), bacterial and viral infection (10–12), cell adhesion or intracellular vesicle transport, and intracellular polarity (3, 4). Triacylglycerols including 3 fatty acids in their structure localize in lipid droplets. Since fatty acids are metabolized in mitochondria by β-oxidation leading to the generation of adenosine 5'-triphosphate (ATP) (13, 14), triacylglycerols and fatty acids serve as the energy source for cells. Bioactive lipid mediators, such as eicosanoids and specialized pro-resolving lipid mediator (SPMs) have a wide variety of physiological functions, such as inflammation (15, 16), resolution (17–19), immune responses (17, 19, 20), blood pressure regulation (21, 22), and pain stimulation (23, 24) through specific receptors. Since lipid molecules are essential components for biological responses and are related to various diseases, enzymes related to lipid synthesis and lipid metabolism, and lipid receptors have been focused as the target molecules of drug discovery, and various effective drugs, such as cyclooxygenase inhibitors (25), cysteinyl leukotriene receptor inhibitors (26, 27), and hydroxymethylglutaryl-CoA reductase inhibitors (28) have been developed. Furthermore,

Table 1. lipid categories

Category	Specific lipid species
Fatty acyls	Fatty acids, eicosanoids, endocannabinoids, SPMs
Glycerolipids	TAGs, DAGs, MAGs
Glycerophospholipids	PA, PC, PE, PG, PI, PS, cardiolipin
Sphingolipids	SM, sulfatides, sphingosine, ceramides, ganglioside
Sterol lipids	Cholesterol, estradiol, testosterone, bile acids
Prenol lipids	Farnesol, dolichols, vitamin K
Saccharolipids	Lipid A, acyltrehaloses
Polyketides	Aflatoxins, tetracyclines, erythromycin

SPMs, specialized pro-resolving lipid mediators; TAGs, triacylglycerols; DAGs, diacylglycerols; MAGs, monoacylglycerols; PA, phosphatidic acid; PC, phosphatidylcholine; PE, phosphatidylethanolamine; PG, phosphatidylglycerol; PI, phosphatidylinositol; PS, phosphatidylserine; SM, sphingomyelin

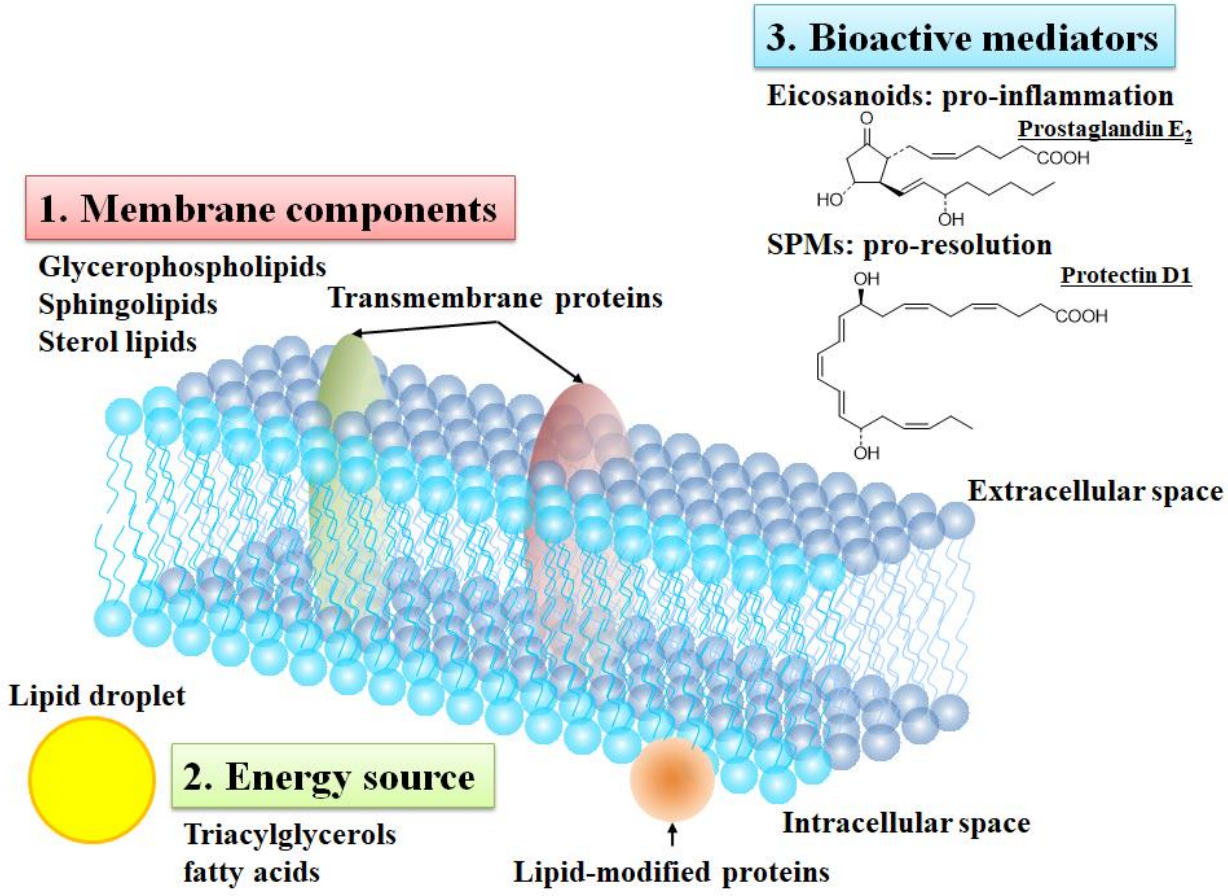

Figure 1. Diverse biological function of lipid molecules. (1–3) Glycerophospholipids, sphingolipids and sterol lipids, which are the major components in cell membranes, are related to maintain cell morphology (1). Triacylglycerols and fatty acids serve as the energy source for cells (2). Bioactive lipid mediators, such as eicosanoids and SPMs have a wide variety of physiological functions, such as inflammation and resolution (3). SPMs, specialized pro-resolving lipid mediators.

drugs using lipid molecules as lead compounds, such as prostaglandin analogs (29) and FTY720 (21, 30) have been also developed. Therefore, lipid biology is one of the most attractive fields for the drug discovery research.

Analytical methods of diverse lipid molecules

Highly sensitive and highly selective analytical methods are required to measure lipid molecules with various structures and concentrations (2). Lipid analysis is roughly divided into two methods: immunoassay, including radioimmunoassay and enzyme immunoassay, and chromatographic methods, including gas chromatography (GC) and liquid chromatography (LC). In general, antibody methods are highly sensitive, do not require pretreatment, and are easy to automate. Therefore, it is advantageous in terms of high-throughput analysis of many samples and there are many applications to prostaglandins (31–34). However, there are disadvantages, including the design of immunogens, the production of antibodies, the problem of cross-reactivity with similar substances, and the inability to analyze multicomponent profiles. In contrast, chromatographic methods are useful for multi-component profile analysis, which is difficult for immunoassay. However, in the case of GC, the derivatization of lipid molecules with poor volatility and stability is essential to improve volatility, isomer separation, or the sensitivity of detectors (31, 35–37). Therefore, LC is suitable for separating lipid molecules. Although UV–visible spectroscopic detectors and fluorescence detectors have been used as LC detectors, mass spectrometry (MS), by which structural information can be provided, is optimal for the separation of lipid analogs that cannot be dealt with only by chromatographic separation. In fact, since the measurement of cell membrane phospholipids using electrospray ionization (ESI)–MS was reported in the 1990's (38, 39), LC/ESI–MS has rapidly penetrated into the lipid research

area as a powerful measurement tool (40, 41). Furthermore, since lipid molecules are susceptible to fragmentation due to the presence of ester bonds, unsaturated bonds, hydroxyl groups or epoxy groups, by using tandem mass spectrometry (MS/MS), it is possible to perform the structure-specific fragmentation by selected reaction monitoring (SRM) (23, 24, 42, 43) or the comprehensive lipid screening by data-dependent scanning (44–46). Therefore, MS-based analytical systems of lipid molecules have been utilized to elucidate the mechanism of diseases and to discover the biomarkers of diseases.

Relationship between lipid biology and viral infection

Lipid molecules are involved in all stages of the viral life cycle, including the viral entry into host cells, the envelope fusion, the viral replication and/or assembly, and the virion assembly and budding (47–49). Therefore, enzymes related to lipid synthesis and lipid metabolism, lipid receptors, and lipid molecules themselves are attractive target molecules for the host defense against viral infection and for the drug discovery. For example, fatty acid biosynthesis is activated for viral replication and assembly (50–54). Fatty acid synthase (FASN) inhibitors exhibit antiviral activity against several viruses, including dengue virus (DENV), West Nile virus, yellow fever virus, respiratory syncytial virus, human parainfluenza 3, and human rhinovirus 16 (55, 56). Similar to FASN inhibitors, phospholipase C-β2 activators and sterol regulatory element binding protein (SREBP) inhibitors exhibit broad-spectrum antiviral activities (57, 58). These evidences demonstrate that the antiviral drugs targeting host lipid enzymes can be expected to have broad-spectrum antiviral activities compared with the antiviral drugs targeting viral proteins. As mentioned above, lipid molecules and their enzymes are involved in DENV infection and lipid enzyme inhibitors, including FASN inhibitors and SREBP inhibitors

exhibit anti-DENV activities. Despite the significant public health concerns posed by DENV, there are currently no effective anti-DENV therapeutic agents. To develop anti-DENV drugs, a better understanding of the detailed mechanisms of DENV infection is needed. Although the activation of both lipid metabolism and lipid synthesis in DENV-infected cells has been reported, there have been no reports of anti-DENV lipid molecules.

This thesis consists of two chapters. In chapter I, MS-based analytical systems of lipid molecules are developed. In chapter II, antiviral lipid molecules against DENV are identified and their mechanisms are investigated.

Chapter I

Development of MS-based analytical systems of lipid molecules

Introduction

MS-based analytical systems of lipid molecules, which widely referred to as “lipidomics”, are roughly divided into two methods: global lipidomics and targeted lipidomics. Global lipidomics is a comprehensive analytical method for lipid molecules and is also divided into two methods: a normal-phase (NP) LC method and a reverse-phase (RP) LC method (40, 59). An NPLC method, which is suitable for separating different lipid classes based on the polar head groups, such as the phosphocholine group of phosphatidylcholine and the phosphoethanolamine group of phosphatidylethanolamine, allows the analysis of the variation between each lipid class (60, 61). Since flammable organic solvents, such as hexane and chloroform are conventionally used as the mobile phase in NPLC, it is difficult to automate the measurement. Recently, a hydrophilic interaction chromatography (HILIC) without flammable organic solvents has been widely used instead of NPLC (40, 62). Previously, the HILIC method was established, and this method has been applied to the analysis of the mechanism of obesity (45). However, NPLC, including HILIC is unsuitable for the analysis of high lipophilic lipid molecules without the polar head groups, such as triacylglycerols and the analysis of each lipid molecular species. In contrast, an RPLC method is suitable for separating different lipid molecular species based on the numbers and the length of fatty acid chains (40, 59). Since an RPLC method enables detailed analysis for each lipid molecular species compared with an NPLC method, an RPLC method has higher coverage than an NPLC method and has been widely used as the first choice for lipidomics (40, 59). Targeted lipidomics is a selective analytical method for specific lipid molecular species and has widely used to analyze a trace amount of bioactive lipid mediators (1,

63–67). Previously, the targeted lipidomics for analyzing oxidized fatty acids was established (42). While, there is room for the improvement to increase the sensitivity for the effective analysis of a trace amount of oxidized fatty acids in biological samples.

MS used to lipidomics is roughly divided into two types: quantitative MS, such as triple quadrupole (QqQ) MS and hybrid triple quadrupole-linear ion trap (QqLIT) MS, and qualitative MS, such as Orbitrap MS and quadrupole time-of-flight (QTOF) MS. QqQ MS and QqLIT MS have high-sensitivity and high-selectivity in SRM, and these techniques are widely used for targeted lipidomics to analyze bioactive lipid mediators in conjunction with appropriate molecular standards (1, 63–67). Orbitrap MS and QTOF MS, which are high-resolution MS, enable very accurate mass analysis [<5 parts per million (ppm)], as well as higher selectivity than QqQ MS and QqLIT MS (68). Furthermore, a comprehensive analysis is possible by setting the mass range without analytical parameters for each molecule. Therefore, Orbitrap MS and QTOF MS have been widely used to global lipidomics. Although many applications of Orbitrap MS and QTOF MS in global lipidomics have been reported (69–75), there are few publications concerning global lipidomics for oxidized fatty acids using high-resolution MS. To explore unknown lipid metabolites in biological samples, the development of a global lipidomics for analyzing them is necessary.

In this chapter, for the purpose of discovery and identification of lipid molecules, including unknown molecules in biological samples, global lipidomics for analyzing oxidized fatty acids and the other lipid molecules was developed using RPLC coupled with “Q Exactive Plus”, which is a high-sensitivity, high-resolution MS. Furthermore, the sensitivity of targeted lipidomics was improved for detecting arachidonic acid (AA) metabolites.

Materials and methods

Ethical approval of the study protocol

This study was conducted in accordance with the guidelines set by Shionogi Innovation Center (Sapporo, Japan).

Chemicals

LC–MS grade methanol (MeOH) and isopropanol, ammonium acetate, dibutyl hydroxytoluene, sodium chloride, dipotassium hydrogen phosphate and potassium dihydrogen phosphate were purchased from Wako Pure Chemical Industries, Ltd. (Osaka, Japan). LC–MS grade acetonitrile and phosphoric acid were obtained from Kanto Chemical Co., Inc. (Tokyo, Japan). LC–MS grade formic acid was purchased from Sigma–Aldrich (St. Louis, MO, USA). Isoflurane was obtained from DS Pharma Animal Health Co., Ltd. (Osaka, Japan). Standards of fatty acids and oxidized fatty acids were purchased from Cayman Chemical Company (Ann Arbor, MI, USA) (see Table 2 for a complete list of compounds). Ultrapure water was obtained using a Milli-Q system (Millipore, Billerica, MA, USA).

Animals

C57BL/6 male mice were purchased from Clea Japan Inc. (Tokyo, Japan). All mice were maintained in microisolator cages, exposed to a 12 hour (h) light–dark cycle, and provided with standard food and water *ad libitum*.

Table 2. Measurement parameters of oxidized fatty acids

No.	Lipid	Molecular Formula	Exact Mass	Precursor Ion	Retention Time (min)	Fragment Ion
001	AA	$C_{20}H_{32}O_2$	304.2402	303.2319	22.99	259.2430
002	5-HETE	$C_{20}H_{32}O_3$	320.2351	319.2273	17.48	115.0401
003	8-HETE	$C_{20}H_{32}O_3$	320.2351	319.2273	16.64	155.0715
004	9-HETE	$C_{20}H_{32}O_3$	320.2351	319.2273	16.79	167.0713
005	11-HETE	$C_{20}H_{32}O_3$	320.2351	319.2273	16.15	167.1077
006	12-HETE	$C_{20}H_{32}O_3$	320.2351	319.2273	16.37	179.1079
007	15-HETE	$C_{20}H_{32}O_3$	320.2351	319.2273	15.53	219.1394
008	16-HETE	$C_{20}H_{32}O_3$	320.2351	319.2273	14.52	233.1550
009	17-HETE	$C_{20}H_{32}O_3$	320.2351	319.2273	14.34	247.1703
010	18-HETE	$C_{20}H_{32}O_3$	320.2351	319.2273	14.13	261.1858
011	19-HETE	$C_{20}H_{32}O_3$	320.2351	319.2273	13.77	275.2016
012	20-HETE	$C_{20}H_{32}O_3$	320.2351	319.2273	14.12	289.2172
013	5-OxoETE	$C_{20}H_{30}O_3$	318.2195	317.2117	17.72	203.1806
014	12-OxoETE	$C_{20}H_{30}O_3$	318.2195	317.2117	16.15	153.1286
015	15-OxoETE	$C_{20}H_{30}O_3$	318.2195	317.2117	15.34	113.0972
016	5,6-EET	$C_{20}H_{32}O_3$	320.2351	319.2273	18.61	191.1803
017	8,9-EET	$C_{20}H_{32}O_3$	320.2351	319.2273	18.19	155.0716
018	11,12-EET	$C_{20}H_{32}O_3$	320.2351	319.2273	17.85	167.1078
019	14,15-EET	$C_{20}H_{32}O_3$	320.2351	319.2273	17.10	219.1393
020	5,6-DHET	$C_{20}H_{34}O_4$	338.2457	337.2379	14.92	145.0506
021	8,9-DHET	$C_{20}H_{34}O_4$	338.2457	337.2379	13.69	127.0765
022	11,12-DHET	$C_{20}H_{34}O_4$	338.2457	337.2379	12.93	167.1078
023	14,15-DHET	$C_{20}H_{34}O_4$	338.2457	337.2379	12.22	207.1391
024	LTB_4	$C_{20}H_{32}O_4$	336.2301	335.2222	10.84	195.1028
025	LTC_4	$C_{30}H_{47}N_3O_9S$	625.3033	624.2949	10.18	272.0889
026	LTD_4	$C_{25}H_{40}N_2O_6S$	496.2607	495.2523	10.41	177.0340
027	LTE_4	$C_{23}H_{37}NO_5S$	439.2392	438.2309	11.13	333.1895
028	14,15-LTC_4	$C_{30}H_{47}N_3O_9S$	625.3033	624.2949	8.08	272.0890
029	14,15-LTE_4	$C_{23}H_{37}NO_5S$	439.2392	438.2309	9.45	120.0125
030	LXA_4	$C_{20}H_{32}O_5$	352.2250	351.2166	6.99	115.0402
031	PGD_2	$C_{20}H_{32}O_5$	352.2250	351.2166	5.64	271.2071
032	PGE_2	$C_{20}H_{32}O_5$	352.2250	351.2166	5.47	271.2069
033	$PGF_{2\alpha}$	$C_{20}H_{34}O_5$	354.2406	353.2323	5.65	193.1235

Table 2. (continued)

No.	Lipid	Molecular Formula	Exact Mass	Precursor Ion	Retention Time (min)	Fragment Ion
034	6-keto-$PGF_{1\alpha}$	$C_{20}H_{34}O_6$	370.2355	369.2272	3.00	163.1129
035	TXB_2	$C_{20}H_{34}O_6$	370.2355	369.2272	4.98	195.1028
036	dhk-PGD_2	$C_{20}H_{32}O_5$	352.2250	351.2166	6.69	175.1128
037	dhk-PGE_2	$C_{20}H_{32}O_5$	352.2250	351.2166	5.93	175.1129
038	dhk-$PGF_{2\alpha}$	$C_{20}H_{34}O_5$	354.2406	353.2323	6.58	291.2332
039	15-deoxy-PGJ_2	$C_{20}H_{28}O_3$	316.2038	315.1955	12.90	271.2069
040	EPA	$C_{20}H_{30}O_2$	302.2246	301.2162	20.98	257.2275
041	5-HEPE	$C_{20}H_{30}O_3$	318.2195	317.2117	15.29	115.0401
042	8-HEPE	$C_{20}H_{30}O_3$	318.2195	317.2117	14.44	155.0714
043	9-HEPE	$C_{20}H_{30}O_3$	318.2195	317.2117	14.59	167.0714
044	11-HEPE	$C_{20}H_{30}O_3$	318.2195	317.2117	14.10	167.1078
045	12-HEPE	$C_{20}H_{30}O_3$	318.2195	317.2117	14.31	179.1079
046	15-HEPE	$C_{20}H_{30}O_3$	318.2195	317.2117	13.83	219.1394
047	18-HEPE	$C_{20}H_{30}O_3$	318.2195	317.2117	13.25	259.1707
048	8,9-EpETE	$C_{20}H_{30}O_3$	318.2195	317.2117	15.99	155.0717
049	11,12-EpETE	$C_{20}H_{30}O_3$	318.2195	317.2117	15.73	167.1077
050	14,15-EpETE	$C_{20}H_{30}O_3$	318.2195	317.2117	15.53	207.1391
051	17,18-EpETE	$C_{20}H_{30}O_3$	318.2195	317.2117	14.86	259.1706
052	5,6-diHETE	$C_{20}H_{32}O_4$	336.2306	335.2222	12.60	145.0501
053	14,15-diHETE	$C_{20}H_{32}O_4$	336.2306	335.2222	10.55	207.1387
054	17,18-diHETE	$C_{20}H_{32}O_4$	336.2306	335.2222	10.14	247.1703
055	DHA	$C_{22}H_{32}O_2$	328.2402	327.2319	22.54	283.2431
056	4-HDoHE	$C_{22}H_{32}O_3$	344.2351	343.2273	17.96	101.0245
057	7-HDoHE	$C_{22}H_{32}O_3$	344.2351	343.2273	16.80	141.0558
058	8-HDoHE	$C_{22}H_{32}O_3$	344.2351	343.2273	16.87	109.0659
059	10-HDoHE	$C_{22}H_{32}O_3$	344.2351	343.2273	16.21	153.0921
060	11-HDoHE	$C_{22}H_{32}O_3$	344.2351	343.2273	16.41	165.0921
061	13-HDoHE	$C_{22}H_{32}O_3$	344.2351	343.2273	15.91	193.1233
062	14-HDoHE	$C_{22}H_{32}O_3$	344.2351	343.2273	16.06	205.1231
063	16-HDoHE	$C_{22}H_{32}O_3$	344.2351	343.2273	15.58	233.1549
064	17-HDoHE	$C_{22}H_{32}O_3$	344.2351	343.2273	15.65	245.1541
065	20-HDoHE	$C_{22}H_{32}O_3$	344.2351	343.2273	15.13	285.1847
066	17-keto-DHA	$C_{22}H_{30}O_3$	342.2195	341.2111	15.49	245.1542

Table 2. (continued)

No.	Lipid	Molecular Formula	Exact Mass	Precursor Ion	Retention Time (min)	Fragment Ion
067	17-keto-DPA	$C_{22}H_{32}O_3$	344.2351	343.2273	16.55	247.1704
068	16,17-EpDPE	$C_{22}H_{32}O_3$	344.2351	343.2273	17.37	233.1539
069	19,20-EpDPE	$C_{22}H_{32}O_3$	344.2351	343.2273	16.74	285.1855
070	7,17-diHDPA	$C_{22}H_{34}O_4$	362.2457	361.2379	10.63	143.0713
071	19,20-diHDPA	$C_{22}H_{34}O_4$	362.2457	361.2379	12.18	273.1862
072	RvD1	$C_{22}H_{32}O_5$	376.2250	375.2171	6.65	141.0558
073	17R-RvD1	$C_{22}H_{32}O_5$	376.2250	375.2171	6.77	141.0559
074	RvD2	$C_{22}H_{32}O_5$	376.2250	375.2171	5.80	175.0765
075	PDX	$C_{22}H_{32}O_4$	360.2301	359.2222	9.93	153.0922
076	7S-MaR	$C_{22}H_{32}O_4$	360.2301	359.2222	9.51	113.0608
077	9-HODE	$C_{18}H_{32}O_3$	296.2351	295.2273	15.40	171.1028
078	13-HODE	$C_{18}H_{32}O_3$	296.2351	295.2273	15.06	195.1392
079	9,10-EpOME	$C_{18}H_{32}O_3$	296.2351	295.2273	17.30	171.1027
080	12,13-EpOME	$C_{18}H_{32}O_3$	296.2351	295.2273	16.94	195.1391
081	9-OxoODE	$C_{18}H_{30}O_3$	294.2150	293.2117	15.49	185.1185
082	13-OxoODE	$C_{18}H_{30}O_3$	294.2150	293.2117	14.95	113.0973
083	9,10-diHOME	$C_{18}H_{34}O_4$	314.2457	313.2373	11.98	201.1133
084	12,13-diHOME	$C_{18}H_{34}O_4$	314.2457	313.2373	11.34	183.1390
085	9-HOTrE	$C_{18}H_{30}O_3$	294.2150	293.2117	13.25	171.1027
086	9-OxoOTrE	$C_{18}H_{28}O_3$	292.2038	291.1960	13.41	185.1183
087	13-HOTrE	$C_{18}H_{30}O_3$	294.2150	293.2117	13.30	195.1390
088	13-HOTrEγ	$C_{18}H_{30}O_3$	294.2150	293.2117	13.64	193.1235
089	5-HETrE	$C_{20}H_{34}O_3$	322.2508	321.2430	19.79	115.0401
090	8-HETrE	$C_{20}H_{34}O_3$	322.2508	321.2430	17.38	157.0870
091	15-HETrE	$C_{20}H_{34}O_3$	322.2508	321.2430	16.71	221.1548
092	AA-d8	$C_{20}H_{24}D_8O_2$	312.2904	311.2826	22.87	267.2928
093	15-HETE-d8	$C_{20}H_{24}D_8O_3$	328.2854	327.2775	15.35	226.1830
094	5-OxoETE-d7	$C_{20}H_{23}D_7O_3$	325.2634	323.2493	17.61	209.2186
095	5,6-EET-d11	$C_{20}H_{21}D_{11}O_3$	331.3042	330.2964	18.46	202.2498
096	14,15-DHET-d11	$C_{20}H_{23}D_{11}O_4$	349.3148	348.3069	12.09	207.1391
097	LTC_4-d5	$C_{30}H_{42}D_5N_3O_9S$	630.3347	629.3269	10.16	272.0900
098	LTD_4-d5	$C_{25}H_{35}D_5N_2O_6S$	501.2921	500.2843	10.37	177.0341
099	LXA_4-d5	$C_{20}H_{27}D_5O_5$	357.2564	356.2485	6.96	115.0403

Table 2. (continued)

No.	Lipid	Molecular Formula	Exact Mass	Precursor Ion	Retention Time (min)	Fragment Ion
100	PGD_2-d4	$C_{20}H_{28}D_4O_5$	356.2501	355.2423	5.62	275.2303
101	PGE_2-d4	$C_{20}H_{28}D_4O_5$	356.2501	355.2423	5.42	275.2316
102	TXB_2-d4	$C_{20}H_{30}D_4O_6$	374.2606	373.2528	4.92	173.1124
103	15-deoxy-PGJ_2-d4	$C_{20}H_{24}D_4O_3$	320.2290	319.2211	12.85	275.2319
104	DHA-d5	$C_{22}H_{27}D_5O_2$	333.2716	332.2638	22.44	288.2746
105	RvD1-d5	$C_{22}H_{27}D_5O_5$	381.2564	380.2485	6.49	141.0559
106	RvD2-d5	$C_{22}H_{27}D_5O_5$	381.2564	380.2485	5.70	175.0762
107	9-HODE-d4	$C_{18}H_{28}D_4O_3$	300.2603	299.2524	15.28	172.1091

OxoETE, oxoeicosatetraenoic acid; DHET, dihydroxyeicosatrienoic acid; LXA_4, lipoxin A_4; TX, thromboxane; dhk-PG, 13,14-dihydro-15-keto prostaglandin; EpETE, epoxyeicosatetraenoic acid; diHETE, dihydroxyeicosatetraenoic acid; EpDPE, epoxydocosapentaenoic acid; DPA, docosapentaenoic acid; diHDPA, dihydroxydocosapentaenoic acid; RvD, resolven D; PDX, protectin DX; MaR, maresin; HODE, hydroxyoctadecadienoic acid; EpOME, epoxy octadecenoic acid; OxoODE, oxooctadecadienoic acid; diHOME, dihydroxyoctadecenoic acid; HOTrE, hydroxy octadecatrienoic acid; OxoOTrE, oxooctadecatrienoic acid.

Preparation of standard solutions of oxidized fatty acids

Primary stock solutions of 91 analytes and 16 internal standards (ISs) were prepared in MeOH. The working solutions of oxidized fatty acids and fatty acids were prepared from the primary stock solutions at 1 ng/μl and 10 ng/μl, respectively. The working solutions of fatty acids included AA, eicosapentaenoic acid (EPA), and docosahexaenoic acid (DHA). IS working solutions were prepared from primary stock solutions in 10 mM dibutyl hydroxytoluene in MeOH at 300 pg/μl (AA-d8 and DHA-d5 were at 1000 pg/μl). Standard solutions of oxidized fatty acids were freshly prepared by diluting the working solutions with MeOH to a final concentration of 10 pg/μl containing 30 pg/μl of IS. Similarly, standard mixtures of fatty acids were freshly prepared to a final concentration of 300 pg/μl containing 100 pg/μl of AA-d8 and DHA-d5.

Oxidized fatty acids extraction from mouse lung homogenates

After 8-week-old mice were sacrificed (n = 3), collected lung tissues were stored at −80°C until lipid extraction. After preparation of 25% (mass fraction) homogenates with 10 mM dibutyl hydroxytoluene in MeOH/ultrapure water (1/9, *v/v*) using a Micro Smash MS-100R cell disruptor (Tomy Seiko Co., Ltd., Tokyo, Japan) at 4,000 rpm for 1 minute (min) at 4°C, 10 μl of IS working solution was added to 50 μl aliquots of the lung homogenates along with 450 μl MeOH. The mixtures were vortex-mixed vigorously for 10 min at 10°C and then centrifuged at 9,000 × *g* for 5 min at 4°C. The upper layer was transferred to a silicone-coated tube, dried under a gentle stream of nitrogen at 40°C, and reconstituted in 100 μl of MeOH. This MeOH solution was extracted according to my previous report (42). Briefly, the MeOH solution and 300 μl of 20 mM potassium phosphate solution (pH 7.0) were mixed and placed directly into a preactivated

MonoSpin C18-AX column (GL Sciences Inc., Tokyo, Japan). This column was centrifuged at 9,000 × *g* for 1 min at 4°C and then washed with 300 µl of 5% NaCl solution by centrifugation. Finally, the analytes that were adsorbed onto the column were eluted twice with 300 µl of 5% NaCl/MeOH (1/9, *v/v*). The eluate was dried under a gentle stream of nitrogen at 40°C, reconstituted in 100 µl of MeOH, and 4 µl was introduced into the Q Exactive Plus system.

Oxidized fatty acids analysis by Q Exactive Plus system

The separation of oxidized fatty acids was undertaken on an Ultimate 3000 RSLC system (Thermo Fisher, Rockford, IL, USA). Separation was achieved with an Acquity UPLC BEH C18 column [100 mm × 2.1 mm inner diameter (i.d.), 1.7 µm; Waters Corp., Milford, MA, USA]. The autosampler and column were maintained at 4°C and 60°C, respectively. Mobile phase A was water/1 M ammonium acetate/5 mM phosphoric acid/formic acid (990/10/1/1, *v/v/v/v*) and mobile phase B was acetonitrile/isopropanol/1 M ammonium acetate/formic acid (495/495/10/1, *v/v/v/v*). The flow rate was 0.4 mL/min. The gradient program was: 0.00–25.00 min (from 25% to 70% B), 25.01–28.00 min (100% B), and 28.01–30.00 min (25% B). After separation by LC, we applied high mass accuracy MS analysis and data-dependent tandem mass spectrometry (dd-MS^2) analysis using a Q Exactive Plus Hybrid Quadrupole-Orbitrap Mass Spectrometer (Thermo Fisher). The Q Exactive Plus system was equipped with a high-resolution mass analyzer, an Orbitrap analyzer, and a heated-ESI probe, and this system was operated by Xcalibur 3.0 (Thermo Fisher). Oxidized fatty acid analysis was performed using MS full scan mode ranging from 200 to 750 in negative ion mode with the following source parameters: MS^1 resolving power, 70,000; MS^2 resolving power, 17,500; capillary temperature, 350°C; auxiliary gas heater temperature, 425°C; ion spray voltage, 2.5 kV; Maximum injection time (IT) of MS^1, 100

millisecond (ms); automatic gain control (AGC) target of MS^1, 1×10^6; Maximum IT of MS^2, 50 ms; AGC target of MS^2, 5×10^4; stepped normalized collision energy, 15, 25, and 35 eV; isolation window, 2.0 *m/z*; apex trigger, between 2 second (s) and 7 s; and dynamic exclusion, 5 s. The X, Y, and Z positions of the heated-ESI probe were set to 0, 2, and C, respectively. Nitrogen was used as the collision gas for all metabolites. The inclusion list, which contains 63 *m/z* values of oxidized fatty acids, was set to conduct effective fragmentation. The precursor ions for MS^2 analysis were selected from the list automatically, triggered by peak intensity information in full scan. If any molecules in the inclusion list were not present, other molecules were picked up in order of peak intensity. The Orbitrap analyzer (Thermo Fisher) was calibrated before analysis according to the manufacturer's instructions, using a mixture of acetic acid, caffeine, sodium dodecyl sulfate, sodium taurocholate, Met-Arg-Phe-Ala peptide, n-butylamine, and Ultramark 1621.

Identification of oxidized fatty acids

Identification of oxidized fatty acids was performed using Qual Browser software in Xcalibur 3.0. The precursor and product tolerance was set to a 10 ppm mass window.

Glycerolipid, glycerophospholipid, and sphingolipid extraction from lung homogenates

Glycerolipid, glycerophospholipid, and sphingolipid extraction was conducted according to a previous report (69). Briefly, aliquots of lung homogenate solution (10 µl) were transferred to silicone-coated tubes followed by additions of 10 ng/µl ISs working solution (10 µl) and water (790 µl). IS working solution included: 16:0-d31 ceramide, d5-(18:0/0:0/18:0) diacylglycerol, 16:0-d31 lysophosphatidylcholine, 13:0 lysophosphatidylinositol, 16:0-d31-18:1 phosphatidic

acid, 16:0-d31-18:1 phosphatidylcholine, 16:0-d31-18:1 phosphatidylethanolamine, 16:0-d31-18:1 phosphatidylglycerol, 16:0-d31-18:1 phosphatidylinositol, 16:0-d31-18:1 phosphatidylserine, 16:0-d31 sphingomyelin, sphingosine-d7, sphinanine-d7, sphingosine-1-phosphate-d7, and d5-(17:0/17:1(10Z)/17:0) triacylglycerol. Each IS standards was purchased from Avanti Polar Lipids, Inc. (Alabaster, AL, USA). An 800 µl aliquot of 1-butanol was added and the mixture was vortexed vigorously for 10 min at room temperature. After centrifugation at 9,000 × *g* for 5 min at room temperature, the upper layer was transferred to another silicone-coated tube. The remaining aqueous layer was extracted again with 1-butanol (500 µl). The combined upper layers from both extractions were dried under a gentle stream of nitrogen at 40°C, reconstituted in 200 µl of methanol/chloroform (1/1, *v/v*), and 1 µl of the reconstituted solution was introduced into the LC/ESI–MS/MS system.

Glycerolipid, glycerophospholipid, and sphingolipid analysis by Q Exactive Plus system

Glycerolipids, glycerophospholipids, and sphingolipids were analyzed as previously described. The gradient program for HPLC methods was: 0.00–43.00 min (from 40% to 100% B), 43.01–48.00 min (100% B), and 48.01–50.00 min (40% B). Lipid analysis was performed using MS full scan mode ranging from 200 to 1,300 in positive ion mode or negative ion mode. The source parameters in positive ion mode were: MS^1 resolving power, 70,000; MS^2 resolving power, 17,500; capillary temperature, 350°C; auxiliary gas heater temperature, 425°C; ion spray voltage, 3.8 kV; Maximum IT of MS^1, 100 ms; AGC target of MS^1, 1×10^6; Maximum IT of MS^2, 50 ms; AGC target of MS^2, 5×10^4; stepped normalized collision energy, 25, 35, and 45 eV; isolation window, 2.0 *m/z*; apex trigger, between 2 s and 7 s; and dynamic exclusion, 5 s. The X, Y, and Z positions of the heated-ESI probe were set to 0, 2, and C, respectively. Nitrogen was

used as the collision gas for all metabolites. The source parameters in negative ion mode followed the analytical method for oxidized fatty acids except for the stepped normalized collision energy; this parameter was set to 25, 35, and 45 eV. The inclusion list, which contains 2,053 *m/z* values of lipid molecular species in the LIPID MAPS database for the positive ion mode, and 2,138 *m/z* values for the negative ion mode, was set to conduct effective fragmentation. The Orbitrap analyzer (Thermo Fisher) was calibrated in positive ion mode and negative ion mode according to the manufacturer's instructions.

Identification by Lipid Search

Identification of lipid molecular species was performed using Lipid Search v4.1 software (Mitsui Knowledge Industry, Tokyo, Japan). The product search mode was used, and identification was based on the accurate mass of precursor ions and MS^2 special patterns. The precursor tolerance was set to a 6.5 ppm mass window and the product tolerance was set to an 8 ppm mass window. The absolute intensity threshold of precursor ions was set to 50,000, and the relative intensity threshold of product ions was set to 1.0%. The m-score threshold was set to 1.0.

Oxidized AA analysis by the API5000 system

Primary stock solutions of 94 analytes (Cayman Chemical Company) and 17 ISs were prepared in MeOH. The working solutions of oxidized fatty acids and fatty acids were prepared from primary stock solutions at 1 ng/µl or 10 ng/µl, respectively. IS working solutions were prepared from primary stock solutions in 10 mM dibutyl hydroxytoluene in MeOH at 300 pg/µl (AA-d8 and DHA-d5 were at 1,000 pg/µl). Calibration standards of oxidized fatty acids were prepared freshly when required by diluting the working solutions with MeOH to 0.01, 0.03, 0.05,

0.1, 0.3, 1, 3, 10, 30 and 100 pg/µl (concentrations of fatty acids were 0.1, 0.3, 0.5, 1, 3, 10, 30, 100, 300 and 1,000 pg/µl). Calibration standards contained IS at 6 pg/µl (concentrations of AA-d8 and DHA-d5 were both 20 pg/µl).

Lipid separation was performed on an Acquity UPLC system (Waters Corp.) and achieved with an Acquity UPLC BEH C18 column (100 mm × 2.1 mm i.d., 1.7 µm; Waters Corp.). The autosampler and column were maintained at 4 and 60°C, respectively. Mobile phase A was water/5 mM phosphoric acid/acetic acid (1,000/1/1, *v/v/v*) and mobile phase B was acetonitrile/isopropanol/acetic acid (500/500/1, *v/v/v*) at a flow rate of 0.4 mL/min. The gradient program was 0.00–15.00 min (from 25% to 80% B), 15.01–17.50 min (100% B) and 17.51–20.00 min (25% B). An FCV-20AH2 system (Shimadzu, Kyoto) was used as a valve switch to allow for introduction of the sample to the separation column between 1.00 and 15.00 min. MS analysis was carried out in scheduled multiple reaction monitoring (MRM) mode using an API5000 Mass Spectrometer (AB SCIEX, Foster City, CA, USA) equipped with an ESI source. Nitrogen was used as the collision gas for all metabolites. Oxidized fatty acids were detected in negative ESI mode with the following source parameters: curtain gas, 15 psi; ion source gas 1, 50 psi; ion source gas 2, 60 psi; ionspray voltage, −4500 V; collision gas, 8 psi; temperature, 500°C; interface heater, “on”; entrance potential, −10 V; collision cell exit potential, −10 V; MRM detection window, 60 s; target scan time, 1 s. Acquisition and processing of data were performed with Analyst v1.6.2 (AB Sciex).

Results

Global lipidomics

Initially, global lipidomics for analyzing oxidized fatty acids was investigated. Standard mixtures of oxidized fatty acids (10 pg/μl) were measured using the Q Exactive Plus system. Table 2 shows the exact mass, the retention time, and the structure-specific fragment ions from each oxidized fatty acid. For most of the molecules, the molecular ion peaks were well separated, and the peak intensity was $>10^4$ (Figure 2). Next, oxidized fatty acids in mouse lung tissues were analyzed. The background of the extracted ion current chromatograms was quite low in the accurate mass analysis (Figure 3). Various oxidized fatty acids could be detected and 12/15-lipoxygenase (LOX) metabolites, such as 13-hydroxyoctadecadienoic acid, 12-hydroxyeicosatetraenoic acid (HETE), 12-hydroxyeicosapentaenoic acid (HEPE), and 14-hydroxydocosahexesaenoic acid (HDoHE) were the main species detected. In addition, several unknown molecular ion peaks were observed, and some of them were identified as 12/15-LOX metabolites, such as 12-hydroxyeicosatrienoic acid (HETrE) and 14-hydroxydocosapentaenoic acid (HDoPE) by high-resolution dd-MS^2 (Figures 4 and 5). For DHA metabolites, several unknown molecular ion peaks were detected in mouse lung tissues (Figure 6). By high-resolution dd-MS^2, the molecular ion peaks with retention times of 14.5 min, 14.8 min, and 15.3 min were identified as 18-HDoHE, 22-HDoHE, and 19-HDoHE, respectively (Figure 6B, 6C, and 6D). By detailed analysis of the molecular ion peak at 14.6 min using high-resolution dd-MS^2, accurate masses of the characteristic fragment ions, such as *m/z* 299.2015 and *m/z* 299.2384 were obtained (Figure 6E and 6F). By composition analysis using accurate mass, the chemical

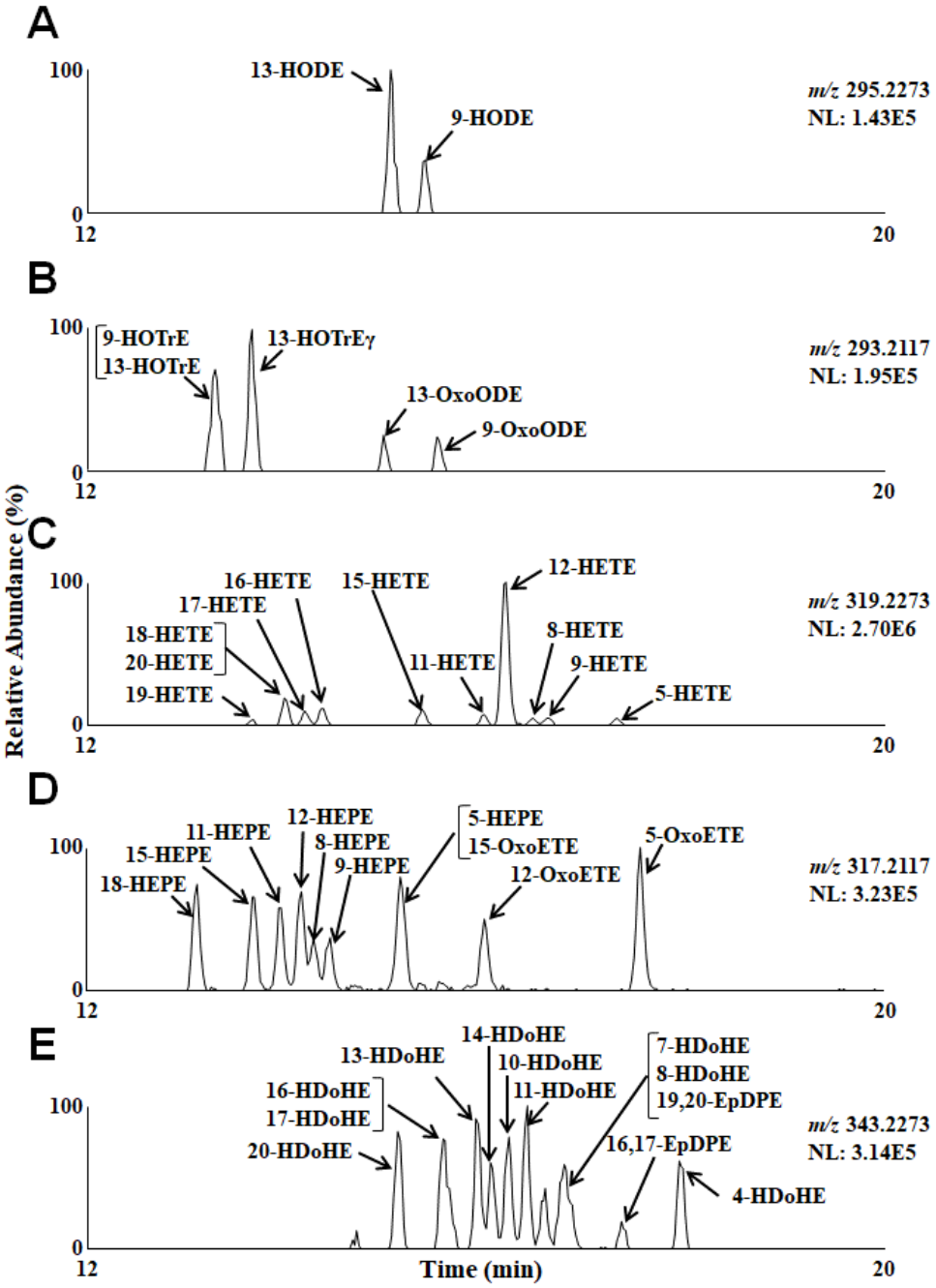

Figure 2. Extracted ion current chromatograms of commercially available mono-oxidized fatty acids. (A–E) Extracted ion current chromatograms of 10 pg/µl commercially available mono-oxidized fatty acids derived from linoleic acid (A), linolenic acid (B), AA (C), EPA (D), and DHA (E). NL, normalized intensity level (counts per second). NL indicates 100% of relative abundance in each extracted ion current chromatogram.

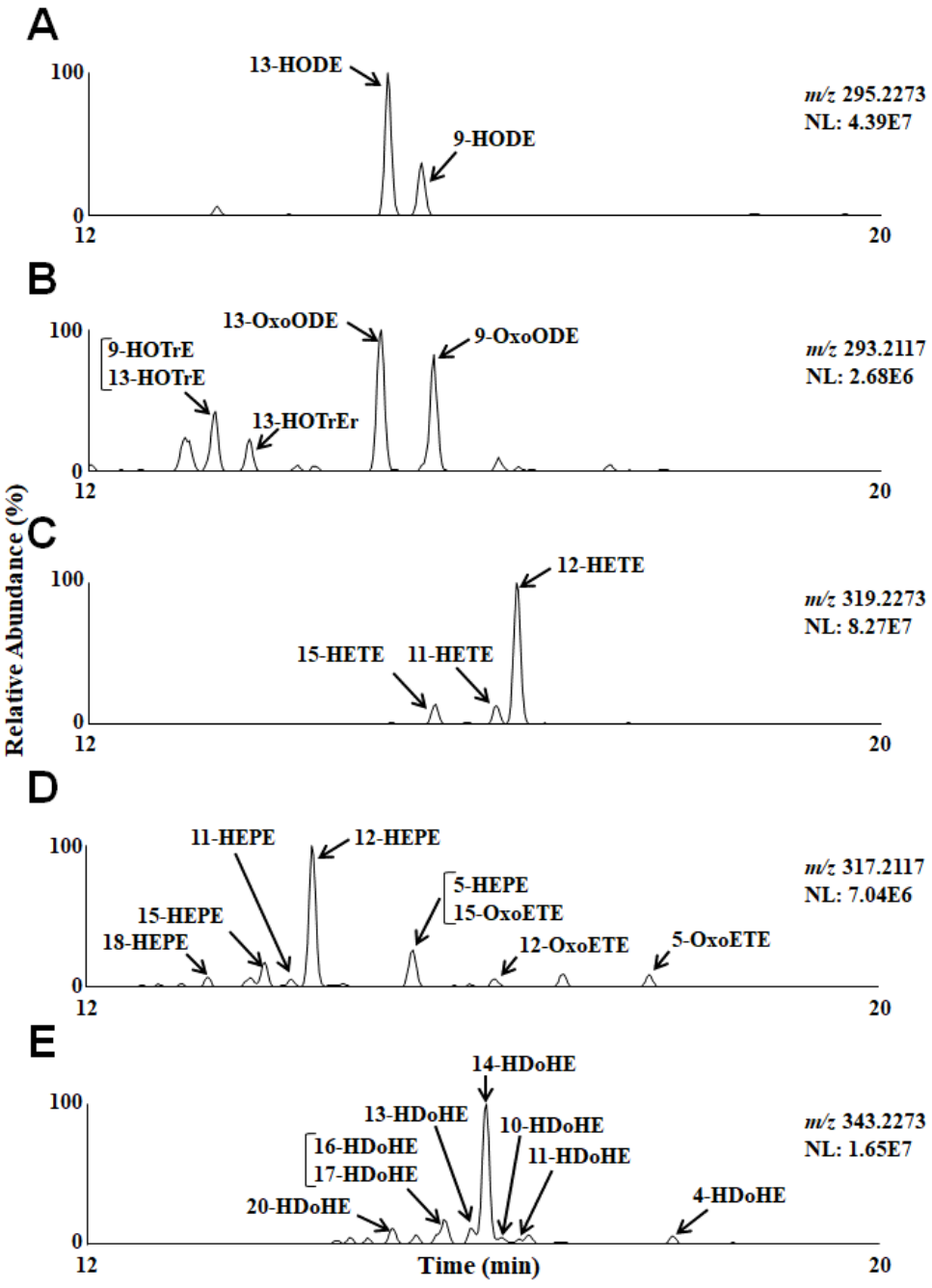

Figure 3. Extracted ion current chromatograms of mono-oxidized fatty acids in lung homogenates. (A–E) Extracted ion current chromatograms of mono-oxidized fatty acids in lung homogenates derived from linoleic acid (A), linolenic acid (B), AA (C), EPA (D), and DHA (E). NL, normalized intensity level (counts per second). NL indicates 100% of relative abundance in each extracted ion current chromatogram.

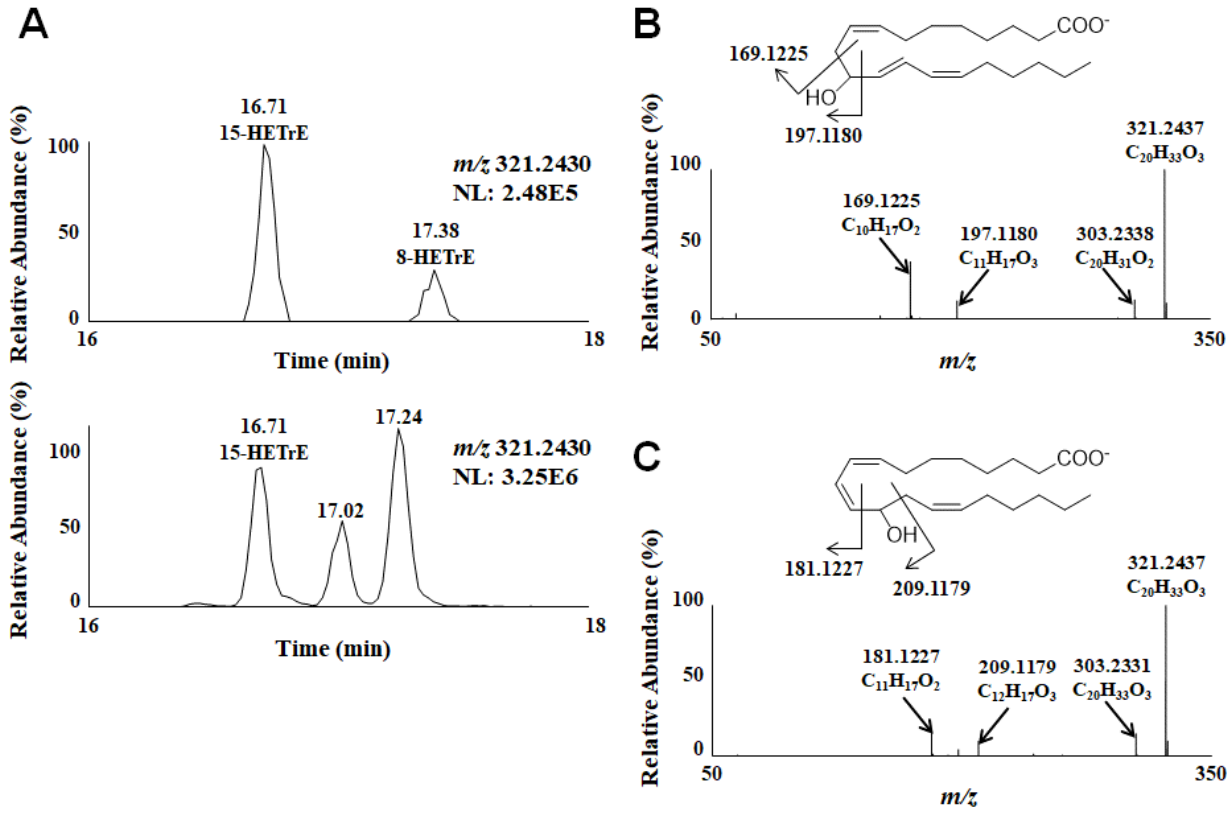

Figure 4. Structural analysis of mono-oxidized fatty acids derived from eicosatrienoic acid using high-resolution dd-MS^2. (A) Extracted ion current chromatogram of 10 pg/µl commercially available mono-oxidized fatty acids (upper) and mono-oxidized fatty acids in lung homogenates (lower) derived from eicosatrienoic acid. (B–C) Higher energy collisional dissociation mass spectra of the molecular ion peaks at 17.02 min (B) and 17.24 min (C) by high-resolution dd-MS^2. NL, normalized intensity level (counts per second). NL indicates 100% of relative abundance in each extracted ion current chromatogram.

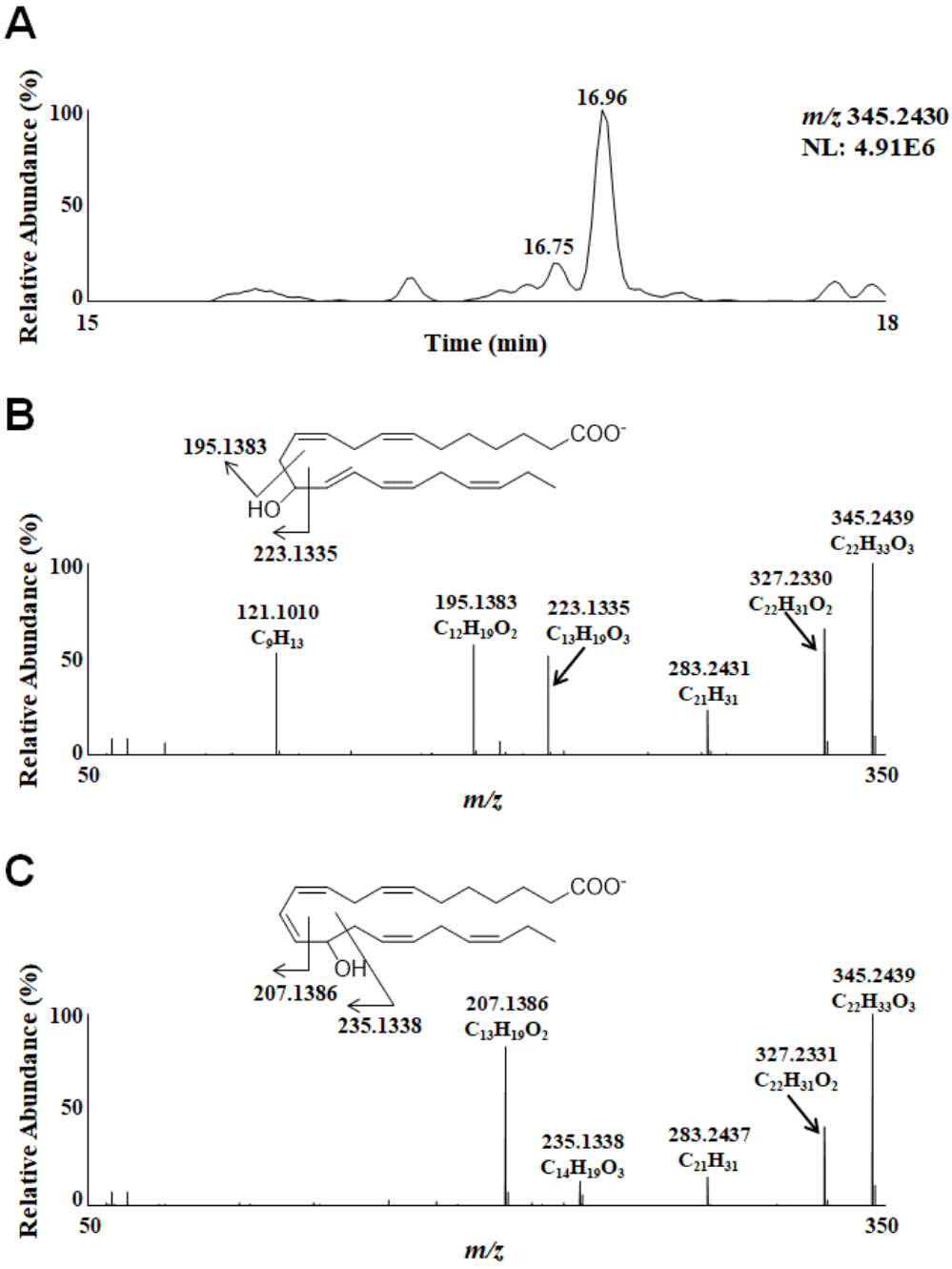

Figure 5. Structural analysis of mono-oxidized fatty acids derived from docosapentaenoic acid using high-resolution dd-MS^2. (A) An extracted ion current chromatogram of mono-oxidized fatty acids derived from docosapentaenoic acid in lung homogenates. (B–C) Higher energy collisional dissociation mass spectra of the molecular ion peaks at 16.75 min (B) and at 16.96 min (C) by high-resolution dd-MS^2. NL, normalized intensity level (counts per second). NL indicates 100% of relative abundance in each extracted ion current chromatogram.

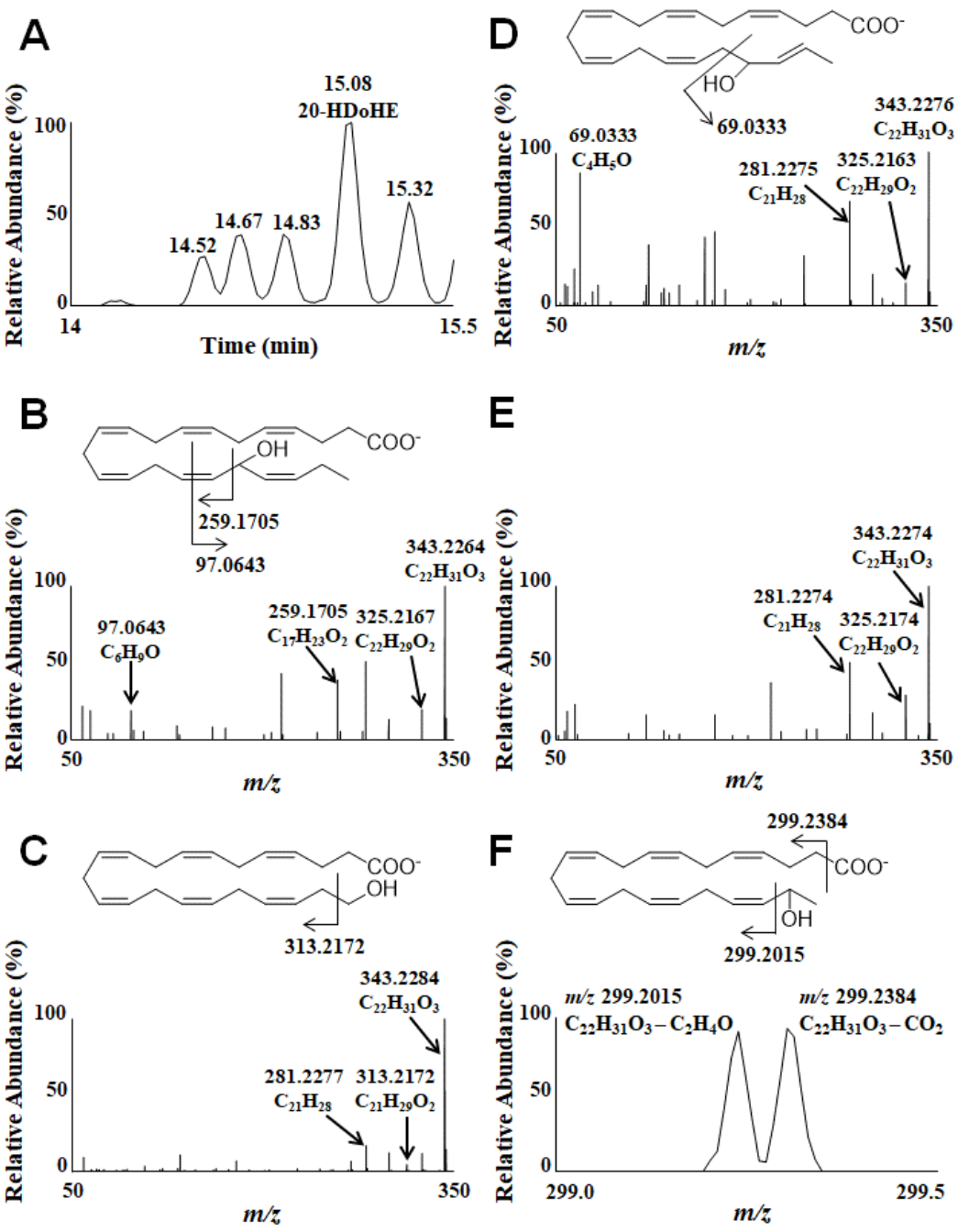

Figure 6. Structural analysis of DHA metabolites using high-resolution dd-MS^2. (A) Extracted ion current chromatogram of mono-oxidized fatty acids derived from DHA in lung homogenates. (B–D) Higher energy collisional dissociation mass spectra of the molecular ion peaks at 14.52 min (B), 14.83 min (C) and 15.32 min (D) by high-resolution dd-MS^2. (E) Higher energy collisional dissociation mass spectrum of the molecular ion peak at 14.67 min by high-resolution dd-MS^2; the mass spectrum around *m/z* 299 is enlarged (F). The left peak (*m/z* 299.2015) and right peak (*m/z* 299.2384) were $[C_{22}H_{31}O_3 - C_2H_4O]^-$ and $[C_{22}H_{31}O_3 - CO_2]^-$, respectively.

formulae of *m/z* 299.2015 and *m/z* 299.2384 were presumed to be $C_{20}H_{27}O_2$ and $C_{21}H_{31}O$, respectively. Because the chemical formula of deprotonated HDoHE is $C_{22}H_{31}O_3$, the former and the latter were considered to be $[C_{22}H_{31}O_3 - C_2H_4O]^-$ and $[C_{22}H_{31}O_3 - CO_2]^-$, respectively. Thus, the ion peak at 14.6 min was identified as 21-HDoHE. A similar fragment ion was also detected from 19-HETE, which is ω-1 hydroxy AA (Table 2). Therefore, it was confirmed that oxidized fatty acids can be measured using this system, and differences in molecular weight of <50 millidalton (mDa), which cannot be distinguished by QqQ MS and QqLIT MS, could be discriminated unambiguously using high-resolution dd-MS^2.

Furthermore, global lipidomics for analyzing glycerolipids, glycerophospholipids and sphingolipids in mouse lung tissues was constructed (Table 3). This data indicated that 2,467 lipid molecules and 1,070 lipid molecules were identified in positive ion mode and in negative ion mode, respectively. Interestingly, some lipid molecules, such as triacylglycerols, diacylglycerols and ceramide were predominantly detected in positive ion mode, whereas some lipid molecules, such as phosphatidic acid, platelet activating factor (PAF) and dimethylphosphatidylethanolamine were predominantly detected in negative ion mode. These data demonstrated that the selection of the measurement mode is an important point for the analysis of lipid molecules with different polarities.

Table 3. Number of lipids identified from mouse lung tissue

Lipid class	Positive ion mode	Negative ion mode
Ceramide	37	1
Diacylglycerol	146	0
Lysophosphatidic acid	0	4
Lysophosphatidylcholine	150	14
Lysophosphatidylethanolamine	76	25
Lysophosphatidylglycerol	3	14
Lysophosphatidylinositol	2	9
Lysophosphatidylserine	14	18
Phosphatidic acid	8	78
Platelet activating factor	0	49
Phosphatidylcholine	626	50
Phosphatidylethanolamine	647	230
Phosphatidylglycerol	78	81
Phosphatidylinositol	19	52
Phosphatidylserine	176	190
Sphingomyelin	100	64
Sphingosine	6	0
Triacylglycerol	369	0
Dimethylphosphatidylethanolamine	10	191
Total	2467	1070

Targeted lipidomics

Although ammonium acetate was added to the mobile phase as a buffer to stabilize the retention of analytes in my previous method, in new method, ammonium acetate was excluded from the mobile phase because a large amount of salt is a factor in reducing the sensitivity. Furthermore, formic acid was changed to acetic acid with a higher acid dissociation constant to improve the ionization efficiency of oxidized fatty acids. MRM conditions for each molecule are summarized in Table 4. By changing the composition of mobile phase, the sensitivity of this method was prominently improved compared with my previous method. For example, the peak intensities of leukotriene B_4 (LTB_4), prostaglandin E_2 (PGE_2), prostaglandin D_2 (PGD_2) and 5,6-epoxyeicosatrienoic acid (EET) were improved from 1.7e4 to 1.0e5 (LTB_4), from 1.8e4 to 1.2e5 (PGE_2), from 2.6e4 to 1.8e5 (PGD_2), and from 1.0e4 to 6.0e4 (5,6-EET), respectively (Figure 7). The signal-to-noise ratios of LTB_4, PGE_2, PGD_2 and 5,6-EET were also improved from 140.2 to 828.8 (LTB_4), from 463.5 to 1,011.9 (PGE_2), from 646.5 to 1,528.1 (PGD_2), and from 133 to 1,253.3 (5,6-EET), respectively. Furthermore, the lower limit of quantification of various molecules, such as LTB_4, PGD_2, PGE_2, 5,6-EET and 12-HETE was improved more than 10 times (Table 5).

Table 4. Optimized SRM pairs and parameters of oxidized AA

Lipid	Calibrated range (pg/µl)	Precursor Ion	Product Ion	Declustering Potential	Collision energy	Retention Time (min)	Internal Standard
AA	0.5–1,000	303	259	−80	−15	13.79	AA-d8
5-HETE	0.01–100	319	115	−100	−25	10.71	15-HETE-d8
8-HETE	0.03–100	319	155	−100	−25	10.23	15-HETE-d8
9-HETE	0.1–100	319	151	−100	−25	10.32	15-HETE-d8
11-HETE	0.01–100	319	167	−100	−25	9.94	15-HETE-d8
12-HETE	0.01–30	319	179	−100	−25	10.07	15-HETE-d8
15-HETE	0.03–100	319	219	−100	−15	9.59	15-HETE-d8
16-HETE	0.1–100	319	189	−80	−25	9.03	15-HETE-d8
17-HETE	0.05–100	319	247	−100	−25	8.93	15-HETE-d8
18-HETE	0.03–100	319	261	−80	−25	8.82	15-HETE-d8
19-HETE	1–100	319	231	−120	−25	8.13	15-HETE-d8
20-HETE	1–100	319	289	−120	−25	8.32	15-HETE-d8
5-oxoETE	0.05–100	317	203	−120	−25	10.90	5-oxoETE-d7
15-oxoETE	0.03–100	317	113	−120	−25	9.52	5-oxoETE-d7
5,6-EET	0.01–100	319	191	−100	−15	11.35	5,6-EET-d11
8,9-EET	0.03–100	319	155	−100	−15	11.11	5,6-EET-d11
11,12-EET	0.01–100	319	167	−100	−25	10.92	5,6-EET-d11
14,15-EET	0.05–100	319	219	−100	−15	10.50	5,6-EET-d11
5,6-DHET	0.03–100	337	145	−120	−25	9.31	14,15-DHET-d11
8,9-DHET	0.03–100	337	127	−120	−35	8.61	14,15-DHET-d11
11,12-DHET	0.03–100	337	167	−120	−25	8.17	14,15-DHET-d11
14,15-DHET	0.01–100	337	207	−120	−25	7.75	14,15-DHET-d11
LTB_4	0.01–100	335	195	−100	−25	6.97	LTB_4-d4
LXA_4	0.03–100	351	115	−80	−25	4.81	LXA_4-d5
PGD_2	0.03–100	351	189	−80	−25	4.03	PGD_2-d4
PGE_2	0.03–100	351	189	−80	−25	3.89	PGE_2-d4
$PGF_{2\alpha}$	0.03–100	353	193	−80	−35	3.99	PGE_2-d4
6-keto-$PGF_{1\alpha}$	0.01–100	369	163	−80	−35	2.42	TXB_2-d4
TXB_2	0.03–100	369	195	−80	−25	3.7	TXB_2-d4
dhk-PGE_2	0.03–100	351	175	−80	−35	4.21	PGE_2-d4
15-deoxy-PGJ_2	0.03–100	315	271	−80	−25	8.14	15-deoxy-PGJ_2-d4
AA-d8	—	311	267	−120	−25	13.73	—
15-HETE-d8	—	327	226	−80	−15	9.50	—
5-oxoETE-d7	—	323	209	−120	−25	10.82	—
5,6-EET-d11	—	331	202	−100	−15	11.28	—

Table 4. (continued)

Lipid	Calibrated range (pg/μl)	Precursor Ion	Product Ion	Declustering Potential	Collision energy	Retention Time (min)	Internal Standard
14,15-DHET-d11	—	348	207	−80	−25	7.69	—
LTB_4-d4	—	339	197	−120	−25	6.96	—
LXA_4-d5	—	356	115	−80	−25	4.77	—
PGD_2-d4	—	355	193	−80	−25	4.00	—
PGE_2-d4	—	355	193	−80	−25	3.87	—
TXB_2-d4	—	373	173	−80	−35	3.70	—
15-deoxy-PGJ_2-d4	—	319	275	−120	−25	8.12	—

OxoETE, oxoeicosatetraenoic acid; DHET, dihydroxyeicosatrienoic acid; LXA_4, lipoxin A_4; TX, thromboxane; dhk-PG, 13,14-dihydro-15-keto prostaglandin.

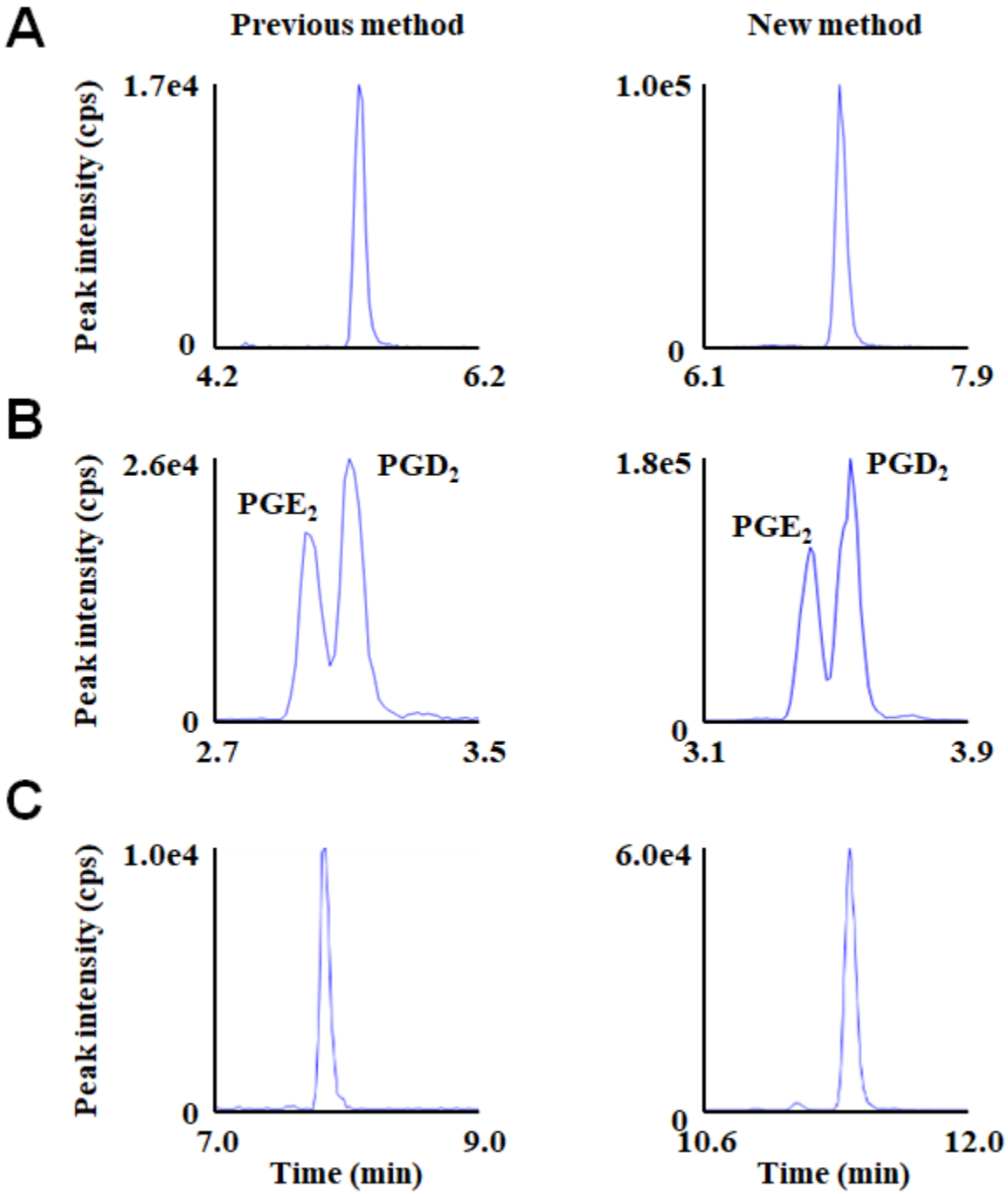

Figure 7. Comparison of extracted ion current chromatograms of 10 pg/μl oxidized fatty acids. (A–C) Extracted ion current chromatograms of LTB_4 (A), PGD_2 and PGE_2 (B), and 5,6-EET (C) were compared between the methods. The newly established method showed greater peak intensity than previous methods. Cps, count per second.

Table 5. The comparison of the lower limit of quantification

Lipid	Previous method (pg/μl)	New method (pg/μl)
5-HETE	0.3	0.01
8-HETE	0.3	0.03
11-HETE	0.3	0.01
12-HETE	0.3	0.01
15-HETE	0.3	0.03
16-HETE	1	0.1
18-HETE	0.3	0.03
5,6-EET	0.3	0.01
8,9-EET	1	0.03
11,12-EET	0.3	0.01
LTB_4	0.3	0.01
LXA_4	0.3	0.03
PGD_2	0.3	0.03
PGE_2	0.3	0.03
$PGF_{2\alpha}$	0.3	0.03
6-keto-$PGF_{1\alpha}$	0.1	0.01
TXB_2	0.3	0.03
dhk-PGE_2	1	0.03
15-deoxy-PGJ_2	0.3	0.03

LXA_4, lipoxin A_4; TX, thromboxane; dhk-PG, 13,14-dihydro-15-keto prostaglandin.

Discussion

Lipidomics have been applied to the identification and validation of lipid molecules and such information is thought to be extremely valuable in the understanding of some diseases. In particular, small amounts of fatty acid metabolites as lipid mediators and/or biomarkers have been thoroughly investigated because of their important pathological and physiological roles in diseases, such as cardiovascular disease, influenza infection, and severe asthma (18, 76–80). These investigations have developed concomitant with the development of MS (41, 81). The investigation of lipid profiles in targeted tissues is important to better understand diseases. In lipid-rich tissues, such as brain, lung, and liver, variation of lipid profiles is expected under pathological conditions. Global lipidomics is a powerful tool to explore the molecules indicating the correlation(s) with disease; the discovery of unknown molecules related to pathologies can also be expected. However, there has been little application of high-resolution MS for analyzing oxidized fatty acids. Because of the extensive structural diversity of lipid molecules, it is considered that unknown lipid metabolites related to diseases will remain undetected. Therefore, for the purpose of the discovery and identification of unknown lipid metabolites in biological samples, global lipidomics for analyzing oxidized fatty acids was constructed using mouse lung as the model tissue.

The separation of mono-oxidized fatty acids in full scan mode is considered difficult because the exact mass of mono-oxidized fatty acids derived from the same fatty acid is the same and their retention behavior is very similar. However, here, aside from a few molecules, each molecular ion peak was well separated in full scan mode. Using Q Exactive Plus, oxidized fatty

acids could be globally measured by setting the mass range without analytical parameters for each molecule. Although the exact position of double bonds in fatty acids cannot be fully determined by MS, 11-HETrE and 12-HETrE in mouse lung tissues might not be derived from Mead acid (MA). In the case of AA, which has four double bonds (in the 5–6, 8–9, 11–12, and 14–15 positions), the accurate masses of major fragment ions of 11-HETE and 12-HETE were *m/z* 167.1080 and *m/z* 179.1080, respectively. Because MA has three double bonds (positions 5–6, 8–9, and 11–12), the accurate masses of major fragment ions of 11-HETrE and 12-HETrE derived from MA were *m/z* 167.1072 and *m/z* 179.1072, respectively. However, the accurate masses of major fragment ions of 11-HETrE and 12-HETrE in mouse lung tissues were *m/z* 169.1225 and *m/z* 181.1227, respectively. These actual values were about 2 Da higher than expected, and these metabolites may have only one double bond in the 5–6 or 8–9 position and two double bonds after position 10. Hence, 11-HETrE and 12-HETrE in mouse lung tissues are not derived from MA, and they are probably derived from dihomo-γ-linolenic acid, which has double bonds in the 8–9, 11–12, and 14–15 positions. Similarly, 13-HDoPE and 14-HDoPE in mouse lung tissues were derived from ω-3 docosapentaenoic acid, not ω-6 docosapentaenoic acid, as determined from their fragment ions. In this way, it is possible to infer the molecular structure of unknown molecules using accurate mass analysis and high-resolution dd-MS^2. Global lipidomics for analyzing glycerolipids, glycerophospholipids, and sphingolipids was also constructed, and this system has already been applied to investigate the role of some lipids in the development of obesity and Olmsted syndrome (82–85). Because intravital fatty acids are generally liberated from glycerophospholipids in cell membranes by phospholipases, it is important to obtain simultaneous information about substrates and products from the same samples. To the best of my knowledge, this is the first report to approach global lipidomics using

the same conditions (e.g., mobile phase, LC column, and LC–MS device) to analyze oxidized fatty acids and glycerophospholipids in the same samples, changing only the extraction procedure and the measurement method.

Furthermore, the sensitivity of my previous targeted lipidomics was improved by changing the composition of mobile phase. This approach has already been applied to investigate the role of some lipids in the development of pain and Olmsted syndrome (23, 24, 43, 85). In particular, this system was indispensable for analyzing a trace amount of PGE_2 and 5,6-EET in synovial fluids from patients with osteoarthritis (23).

Summary

Global lipidomics for analyzing oxidized fatty acids using RPLC coupled with Q Exactive Plus MS was developed. In this system, oxidized fatty acids in mouse lung tissue samples were globally analyzed by high-resolution accurate mass analysis, and multiple unknown lipid metabolites, such as 12-HETrE, 14-HDoPE and 21-HDoHE were identified by accurate mass analysis and high-resolution dd-MS^2. Using high-resolution MS and high-resolution dd-MS^2, the differences in molecular weight of <50 mDa, which cannot be distinguished by QqQ MS and QqLIT MS, could be discriminated unambiguously. The global lipidomics for glycerolipids, glycerophospholipids and sphingolipids in mouse lung tissues was also constructed using RPLC coupled with Q Exactive Plus MS. Thousands of lipid molecules were detected and identified in this system, and it is important to select the measurement mode for analyzing lipid molecules with different polarities. Furthermore, the sensitivity of my previous targeted lipidomics was improved by changing the composition of mobile phase. Compared with my previous method, the lower limit of quantification of various molecules, such as LTB_4, PGD_2, PGE_2, 5,6-EET and 12-HETE was improved more than 10 times in new method.

Chapter II

Inhibition of dengue virus infection by 1-stearoyl-2-arachidonoyl-phosphatidylinositol *in vitro*

Introduction

Dengue fever (DF) is an acute febrile infectious disease caused by the mosquito-borne DENV. According to one recent estimate, 390 million dengue infections occur annually, with 96 million symptomatic cases (86). Another study estimated that 3.9 billion people in 128 countries are at risk of DENV infection (87). The acute disease can progress to more severe forms, which include dengue hemorrhagic fever and dengue shock syndrome (collectively referred to as "severe dengue") (88), severe hemorrhage, and serious organ failure, all of which can lead to death (89–91). The main treatment for DF is palliative, and acetaminophen is used to treat fever and relieve pain (92). Despite the global public health concern posed by this virus, there are currently no effective anti-DENV drugs. A better understanding of the mechanisms behind DENV infection is needed to develop new drugs for this condition.

DENV is a positive-sense single-stranded RNA virus that is a member of the genus *Flavivirus* in the family *Flaviviridae*, and it is split into four serotypes (DENV1, DENV2, DENV3, and DENV4). The DENV genome, approximately 11 kilobase (kb) in size, encodes three structural proteins and seven nonstructural proteins (NSs), which are essential for viral replication. Host cell surface receptors, such as T cell immunoglobulin and mucin domain-containing protein 1 (TIM-1), AXL receptor tyrosine kinase (AXL), and CD300a, mediate DENV entry into cells (93–96). Viral replication and assembly occurs on the surface of the endoplasmic reticulum, and the viral particle maturation occurs through the *trans*-Golgi network (97). DENV hijacks the host cell machinery to produce its viral proteins and to replicate the viral RNA genome.

Activation of both lipid metabolism and lipid synthesis in DENV-infected cells has been reported (53, 98). In DENV-infected cells, the lipid droplet size and intracellular triacylglycerol levels are reduced, the levels of intracellular free fatty acids are increased, and β-oxidation is activated, followed by the generation of ATP. Notably, ATP is essential for DENV replication, and lipid droplets act as the energy source for DENV replication (50). Levels of phospholipids and sphingolipids, which can change the physical properties of the bilayer, including its curvature and permeability, are elevated in DENV-infected cells compared with uninfected cells (99). FASN is an essential component of the DENV replication complex, and accelerates lipid synthesis (55). Rab18 is required to recruit FASN to the sites of DENV replication and to interact with DENV NS3 to promote fatty acid synthesis (100). Changes in the dynamics of serum lipid molecules, such as the bile acids, polyunsaturated fatty acids, phospholipids, and sphingolipids, have been reported in patients with DF (101–104). Although these findings suggest that lipid molecules modulate DENV infection, there have been no reports of anti-DENV lipid molecules. In this chapter, lipid screening was conducted to assess lipid molecules for their ability to attenuate DENV infection. Furthermore, the effects of anti-DENV lipid molecules on viral replication, viral entry, and/or DENV infection–induced inflammatory responses were investigated.

Materials and methods

Materials

Antibiotic–Antimycotic (100×), Dulbecco's modified Eagle's medium (DMEM), fetal bovine serum (FBS), Roswell Park Memorial Institute (RPMI) 1640 medium, 0.25% trypsin–ethylenediaminetetraacetic acid (EDTA), 2-mercaptoethanol, and UltraPure 1 M Tris-HCl buffer, pH7.5 were purchased from Thermo Fisher Scientific Inc. (Rockford, IL, USA). Fatty acid metabolite standards were purchased from Cayman Chemical Company (Ann Arbor, MI, USA). Phospholipid standards were purchased from Avanti Polar Lipids, Inc. (Alabaster, AL, USA). Minimal essential medium (MEM) was purchased from Nissui Pharmaceutical Co., Ltd (Tokyo, Japan). Guanidine thiocyanate and 3,3′,5,5′-Tetramethylbenzidine (TMB) was purchased from Nacalai Tesque, Inc. (Kyoto, Japan). Antibody against dengue virus types 1–4 (D1-11[3]) was purchased from GeneTex, Inc. (Irvine, CA, USA). Horseradish peroxidase (HRP)-linked anti-mouse IgG secondary antibody was purchased from GE Healthcare UK Ltd (Little Chalfont, England). LC–MS grade methanol, isopropanol, ammonium acetate, calcium chloride ($CaCl_2$), sodium chloride (NaCl), ethanol, sodium hydrogen carbonate, sodium dextran sulfate 5,000, dimethyl sulfoxide, potassium acetate, proteinase K, and Dulbecco's phosphate-buffered saline (D-PBS) (−) were purchased from Wako Pure Chemical Industries, Ltd (Osaka, Japan). LC–MS grade acetonitrile and phosphoric acid were obtained from Kanto Chemical Co., Inc. (Tokyo, Japan). LC–MS grade formic acid, chloroform, ammonium chloride (NH_4Cl), resazurin, L-glutamine, 30% bovine serum albumin (BSA) in D-PBS(−), and phorbol 12-myristate 13-acetate (PMA) were purchased from Sigma–Aldrich (St. Louis, MO, USA). Phospholipid standards

were purchased from Avanti Polar Lipids, Inc. (Alabaster, AL, USA). Lipopolysaccharide (LPS) and flagellin were purchased from InvivoGen (San Diego, CA, USA). Recombinant human interferon γ (IFN-γ) was purchased from R&D Systems, Inc. (Minneapolis, MN, USA). Recombinant human CD14 was purchased from R&D Systems, Inc. (Minneapolis). Ultrapure water was obtained with a Milli-Q system (Millipore, Billerica, MA, USA).

Cells and viruses

A549, BHK-21, HepG2, and Huh-7 cells were purchased from the American Type Culture Collection (Manassas, VA, USA). THP-1 cells were kindly provided by Dr. Keita Matsuno (Hokkaido University, Sapporo, Japan). A549, BHK-21, HepG2, and Huh-7 cells were maintained in DMEM supplemented with 10% FBS and 1% Antibiotic–Antimycotic (100×) at 37°C in a humidified incubator under 5% CO_2. THP-1 cells were maintained in RPMI 1640 supplemented with 10% FBS and 1% Antibiotic–Antimycotic (100×). In cell-based assays, A549, BHK-21, HepG2 and Huh-7 cells were used in MEM supplemented with 2% FBS and 2 mM L-glutamine at 37°C in a humidified incubator under 5% CO_2. THP-1 cells were cultured in RPMI 1640 supplemented with 2% FBS and 1% Antibiotic–Antimycotic (100×) for cell-based assays.

DENV1 (D1/hu/PHL/10-07), DENV2 (D2/hu/INDIA/09-74, accession number LC367234), DENV3 (D3/hu/Thailand/00-40), and DENV4 (D4/hu/Solomon/09-11) were kindly provided by Dr. Tomohiko Takasaki (Kanagawa Prefectural Institute of Public Health, Chigasaki, Japan). All DENV serotypes were propagated in BHK-21 cells. BHK-21 cells were separately infected with each DENV serotype at a multiplicity of infection (MOI) of 0.01 and incubated for 3 h at 37°C. After incubation, the nonadherent viruses were removed, and fresh medium (MEM

supplemented with 2% FBS and 2 mM L-glutamine) was added. The infected cells were incubated at 37°C until they showed a cytopathic effect. The supernatants containing DENV were recovered and stored at −80°C. The viral titer of each DENV, including the 50% tissue culture infective dose ($TCID_{50}$) and the number of plaque-forming units, was calculated with a resazurin reduction assay using BHK-21 cells (protocol described below) and a previously described plaque-forming assay (105), respectively.

Preparation of lipid molecules

All lipid molecules dissolved in chloroform, methanol/chloroform (1/1, *v/v*), or ethanol were sufficiently dried under a gentle stream of nitrogen at room temperature, then reconstituted in dimethyl sulfoxide to a concentration of 1 mM. The lipid molecules were either added directly to plates or were added after their dilution with MEM supplemented with 2 mM L-glutamine. In the assay using THP-1 cells, the lipid molecules were added after their dilution with RPMI 1640 supplemented with 2% FBS and 1% Antibiotic–Antimycotic (100×).

Lipid screening

One each of 134 lipid molecule species (50 µl) and 100 µl of BHK-21 cells (3.0×10^4 cells) were added to 96-well microplates and incubated for 1 h at 37°C (n = 2). The cells were then infected with DENV2 (50 µl; 5 $TCID_{50}$) for 120 h at 37°C. The final concentration of each lipid molecule was 10 µM. Resazurin (0.24 mg/ml; 20 µl) in D-PBS(−) was added to the cells, which were then incubated at 37°C for 2 h. The fluorescence intensity was measured at 531 nm (excitation) and 590 nm (emission) with an EnVision Xcite Multilabel Reader (Perkin Elmer, Waltham, MA, USA). The anti-DENV2 activities of the lipid molecules were calculated with the

following equation, in which A is the mean fluorescence intensity of the uninfected cells; B is the mean fluorescence intensity of the DENV2-infected cells; and C is the individual fluorescence intensity of the DENV2-infected cells treated with lipid molecules:

$$\text{Anti-DENV2 activity (\%)} = (C - B) / (A - B) \times 100.$$

The cytotoxic effects of the lipid molecules on BHK-21 cells were evaluated with the method described above, using uninfected BHK-21 cells.

Resazurin reduction assay

Lipid molecules (50 µl) and 100 µl of BHK-21 cells (3.0×10^4 cells) were added to Nunc MicroWell 96-well Microplates (Thermo Fisher) and incubated for 1 h at 37°C. The cells were infected with 50 µl of DENV2 (10 $TCID_{50}$) for 96 h at 37°C. Except for 1-stearoyl-2-arachidonoyl (SA) -phosphatidylinositol (PI), the final concentration of all lipid molecules was 10 µM. Resazurin (0.24 mg/ml; 20 µl) in D-PBS(−) was added, and the cells were incubated at 37°C for 2 h after DENV2 infection. The fluorescence intensity, anti-DENV2 activities, and cytotoxic effects of the lipid molecules were measured as previously described.

Quantification of intracellular DENV RNA with reverse transcriptase-quantitative real-time polymerase chain reaction (RT-qPCR)

Samples (100 µl) of BHK-21, A549, Huh-7 and HepG2 cells (3.0×10^4 cells) were seeded in 96-well microplates and incubated overnight at 37°C. SAPI (50 µl), distearoyl-PI (DSPI) (50 µl), or SA-phosphatidylcholine (PC) (50 µl) was added to the cells, and they were incubated at 37°C for 1 h. The cells were then infected with DENV2 (50 µl; MOI of 0.01 for BHK-21, A549 and Huh-7 cells; MOI of 0.1 for HepG2 cells) at 37°C for 72 h. Alternately, A549 cells were infected

with DENV1 or DENV3 (50 µl; MOI of 0.01) at 37°C for 72 h or with DENV4 (50 µl; MOI of 0.01) at 37°C for 48 h. The final concentration of SAPI was 10, 5, 2.5, or 1.25 µM. The final concentrations of DSPI and SAPC were each 10 µM. After DENV infection, the cell supernatants were removed, and the infected cells were washed with proteinase K in D-PBS(−) (1 µg/ml; 200 µl) for 45 min at 4°C to eliminate the viruses bound to the cell surfaces (93, 95, 106). The intracellular RNA was extracted with 100 µl of lysis buffer [10 mM Tris-HCI (pH7.5), 4 M guanidine thiocyanate, and 1% 2-mercaptoethanol] and purified using Wizard SV 96 Binding Plates (Promega KK, Osaka, Japan), in accordance with the manufacturer's instructions. RT-qPCR was performed with the EXPRESS One-Step Superscript RT-qPCR Kit, universal (Thermo Fisher) and QuantStudio 7 Flex Real-Time PCR System (Thermo Fisher), in accordance with the manufacturer's instructions. Primer sets for DENV2, glyceraldehyde-3-phosphate dehydrogenase (*Gapdh*), and β-actin (*ACTB*) (Hs01060665_g1) were purchased from Thermo Fisher, and the primer sequences for DENV2 and *Gapdh* were:
DENV2 forward, 5′-AGTGGACACGAGAACCCAAGA-3′; DENV2 reverse, 5′-TTCGGCCGTGATTTTCATTAG-3′; DENV2 probe, 5′-FAM-AAAAGAAGGCACGAAGAA-MGB-3′; *Gapdh* forward, 5′-GGTCGGAGTGAACGGATTTG-3′; *Gapdh* reverse, 5′-AGTGAAGGCAGCCCTGGTAA-3′; *Gapdh* probe, 5′-VIC-CCGTATTGGACGCCTG-MGB-3′ (105). *Gapdh* and *ACTB* were used as the internal controls.

Lipid extraction

A549 cells (500 µl; 1.5×10^5 cells) were seeded in Nunc Cell Culture 24-Well Plates (Thermo Fisher) and incubated overnight at 37°C. SAPI (250 µl), DSPI (250 µl), or SAPC (250 µl) was added, after which the cells were incubated at 37°C for 1 h. The cells were then infected

with DENV2 (250 µl; MOI of 0.1) for 3, 24, 48, or 72 h at 37°C. The final lipid molecule concentrations were each 10 µM. At each timepoint, the supernatants were recovered and stored at −80°C until use in a lipid analysis. The infected cells were washed with proteinase K in D-PBS(−) (1 µg/ml; 1 ml) for 45 min at 4°C and collected with 0.05% trypsin–EDTA in D-PBS(−) (500 µl). Aliquots of the cell suspensions (500 µl) were transferred to 2 ml silicone-coated tubes, and 1 ml of 500 ng/ml IS in methanol/chloroform (1/1, *v/v*) was added to each tube. The IS included 16:0-$_{d31}$-18:1 PC and 16:0-$_{d31}$-18:1 PI. Aliquots of the supernatants (100 µl) diluted with water (200 µl) were also transferred to 2 ml silicone-coated tubes, and 1 ml of 500 ng/ml IS was added to each tube. The mixtures were vortexed vigorously for 5 min at room temperature and centrifuged at 20,000 × *g* for 5 min at room temperature. The chloroform layer (lower layer) of each mixture was transferred to another silicone-coated tube, dried under a gentle stream of nitrogen at 40°C, and reconstituted in 200 µl of methanol/chloroform (1/1, *v/v*). An aliquot (2 µl) was then was introduced into the LC/ESI–MS/MS system.

Lipid analysis

The lipid analysis was performed as described in my previous report (44), with some modification. Briefly, the lipid molecules were separated on an Ultimate 3000 RSLC system (Thermo Fisher) with an Acquity UPLC BEH C18 column (100 mm × 2.1 mm i.d., 1.7 µm; Waters Corp.). The autosampler and column were maintained at 10°C and 60°C, respectively. Mobile phase A was water/1 M ammonium acetate/5 mM phosphoric acid/formic acid (990/10/1/1, *v/v/v/v*), and mobile phase B was acetonitrile/isopropanol/1 M ammonium acetate/formic acid (495/495/10/1, *v/v/v/v*). The flow rate was 0.4 ml/min. The gradient program for the LC method was: 0.00–1.00 min (70% B), 1.01–15.00 min (from 70% to 90% B), 15.01–

18.00 min (100% B), and 18.01–20.00 min (70% B). After the separation process, a high-mass-accuracy MS analysis and a data-dependent MS/MS analysis were performed with a Q Exactive Plus Hybrid Quadrupole-Orbitrap Mass Spectrometer (Thermo Fisher). The lipid analysis was performed in the MS full-scan mode, ranging from 200 to 1,300, in negative ion mode. The source parameters in negative ion mode were: MS^1 resolving power, 70,000; MS^2 resolving power, 17,500; capillary temperature, 350°C; auxiliary gas heater temperature, 425°C; ion spray voltage, 2.5 kV; maximum IT of MS^1, 100 ms; AGC target of MS^1, 1×10^6; maximum IT of MS^2, 50 ms; AGC target of MS^2, 5×10^4; stepped normalized collision energy, 25, 35, and 45 eV; isolation window, 2.0 *m/z*; apex trigger, between 2 s and 7 s; and dynamic exclusion, 5 s. The X, Y, and Z positions of the heated-ESI probe were set to 0, 2, and C, respectively. Nitrogen was used as the collision gas for all metabolites. Calibration curves of SAPI, DSPI, and SAPC were constructed from 10–1,000 ng/ml for quantification.

Solid-phase binding assay

The binding potential between DENV2 and phospholipids was evaluated as described in previous reports (107–110), with some modification. An aliquot (50 µl) of SAPI, DSPI, SA-phosphatidic acid (PA), SAPC, SA-phosphatidylethanolamine (PE), SA-phosphatidylglycerol (PG), or SA-phosphatidylserine (PS) in ethanol was added directly to 96-well microplates (500 pmol). The ethanol was dried under a gentle stream of nitrogen at 40°C. The wells were then hydrated and blocked with 150 µl of blocking buffer [20 mM Tris (pH 7.5), 100 mM NaCl, 10 mM $CaCl_2$, 3% BSA] for 1 h at room temperature. Various concentrations of DENV2 (50 µl) were added to the cells, which were then incubated for 2 h at 37°C. The wells were washed three times with 150 µl of wash buffer [20 mM Tris (pH 7.5), 100 mM NaCl, 10 mM $CaCl_2$], after

which 100 µl/well of anti-DENV2 primary antibody (1:500) was added. Following an incubation at 37°C for 1 h, the wells were washed three times with 150 µl of wash buffer before 100 µl/well of HRP-linked anti-mouse IgG secondary antibody (1:2,000) was added. The cells and antibody were incubated for 1 h at room temperature. After additional washing, TMB substrate (75 µl) was added, and the cells were incubated for 30 min at room temperature in the dark. The reaction was stopped with 25 µl of 1 N HCl. The absorbance was measured at 450 nm with an EnVision Xcite Multilabel Reader.

Concentration dependence of the anti-DENV2 activity of Dextran sulfate (DS)

A549 cells (100 µl; 3.0×10^4 cells) were seeded in 96-well microplates and incubated overnight at 37°C. DS (50 µl; 10, 5, 2.5, 1.25, 0.63, 0.31, 0.16, or 0.078 µg/ml) was added to each well, and the cells were incubated for 1 h at 37°C. The cells were then infected with 50 µl of DENV2 (MOI of 0.1) for 48 h at 37°C. After DENV2 infection, the supernatants were removed, the infected cells were washed, the intracellular RNA was extracted and purified, and RT-qPCR was performed as previously described. *ACTB* was used as the internal control for normalization. The cytotoxic effect of DS on A549 cells was evaluated as previously described.

Preincubation of lipid molecules and DENV2 before viral infection of cells

A549 cells (750 µl; 1.5×10^5 cells) were seeded in 24-Well plates and incubated overnight at 37°C. SAPI (1 mM; 1 µl), DSPI (1 mM; 1 µl), SAPC (1 mM; 1 µl), DS (1 mg/ml; 1 µl), or dimethyl sulfoxide (1 µl), along with 49 µl of MEM supplemented with 2% FBS and 2 mM L-glutamine and 50 µl of DENV2 stock solution were preincubated for 1 h at 37°C. After the dilution of preincubated DENV2, 250 µl of DENV2 (MOI of 0.1) was added to the cells, which

were incubated for 1 h at 4°C to allow viral attachment to the cell surfaces, followed by a second incubation for 1 h at 37°C to allow entry into the host cells. The final concentration of lipid molecules was 0.089 μM. To exclude the possible anti-DENV2 activity of DS, cells were simultaneously inoculated with DENV2 and DS (0.089 μg/ml). This concentration was equal to the concentration of DS that was added to the cells after preincubation with DENV2. After the supernatants were removed and the cells washed with D-PBS(−) (1 ml), 1 ml of MEM supplemented with 2% FBS and 2 mM L-glutamine was added, and the cells were incubated at 37°C for 47 h. The infected cells were washed with proteinase K in D-PBS(−) (1 μg/ml; 1 ml) for 45 min at 4°C, and the intracellular RNA was extracted and purified with the RNeasy Mini Kit (Qiagen, Hilden, Germany). The concentration of RNA was quantified with a NanoDrop 2000 spectrophotometer (Thermo Fisher), and cDNA was synthesized with PrimeScript RT Master Mix (Perfect Real Time) (Takara Bio Inc., Shiga, Japan) on a Veriti 96-well Thermal Cycler (Thermo Fisher), in accordance with the manufacturers' instructions. RT-qPCR was performed as previously described.

Evaluation of the cytotoxicity of NH_4Cl

A549 cells (100 μl; 3.0×10^4 cells) were seeded in 96-well microplates and incubated overnight at 37°C. NH_4Cl (100 μl; 150, 75, 37.5, 18.8, 9.38, 4.69, 2.34, 1.17, or 0 mM) was added to each well, and the cells were incubated for 24 h at 37°C. The cytotoxic effect of NH_4Cl on A549 cells was evaluated as previously described.

Evaluation of the effects of lipid molecules on viral entry

A549 cells (500 µl; 1.5×10^5 cells) were seeded in 24-Well plates and incubated overnight at 37°C. SAPI (250 µl), DSPI (250 µl), SAPC (250 µl), DS (250 µl), or NH_4Cl (250 µl) was added to the cells, and they were incubated for 1 h at 37°C. The cells were then infected with DENV2 (250 µl; MOI of 2) for 3 h at 37°C. The final concentrations of the lipid molecules, DS, and NH_4Cl were 10 µM, 10 µg/ml, and 15 mM, respectively. After the supernatants were removed, the cells were recovered by the addition of 0.25% trypsin–EDTA for 5 min at 37°C and washed twice with D-PBS(−). The intracellular RNA was extracted and purified, and RT-qPCR was performed as previously described.

Analysis of cytokine and chemokine gene expression with RT-qPCR

A549 cells (500 µl; 1.5×10^5 cells) were seeded in 24-Well plates and incubated overnight at 37°C. SAPI (250 µl), DSPI (250 µl), or SAPC (250 µl) was added to the cells, and they were incubated for 1 h at 37°C. The cells were then infected with DENV2 (250 µl; MOI of 0.1) for 6, 24, 48, or 72 h at 37°C. The final lipid molecule concentrations were each 10 µM. At each timepoint, the supernatants were recovered and stored at −80°C until protein quantification. The infected cells were washed with proteinase K in D-PBS(−) (1 µg/ml; 1 ml) for 45 min at 4°C, and the intracellular RNA was extracted and the cDNA synthesized as previously described. RT-qPCR of DENV2 was performed as previously described. The RT-qPCR analysis of cytokine and chemokine gene expression was performed with Fast SYBR Green Master Mix (Thermo Fisher) on the QuantStudio 7 Flex Real-Time PCR System (Thermo Fisher), in accordance with the manufacturer's instructions. The primer sets for C-C motif chemokine ligand (CCL)-5 (HA037446), *CCL20* (HA145215), C-X-C chemokine ligand (CXCL)-1 (HA035284), *CXCL2* (HA262940), *CXCL8* (HA032483), *CXCL10* (HA005084), *CXCL11* (HA249928), interferon β

(*IFN-β*) (HA168826), interleukin (IL) 1α (*IL-1α*) (HA151772), *IL-1β* (HA106116), *IL-6* (HA032507), tumor necrosis factor α (*TNF-α*) (CH000028), tumor necrosis factor superfamily member 10 (*TNFSF10*) (HA038632), and *ACTB* (HA067803) were purchased from Takara Bio, and *ACTB* was used as the internal control.

Determination of cytokine and chemokine concentrations with enzyme-linked immunosorbent assays (ELISAs)

The protein levels of CCL5, CCL20, CXCL8, IFN-β, and IL-6 in the cell supernatants were quantified with Human CCL5/RANTES Quantikine ELISA Kit (R&D Systems), Human CCL20/MIP-3 alpha Quantikine ELISA Kit (R&D Systems), AlphaLISA Human interleukin 8 (IL-8) Biotin-Free Detection Kit (Perkin Elmer), VeriKine Human IFN Beta ELISA Kit (Thermo Fisher), and Human IL-6 Quantikine® ELISA Kit (R&D Systems), respectively. These assays were conducted in accordance with the manufacturers' instructions. The supernatants were prepared as previously described.

Flagellin stimulation assay

A549 cells (500 µl; 1.5×10^5 cells) were seeded in 24-Well plates and incubated overnight at 37°C. SAPI (250 µl), DSPI (250 µl), or SAPC (250 µl) was added, and the cells were incubated for 1 h at 37°C. Flagellin (400 ng/ml; 250 µl) was added, and the cells were incubated for 48 h at 37°C. The final lipid molecule concentrations were each 10 µM. The cell supernatants were recovered and stored at −80°C until use in protein quantification assays. The stimulated cells were washed twice with cold D-PBS(–) (1 ml). Intracellular RNA was extracted, cDNA

was synthesized, and RT-qPCR was performed as previously described. The IL-6 in the supernatants was quantified with the Human IL-6 Quantikine ELISA Kit.

Determination of secreted DENV2 NS1 (sNS1) concentrations with ELISA

The levels of DENV2 sNS1 protein in the supernatants were quantified with the Dengue virus NS1 ELISA kit (Arigo Biolaboratories Corp., Hsinchu, Taiwan), in accordance with the manufacturer's instructions. The supernatants were prepared as previously described.

LPS and IFN-γ co-stimulation assay in macrophage cells differentiated from THP-1 cells stimulated by PMA stimulation and resting cells (PMAr cells)

PMAr cells were prepared as previously described (111). PMA (200 nM; 100 µl) in RPMI 1640 supplemented with 2% FBS and 1% Antibiotic–Antimycotic (100×) and 100 µl of THP-1 cells (1.0×10^5 cells) were added to 96-well microplates and incubated for 72 h at 37°C. After the PMA-containing medium was removed, the cells were washed once with D-PBS(−) (200 µl) and incubated for 5 days in fresh RPMI 1640 medium supplemented with 10% FBS and 1% Antibiotic–Antimycotic (100×) (differentiating to PMAr cells). After the medium was removed, SAPI (100 µl), DSPI (100 µl), or SAPC (100 µl), along with LPS (400 ng/ml; 50 µl) and IFN-γ (80 ng/ml; 50 µl) in RPMI 1640 supplemented with 2% FBS and 1% Antibiotic–Antimycotic (100×) or IFN-γ (40 ng/ml; 100 µl) in RPMI 1640 supplemented with 2% FBS and 1% Antibiotic–Antimycotic (100×), were added, and the cells were incubated for 24 h at 37°C. The final lipid molecule concentrations were each 10 µM. After stimulation, 100 µl of each supernatant was recovered, and the levels of TNF-α protein in them were quantified with the AlphaLISA Human TNF-α Biotin-Free Detection Kit (Perkin Elmer), in accordance with the

manufacturer's instructions. Lastly, resazurin (0.24 mg/ml; 10 µl) in D-PBS(−) was added, and the cells were incubated for 2 h at 37°C. A cytotoxicity assay was performed as previously described.

LPS and soluble CD14 (sCD14) co-stimulation assay of A549 cells

A549 cells (500 µl; 1.5×10^5 cells) were seeded in 24-Well plates and incubated overnight at 37°C. SAPI (250 L), DSPI (250 L), or SAPC (250 L) was added, and the cells were incubated for 1 h at 37°C. LPS (800 ng/ml; 125 µl) and sCD14 (800 ng/ml; 125 µl) were then added, and the cells were incubated for 48 h at 37°C. The final lipid molecule concentrations were each 10 µM. The cells were washed twice with cold D-PBS(–) (1 ml). RT-qPCR was performed using synthesized cDNA from intracellular RNA.

Statistical analysis

All data are shown as means ± standard errors of the means. Comparisons between groups were made with a one-way analysis of variance (ANOVA) followed by a *post hoc* Dunnett's test. The criterion for statistical significance was $p < 0.05$. All statistical analyses were performed with the SAS v9.2 software (SAS Institute, Cary, NC, USA).

Results

Phosphatidylinositol purified from bovine liver (PI-L) has anti-DENV2 activity

Previous studies have reported the antiviral activities of some lipid molecules. For example, 1-palmitoyl-2-oleoly-PG (POPG) inhibits both influenza virus infection and respiratory syncytial virus infection (107, 109, 110), PI purified from soy (PI-S) inhibits respiratory syncytial virus infection (108), and protectin D1 inhibits influenza virus infection (78). Here, a resazurin reduction assay was used to screen 134 lipid molecules, including fatty acid metabolites and phospholipids, and anti-DENV lipid molecules were selected, which inhibited the cytopathic effects elicited in DENV2-infected BHK-21 cells. DENV2 was used for lipid screening because DENV2 has the best growth and induces the cytopathic effect in BHK-21 cells among all DENV serotypes. Of these 134 lipid molecules, 17 showed more than 50% anti-DENV2 activity at a concentration of 10 μM, with no cytotoxic effects (Table 6), so the hit rate was 12.7%. Among these 17 lipid molecules, PI purified from bovine liver (PI-L) had the highest anti-DENV2 activity (94.8%). In contrast, POPG, PI-S, and protectin DX, which is a stereoisomer of protectin D1, showed only weak or negligible anti-DENV2 activity with no cytotoxic effects (Table 7). PI has two fatty acids in its structure (Figure 8A). According to the manufacturer's information, stearic acid (46%) and AA (17%) are the main fatty acid components of PI-L, whereas linoleic acid (50%) and palmitic acid (31%) are the main fatty acid components of PI-S. These data suggest that the differences in the anti-DENV2 activities of PI-L and PI-S are associated with their fatty acid components.

Table 6. Lipid molecules that displayed >50% anti-DENV2 activity with no cytotoxic effects.

No.	Lipid molecule	Anti-DENV2 activity (%)	Cell viability (%)
1	PI-L	94.8	93.0
2	11,12-EET	85.3	89.5
3	8,9-EpETE	83.8	97.1
4	18-HETE	82.1	91.8
5	8-HETrE	79.6	87.9
6	17-HETE	78.7	93.4
7	8-HETE	76.4	92.1
8	LPI (20:4)	74.4	85.0
9	7,8-EpDPE	73.4	96.1
10	14,15-EET	71.1	88.8
11	16-HETE	71.1	88.3
12	5-OxoETE	70.0	91.2
13	19,20-EpDPE	69.1	97.1
14	LPG (16:0)	65.7	84.0
15	5,6-DHET	65.1	91.5
16	11-HETE	63.4	92.0
17	5-HETE	58.4	89.2

EpETE, epoxyeicosatetraenoic acid; LPI (20:4), arachidonoyl lysophosphatidylinositol; EpDPE, epoxydocosapentaenoic acid; OxoETE, oxoeicosatetraenoic acid; LPG (16:0), palmitoyl lysophosphatidylglycerol; and DHET, dihydroxyeicosatrienoic acid.

Table 7. Anti-DENV2 activity and cytotoxicity of POPG, PI-S, and protectin DX.

No.	Lipid molecule	Anti-DENV2 activity (%)	Cell viability (%)
1	POPG	34.7	97.7
2	PI-S	15.5	98.2
3	protectin DX	6.7	100.1

POPG, 1-palmitoyl-2-oleoyl-PG; and PI-S, PI purified from soy.

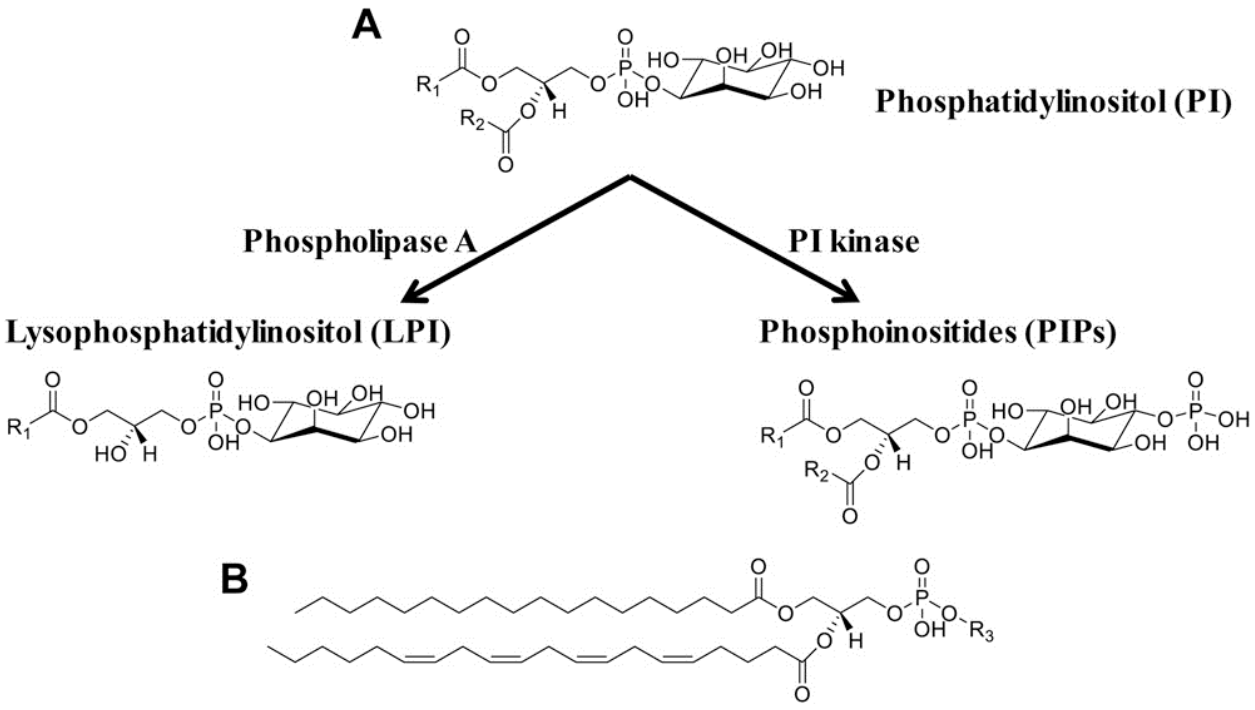

Figure 8. Structures of PI, PI metabolites, and SA-phospholipids. (A–B) Structures of PI and PI metabolites, including lysophosphatidylinositol (LPI) and phosphoinositides (PIPs) (A), and SA-phospholipids (B). R_1, saturated fatty acid or monounsaturated fatty acid; R_2, polyunsaturated fatty acid; and R_3, polar head group. R_3 = H, phosphatidic acid; R_3 = $CH_2CH_2N^+(CH_3)_3$, phosphatidylcholine; R_3 = $CH_2CH_2NH_3^+$, phosphatidylethanolamine; R_3 = $CH_2CHOHCH_2OH$, phosphatidylglycerol; and R_3 = $CH_2CH_2NH_2COOH$, phosphatidylserine.

1-stearoyl-2-arachidonoyl-phosphatidylinositol (SAPI) has anti-DENV2 activity

To identify the specific PI molecular species that have anti-DENV2 activity, the anti-DENV2 activities of five different PI species were investigated with a resazurin reduction assay. Among these, SAPI, which is the most abundant endogenous molecular species of PI, demonstrated the highest anti-DENV2 activity (87.8%) at a concentration of 10 μM, and its 50% effective concentration (EC_{50}) was 4.03 μM (Figure 9A). In contrast, other PI molecular species, such as dipalmitoyl-PI (DPPI) and DSPI, had no anti-DENV2 activity. The anti-DENV2 activities of PI metabolites, including lysophosphatidylinositol (LPI) and SA-phosphoinositides (PIPs) (Figure 8A), were also investigated. Although palmitoyl-LPI [LPI (16:0)] showed weak anti-DENV2 activity (48.3%), no PI metabolites showed anti-DENV2 activity higher than that of SAPI (Figure 9B). The contributions of the polar head groups to the anti-DENV2 activity were investigated with various SA-phospholipids (Figure 8B). SAPA and SAPE showed no anti-DENV2 activity. Although SAPG and SAPS showed weak anti-DENV2 activities, SAPI still demonstrated the highest anti-DENV2 activity (81.4%) (Figure 9C). Interestingly, SAPC exacerbated DENV2 infection. No cytotoxic effects of the PI molecular species, PI metabolites, or SA-phospholipids were observed at concentrations of 10 μM (Figure 9D–9F). These data demonstrate that both the fatty acid components and the phosphoinositol group are important for the anti-DENV2 activity of SAPI.

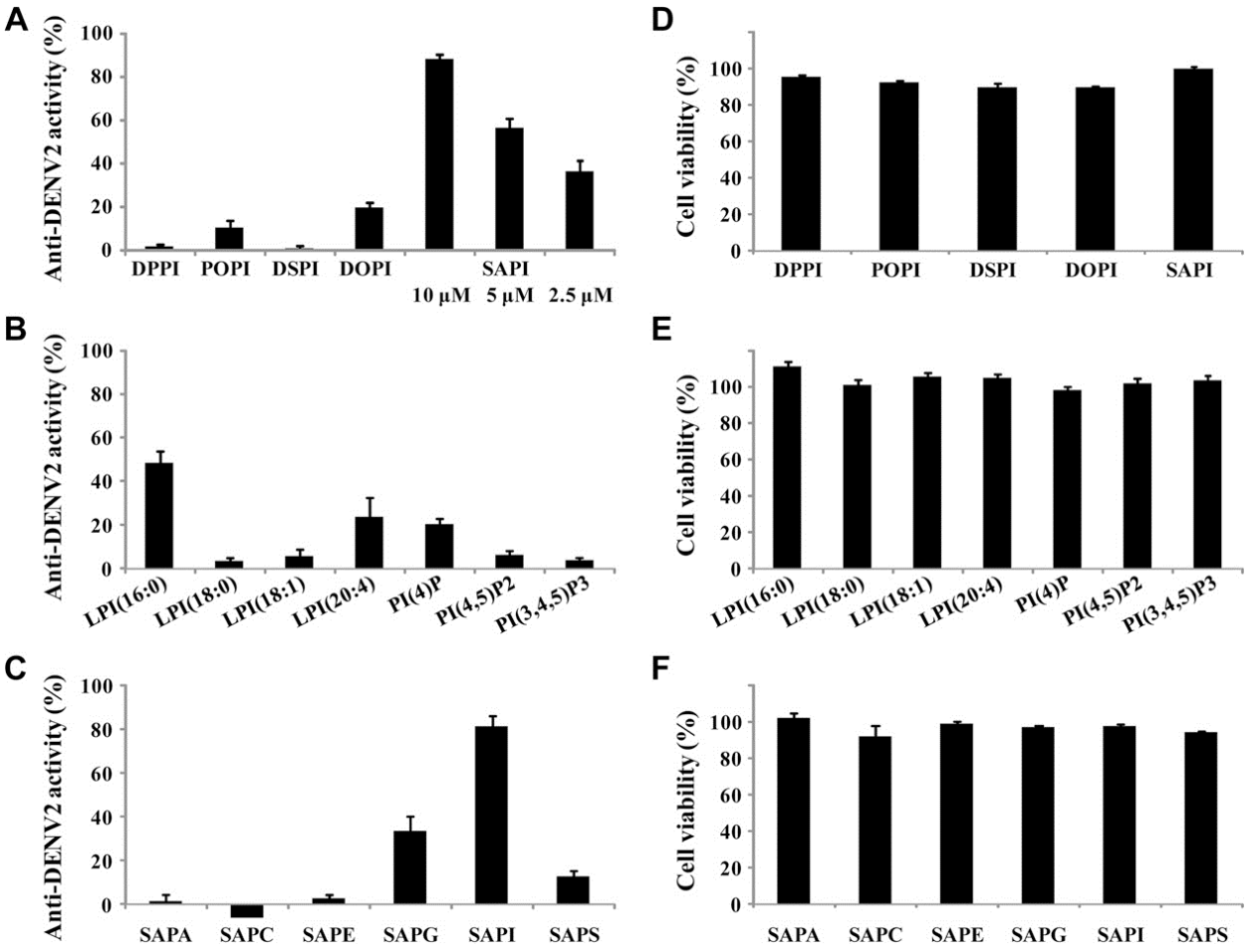

Figure 9. Anti-DENV2 activities of PI molecular species, PI metabolites, and SA-phospholipids in uninfected or DENV2-infected cells. (A–C) The anti-DENV2 activities of PI molecular species (A), PI metabolites (B), and SA-phospholipids (C) were evaluated with a resazurin reduction assay based on cytopathic effects elicited in BHK-21 cells at 96 h after infection with 10 $TCID_{50}$ DENV2. (D–F) The cytotoxic effects of PI molecular species (D), PI metabolites (E), and phospholipids (F) were evaluated with a resazurin reduction assay using uninfected BHK-21 cells. Except for SAPI, the final concentrations of all lipid molecules were each 10 μM. SA-PIPs were used in this experiment. Values are means ± SEM (n = 6). DPPI, dipalmitoyl-PI; POPI, 1-palmitoyl-2-oleoyl-PI; LPI (16:0), palmitoyl-LPI; LPI (18:0), stearoyl-LPI; LPI (18:1), oleoyl-LPI; LPI (20:4), arachidonoyl-LPI; PI(4)P, PI-4-monophosphate; PI(4,5)P2, PI-4,5-diphosphate; PI(3,4,5)P3, PI-3,4,5-triphosphate.

SAPI reduces intracellular DENV RNA in DENV-infected cells

To investigate whether SAPI suppresses DENV replication, intracellular DENV2 RNA was quantified with RT-qPCR. DSPI and SAPC, which showed no anti-DENV2 activity (Figure 9), were used as the negative controls. Compared with the mock-treated group and the DSPI-treated group, the amount of DENV2 RNA was concentration-dependently reduced in all the DENV2-infected cells treated with SAPI, and the amount of DENV2 RNA was reduced more than 10-fold in all the tested cells treated with 10 μM SAPI (Figure 10A–10D). Interestingly, the amount of DENV2 RNA in the SAPC-treated group was 2- to 3-fold higher than that in the mock group. The amounts of intracellular DENV1, DENV3, and DENV4 RNA were also quantified with RT-qPCR, and these amounts were similarly >10-fold lower in A549 cells treated with 10 μM SAPI compared with the mock groups (Figure 10E–10G). These data demonstrate that the anti-DENV activity of SAPI is not specific to certain cell types or viral serotypes.

SAPI is distributed in the supernatants of DENV2-infected and uninfected cells

To investigate its distribution, the SAPI in cellular extracts and supernatants was quantified with LC/ESI–MS/MS (44). The structures of SAPI, DSPI, and SAPC were determined with high-resolution MS and high-resolution MS/MS in negative ion mode (Figure 11). Although SAPI and SAPC were incorporated into both DENV2-infected and uninfected cells in a time-dependent manner compared with the mock groups, the increases in cellular SAPI and SAPC were only approximately 100 ng and 20 ng, respectively (Figure 12A and 12B). In the supernatants of both the DENV2-infected and uninfected cells, approximately 11 μg of SAPI was stably present for 72 h after treatment (Figure 12D). Interestingly, the amount of cellular DSPI in both the DENV2-infected and uninfected cells increased markedly in a time-dependent

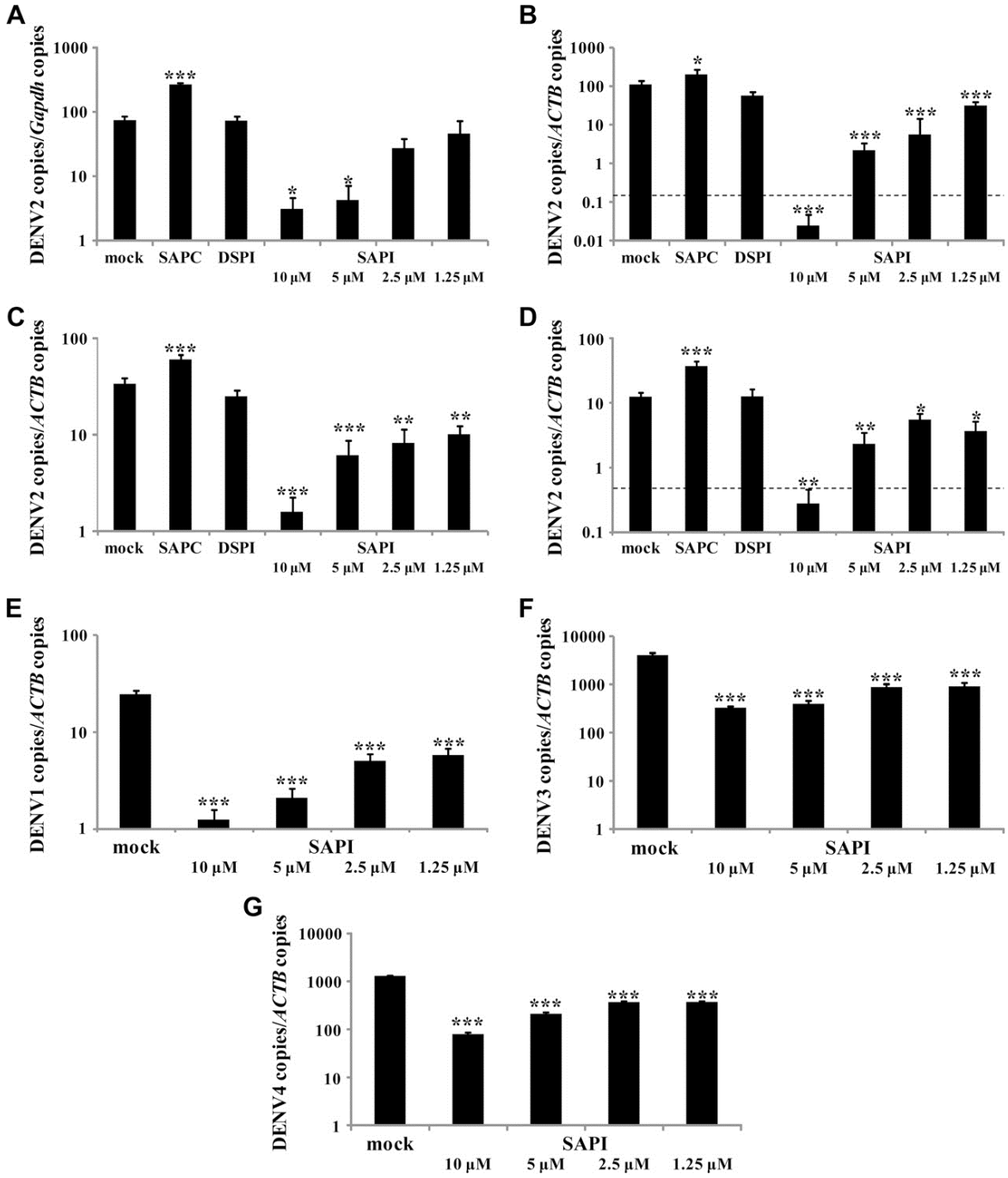

Figure 10. Effect of SAPI on viral replication of all DENV serotypes. (A–D) Amount of DENV2 RNA at 72 h after DENV2 infection at an MOI of 0.01 in BHK-21 cells (A), A549 cells (B), or Huh-7 cells (C) or at an MOI of 0.1 in HepG2 cells (D) was quantified with RT-qPCR. The final concentrations of DSPI and SAPC were each 10 µM. (E–G) Amount of DENV1 RNA (E), DENV3 RNA (F), and DENV4 RNA (G) in A549 cells was quantified with RT-qPCR. Cells were initially infected with DENV1 or DENV3 at an MOI of 0.01 for 72 h or with DENV4 at an MOI of 0.01 for 48 h. *ACTB* and *Gapdh* were used as the internal controls. Values are means ± SEM (n = 4). Data were analyzed in comparison with the mock group using a one-way ANOVA followed by a *post hoc* Dunnett's test. *$p < 0.05$; **$p < 0.01$; ***$p < 0.001$. The dotted line indicates the limit of DENV2 quantification.

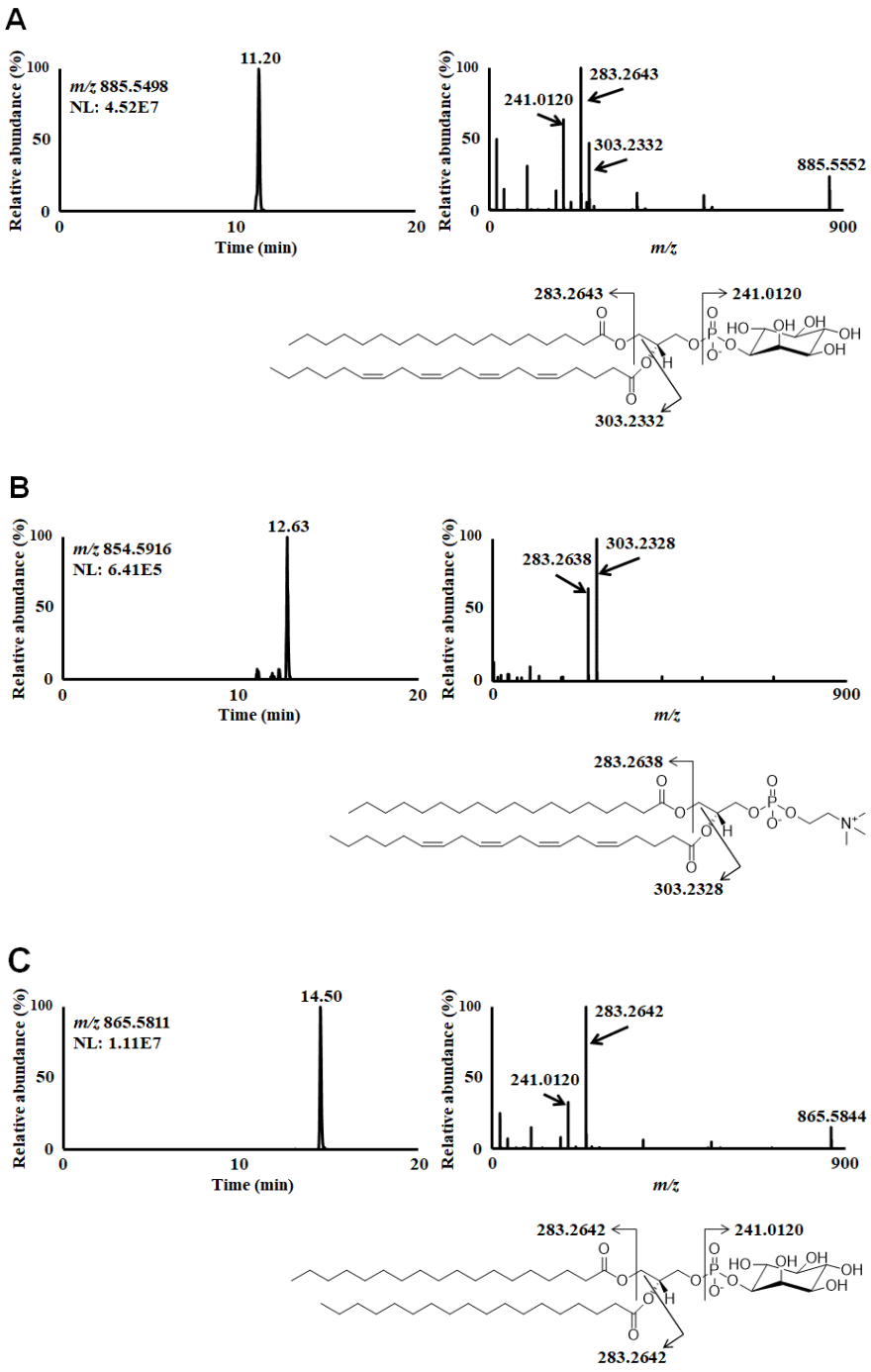

Figure 11. Structural analysis of SAPI, DSPI, and SAPC with high-resolution MS/MS. (A–C) Extracted ion current chromatograms of SAPI (A) and SAPC (B) in the supernatants of DENV2-infected cells and of DSPI (C) in DENV2-infected cells at 3 h after DENV2 infection. High-energy collisional dissociation mass spectra of the molecular ion peaks at 11.20 min (SAPI), 14.50 min (DSPI), and 12.63 min (SAPC) with high-resolution MS/MS.

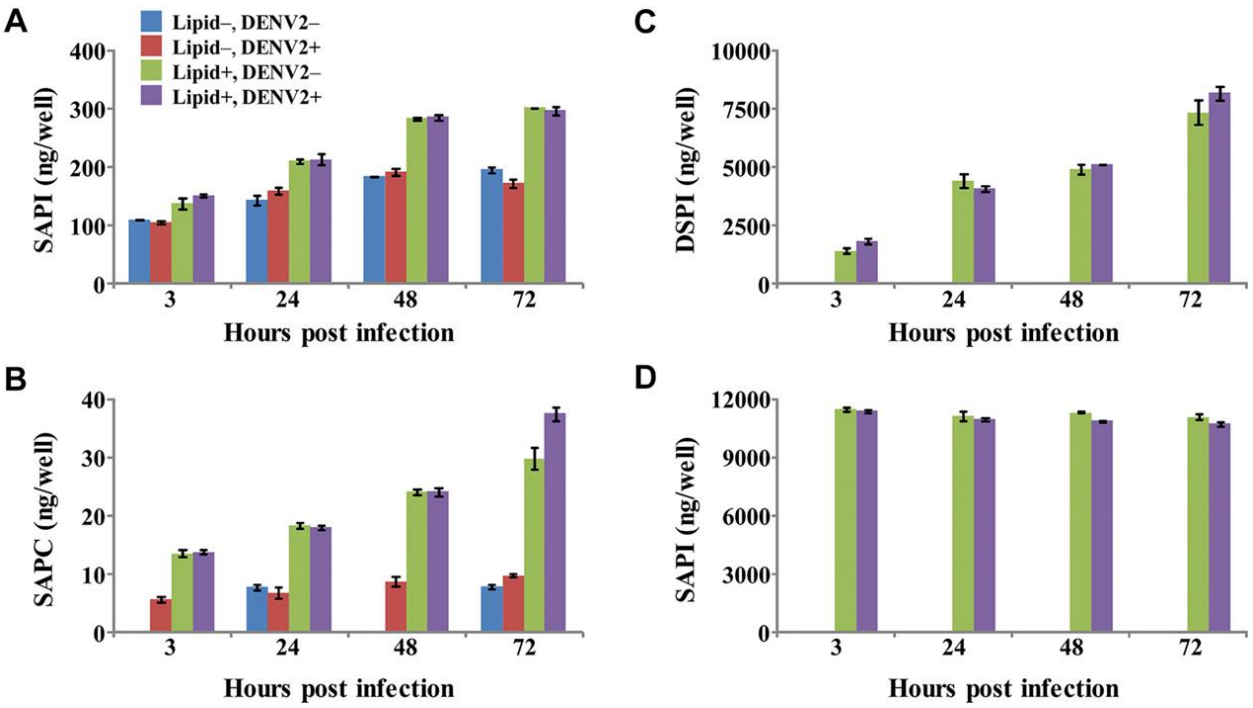

Figure 12. Quantification of lipid molecules in the cellular extracts and in the supernatants of DENV2-infected and uninfected cells. (A–C) Amounts of SAPI (A), SAPC (B), and DSPI (C) in the cellular extracts of A549 cells with or without DENV2 infection at an MOI of 0.1 were quantified with LC/ESI–MS/MS. (D) Amounts of SAPI in the supernatants of A549 cells with or without DENV2 infection at an MOI of 0.1 were quantified with LC/ESI–MS/MS. Values are means ± SEM (n = 3). Lipid– or Lipid+ indicate A549 cells with or without the treatment of lipid molecules, respectively.

manner and was approximately 8 μg at 72 h after DENV2 infection (Figure 12C). There were no differences in the amounts of SAPI, DSPI, or SAPC between the uninfected cells and the DENV2-infected cells. These findings suggest that SAPI exerts its anti-DENV2 activity extracellularly rather than intracellularly.

SAPI does not bind directly to DENV2 particles and does not inhibit the entry of DENV2 into host cells

To investigate the interaction between the lipid molecules and DENV2 particles, the binding affinity of the lipid molecules for DENV2 particles was evaluated with a solid-phase binding assay. The binding affinity of each lipid molecule to the DENV2 particles was dependent on the viral titer, and the strengths of the binding potentials were: DSPI > SAPI = SAPE = SAPS > SAPG > SAPA = SAPC (Figure 13). However, the strengths of the anti-DENV2 activities of the lipid molecules based on the resazurin reduction assay results were: SAPI > SAPG > SAPS > DSPI = SAPA = SAPE > SAPC (Figure 9). These data suggest that there is no correlation between the binding affinity and anti-DENV2 activity of the lipid molecules. To investigate whether the lipid molecules bind directly to the DENV2 particles, the lipid molecules and DENV2 particles were preincubated in culture medium before the virus was allowed to infect the host cells. If the lipid molecules inhibit DENV2 entry into the host cells by binding directly to the DENV2 particles, the complex of lipid molecules and DENV2 particles may be unable to enter the host cells and therefore could be removed in a washing step. Consequently, the amount of intracellular DENV2 particles would be reduced. In this assay, low-molecular-weight DS, which binds to the DENV surface glycoprotein (112), was used as the positive control for adsorption to DENV2 particles. DS displayed anti-DENV2 activity in a concentration-dependent

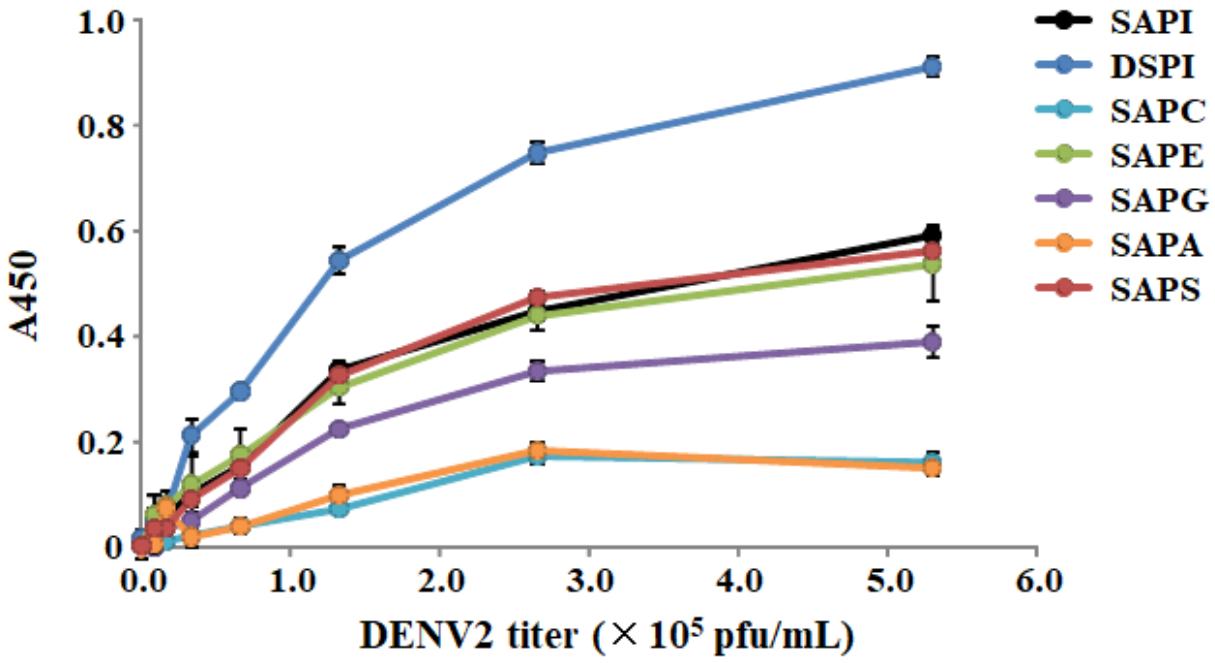

Figure 13. Binding affinities of lipid molecules for various titers of DENV2 particles.

Binding affinities of lipid molecules to various titers of DENV2 particles were evaluated with a solid-phase binding assay. The final lipid molecule concentrations were each 500 pmol. Values are means ± SEM (n = 4).

manner with no cytotoxic effect (Figure 14A and 14B). The results of this assay indicate that the amount of intracellular DENV2 RNA after the DENV2 particles were preincubated with DS was lower than that of the mock and no-preincubation (DS pre^{-}) groups (final concentration of DS: 0.089 μg/ml) (Figure 15A). The amounts of intracellular DENV2 RNA in the SAPI-, DSPI-, and SAPC-treated groups were similar to those in the mock groups. These results suggest that the lipid molecules do not bind directly to DENV2 particles.

The effect of SAPI on the entry of DENV2 into host cells was also investigated. In this assay, NH_4Cl, which inhibits endosomal acidification and viral internalization (113–115), and a high concentration of DS were used as the positive controls for viral entry inhibition. Compared with the mock group, the amount of intracellular DENV2 RNA in the NH_4Cl-treated group was dramatically lower, with no cytotoxicity (Figure 14C), and that in the group treated with a high concentration of DS was significantly lower (Figure 15B). In contrast, the amounts of intracellular DENV2 RNA in the SAPI-, DSPI- and SAPC-treated groups were similar to those in the mock groups. These results demonstrate that SAPI does not inhibit the entry of DENV2 into host cells.

SAPI suppresses the inflammatory response induced by DENV2 infection

PI has anti-inflammatory activity because it antagonizes the stimulation of Toll-like receptors (TLRs), such as TLR2 and TLR4 (116–118). To investigate whether SAPI suppresses the inflammatory response induced by DENV2 infection, the expression of cytokine and chemokine genes and proteins in DENV2-infected cells was analyzed with RT-qPCR and ELISAs, respectively. Initially, PrimerArray, which is a convenient tool for the analysis of gene expression in specific pathways, was used to analyze uninfected and DENV2-infected cells. The PrimerArray results show that the expression levels of 10 genes (*CCL5*, *TNFSF10*, *CCL20*,

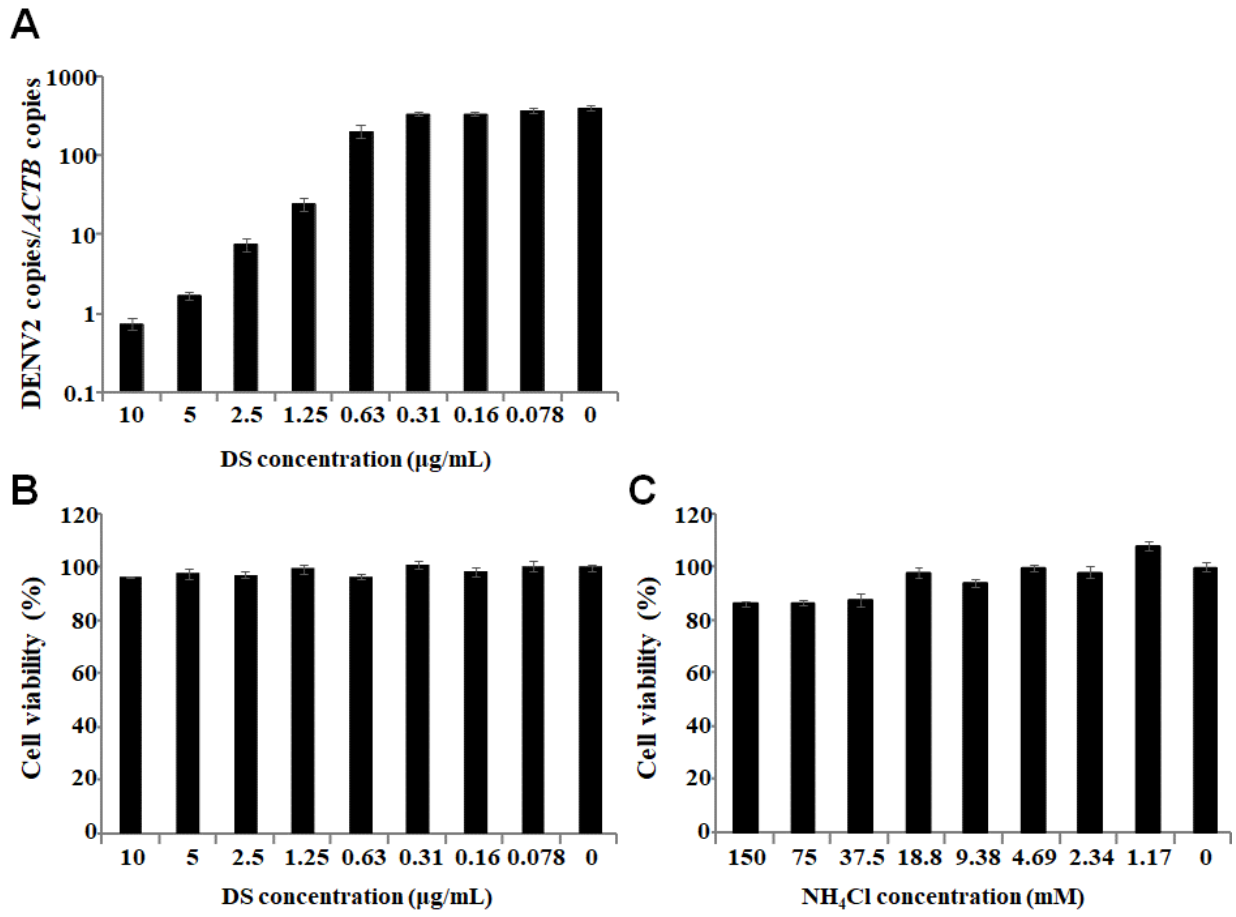

Figure 14. Anti-DENV2 activity of DS in uninfected or DENV2-infected cells and cytotoxicity evaluation of DS and NH_4Cl. (A) The amount of DENV2 RNA in A549 cells at 48 h after infection with DENV2 at an MOI of 0.1 was quantified with RT-qPCR. ACTB was used as the internal control for normalization. (B–C) Cytotoxic effects of DS (B) and NH_4Cl (C) were evaluated with a resazurin reduction assay. Values are means ± SEM (n = 4).

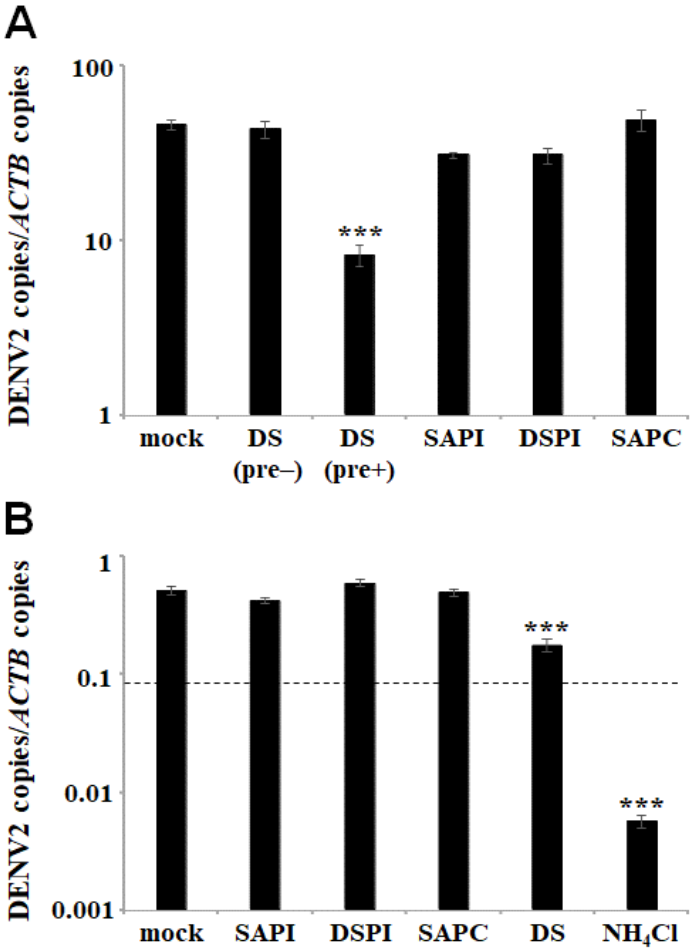

Figure 15. Effect of SAPI on the entry of DENV2 into host cells. (A) Lipid molecules (10 µM) or DS (10 µg/ml) were preincubated with DENV2 particles for 1 h at 37°C before they were used to infect A549 cells. After the preincubated DENV2 was diluted, DENV2 at an MOI of 0.1, together with lipid molecules (final concentration: 0.089 µM) or DS (final concentration: 0.089 µg/ml), was incubated for 1 h at 4°C to allow viral attachment to the cell surfaces, then incubated for 1 h at 37°C to allow entry into the cells. After the supernatants were removed and the cells washed, fresh medium was added to the cells, which were subsequently incubated for 47 h at 37°C. Intracellular DENV2 RNA was quantified with RT-qPCR. DS (pre−) indicates that A549 cells were simultaneously inoculated with DS (0.089 µg/ml) and DENV2 without preincubation. (B) Lipid molecules (10 µM), DS (10 µg/ml), or NH_4Cl (15 mM) were added to A549 cells for 1 h at 37°C before DENV2 infection. The cells were inoculated with DENV2 at an MOI of 2 for 3 h at 37°C. After the supernatants were removed and the cells washed, intracellular DENV2 RNA was quantified with RT-qPCR. *ACTB* was used as the internal control for normalization. Values are means ± SEM (n = 4). Data were analyzed in comparison with the mock group using a one-way ANOVA followed by a *post hoc* Dunnett's test. ***$p < 0.0001$. The dotted line indicates the limit of DENV2 quantification.

IL-1α, *IL-6*, *TSLP*, *CX3CL1*, *CXCL10*, *CXCL2*, and *CXCL8*) at 72 h after DENV2 infection at an MOI of 0.01 were each more than 2-fold higher compared with the corresponding levels in uninfected cells (Table 8). Based on this result, the anti-inflammatory effects of SAPI on DENV2 infection were then investigated.

Intracellular DENV2 RNA increased in a time-dependent manner and reached a plateau at 48 h after DENV2 infection at an MOI of 0.1 in the mock, DSPI-treated, and SAPC-treated groups (Figure 16A). Although the intracellular DENV2 RNA increased in a time-dependent manner in the SAPI-treated group, 20-fold, 30-fold, and 2-fold reductions in the intracellular DENV2 RNA were observed at 24, 48, and 72 h, respectively, after DENV2 infection compared with the mock group (Figure 16A). At 48 h after DENV2 infection, the expression levels of cytokine and chemokine genes *CCL5*, *CCL20*, *CXCL1*, *CXCL2*, *CXCL8*, *CXCL10*, *CXCL11*, *IFN-β*, *IL-1α*, *IL-6*, *TNF-α*, and *TNFSF10* were increased in the mock with DENV2 infection ($DENV2^+$), DSPI-treated, and SAPC-treated groups compared with the mock without DENV2 infection ($DENV2^-$) group. However, these increases in gene expression following DENV2 infection were significantly suppressed in the SAPI-treated group (Figure 16B). Furthermore, the increased expression of all 13 examined genes, including *IL-1β*, was also significantly suppressed by SAPI treatment at 72 h after DENV2 infection (Figure 16C). Next, the levels of some cytokine and chemokine proteins were examined. Compared with the mock ($DENV2^-$) group, the levels of CCL5, CCL20, CXCL8, IFN-β, and IL-6 were increased at 72 h after DENV2 infection in the mock ($DENV2^+$), DSPI-treated, and SAPC-treated groups, but these DENV2-induced increases in protein levels were significantly suppressed in the SAPI-treated group (Figure 16D). Interestingly, SAPI did not suppress the inflammatory response induced by stimulation with flagellin, a TLR5 agonist (Figure 17). These data demonstrate that SAPI

Table 8. The 10 genes detected by PrimerArray as having a >2-fold increase in expression following DENV2 infection.

No.	Gene symbol	Fold difference (n = 4)	
		mean	SEM
1	*CCL5*	118.44	17.327
2	*TNFSF10*	12.07	1.776
3	*CCL20*	8.86	4.288
4	*IL1α*	4.84	0.390
5	*IL-6*	4.24	0.666
6	*TSLP*	3.86	0.741
7	*CX3CL1*	3.28	0.685
8	*CXCL10*	3.04	0.595
9	*CXCL2*	2.41	0.257
10	*CXCL8*	2.24	0.186

CCL, C-C motif chemokine ligand; TSLP, thymic stromal lymphopoietin; CX3CL1, C-X-X-X-C chemokine ligand 1; CXCL, C-X-C chemokine ligand.

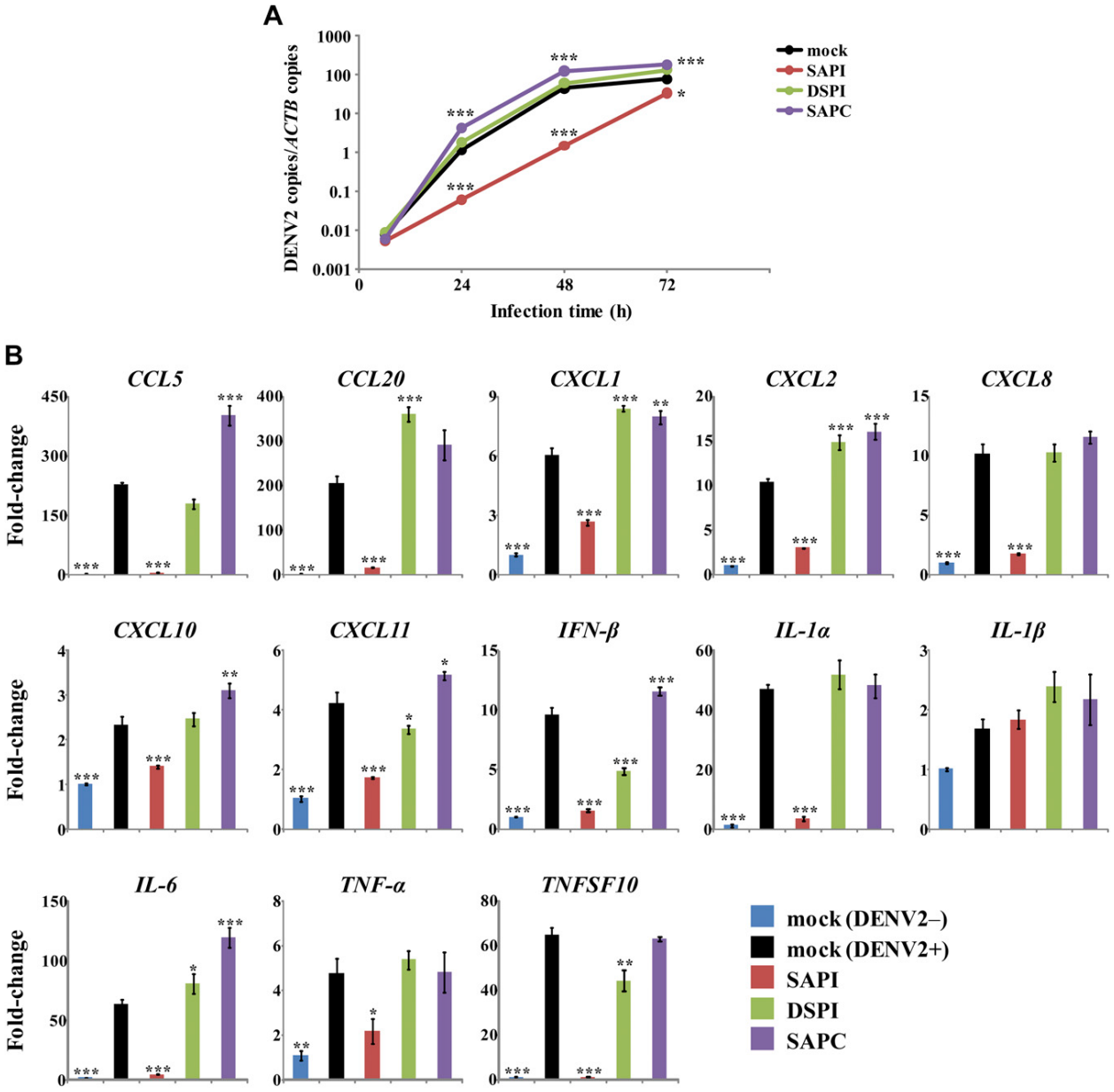

Figure 16. Effect of SAPI on the DENV2 infection-induced production of cytokines and chemokines. (A) Amount of DENV2 RNA in A549 cells after DENV2 infection at an MOI of 0.1 was quantified with RT-qPCR. Lipid molecules were added to cells 1 h before DENV2 infection. The final concentrations of SAPI, DSPI, and SAPC were each 10 μM. *ACTB* was used as the internal control. Values are means ± SEM (n = 4). Data were analyzed in comparison with the mock group using a one-way ANOVA followed by a *post hoc* Dunnett's test. *$p < 0.05$; **$p < 0.01$; ***$p < 0.001$. (B–C) The expressions of cytokine and chemokine genes at 48 h after DENV2 infection (B) and at 72 h after DENV2 infection (C) were analyzed with RT-qPCR. The final concentrations of SAPI, DSPI, and SAPC were each 10 μM. *ACTB* was used as the internal control. Fold changes were calculated with the ΔΔCt method relative to the mock ($DENV2^+$) group. Values are means ± SEM (n = 4). Data were analyzed in comparison with the mock ($DENV2^+$) group using a one-way ANOVA followed by a *post hoc* Dunnett's test. *$p < 0.05$; **$p < 0.01$; ***$p < 0.001$. (D) Amounts of CCL5, CCL20, CXCL8, IFN-β, and IL-6 in the supernatant at 72 h after DENV2 infection were quantified with ELISAs. The final concentrations of SAPI, DSPI, and SAPC were each 10 μM. Values are means ± SEM (n = 4). Data were analyzed in comparison with the mock ($DENV2^+$) group using a one-way ANOVA followed by a *post hoc* Dunnett's test. **$p < 0.01$; ***$p < 0.001$.

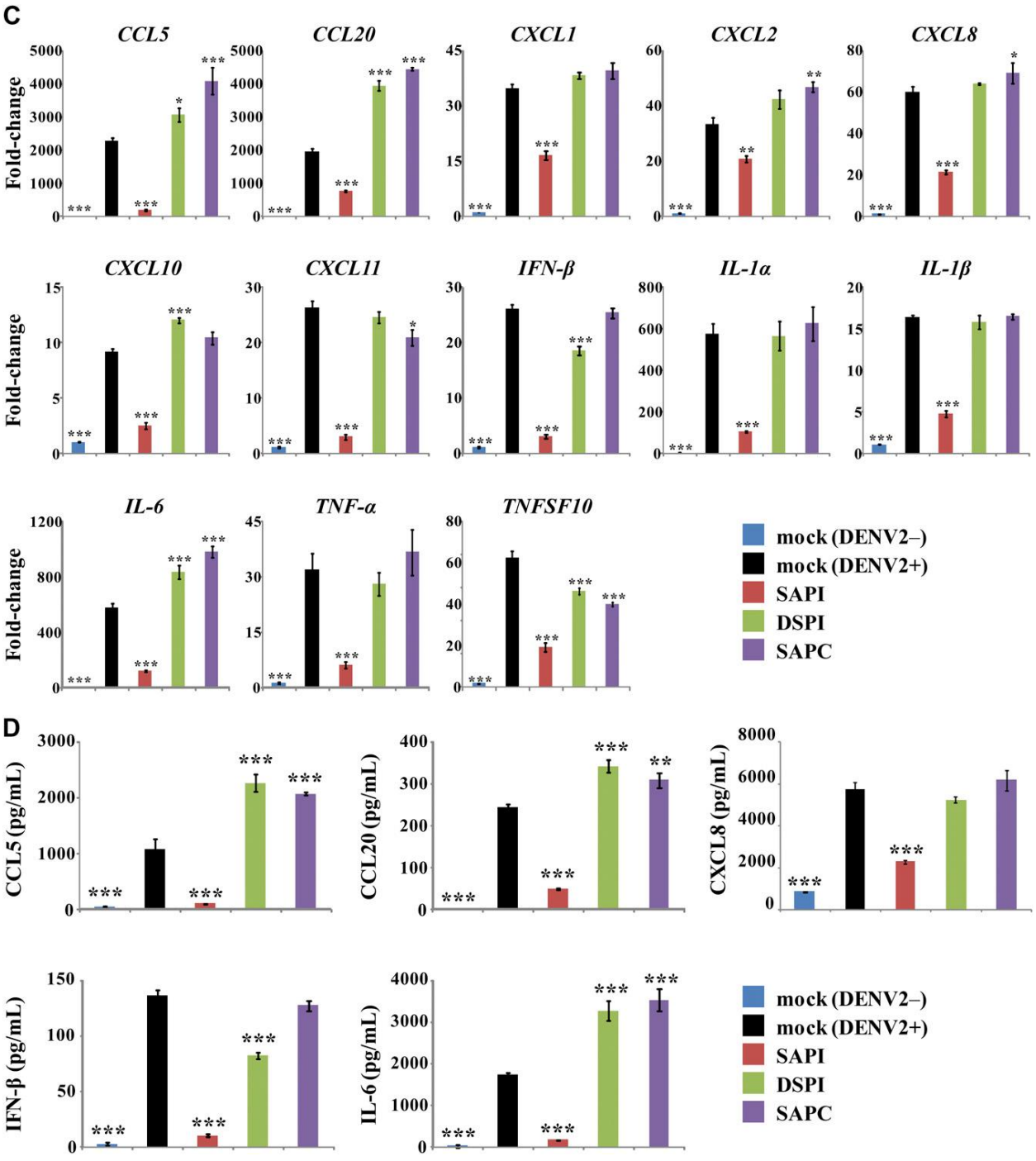

Figure 16. (continued)

specifically suppresses the inflammatory responses induced by DENV2 infection.

DENV2 sNS1 in the supernatant of DENV2-infected cells is reduced by SAPI

DENV sNS1, which forms a hexamer in the supernatants of DENV-infected cells or the circulating blood of DENV patients, induces inflammatory cytokine production and endothelial cell monolayer leakage *via* the activation of TLR4, which together contribute to the development of severe dengue (119–123). To investigate the involvement of sNS1 in the inflammatory response induced by DENV infection, the amount of DENV2 sNS1 in the supernatants of infected and treated cells was quantified with ELISAs. The amount of DENV2 sNS1 was markedly increased at 48 h after DENV2 infection in the mock, DSPI-treated, and SAPC-treated groups, but no increase in DENV2 sNS1 was observed in the SAPI-treated group (Figure 18). Although the level of intracellular DENV2 RNA was dramatically increased 24 h after DENV2 infection in the mock ($DENV2^{+}$), DSPI-treated, and SAPC-treated groups compared with the SAPI-treated group (Figure 16A), no marked increase in the expression of cytokine or chemokine genes was observed at that timepoint (Figure 19). However, at 48 h (Figure 16B) and 72 h (Figure 16C) after DENV2 infection, the expression of cytokine and chemokine genes was dramatically higher in the mock ($DENV2^{+}$), DSPI-treated, and SAPC-treated groups than in the mock ($DENV2^{-}$) group. In contrast, this increased expression was significantly suppressed in the SAPI-treated group. These data suggest that DENV2 sNS1 plays an important role in the initiation of the inflammatory response.

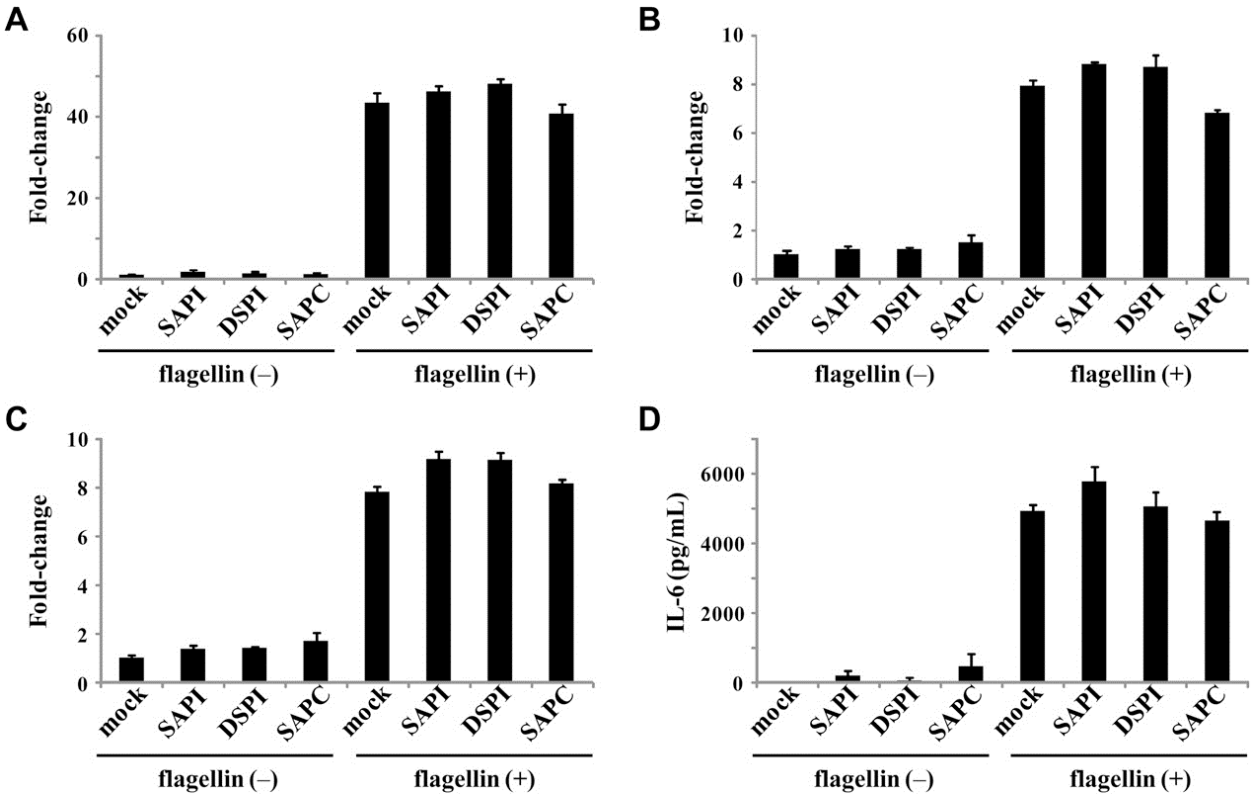

Figure 17. Effect of SAPI on the flagellin stimulation-induced expression of cytokines and chemokines. (A–C) The expression of genes *CCL5* (A), *CXCL8* (B), and *IL-6* (C) in A549 cells at 48 h after flagellin (100 ng/ml) stimulation was analyzed with RT-qPCR. (D) The amount of IL-6 in the supernatant at 48 h after flagellin stimulation was quantified with ELISA. The final concentrations of SAPI, DSPI, and SAPC were each 10 μM. *ACTB* was used as the internal control. Fold changes were calculated with the ΔΔCt method relative to the mock (flagellin^{-}) group. Values are means ± SEM (n = 4).

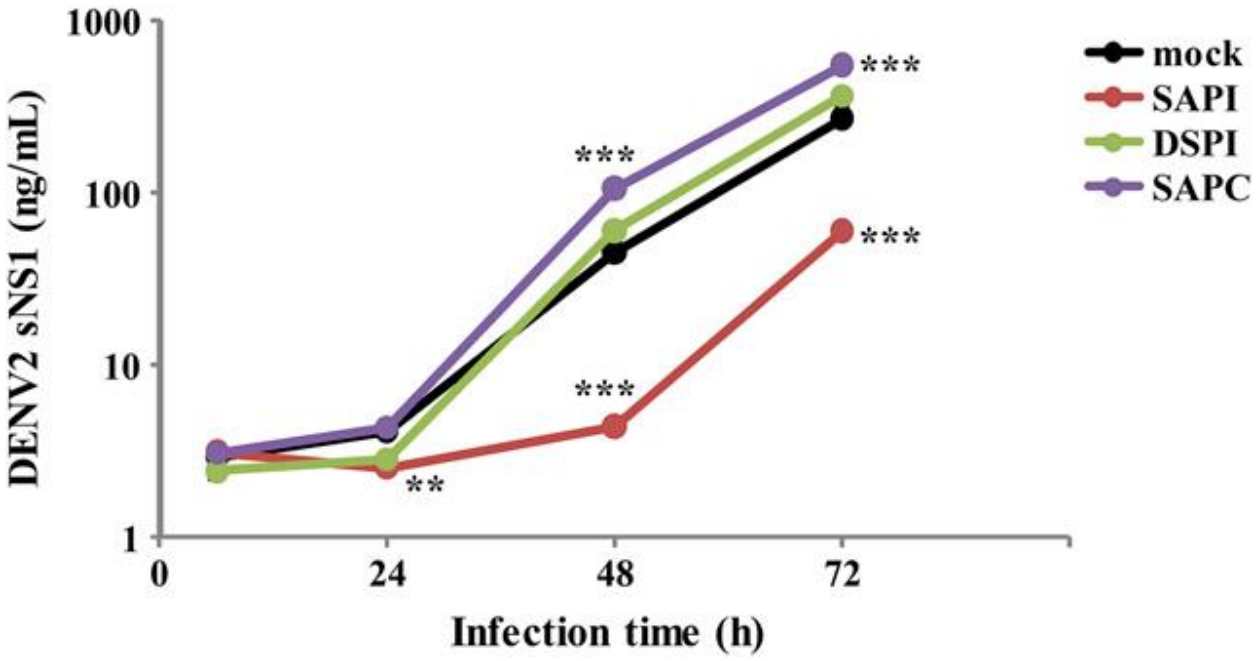

Figure 18. Effect of SAPI on the DENV2 infection-induced production of DENV2 sNS1. The amount of sNS1 in the supernatant after DENV2 infection at an MOI of 0.1 was quantified with ELISA. Final concentrations of SAPI, DSPI, and SAPC were each 10 μM. Values are means ± SEM (n = 4). Data were analyzed in comparison with the mock group using a one-way ANOVA followed by a *post hoc* Dunnett's test. $^{**}p < 0.01$; $^{***}p < 0.001$.

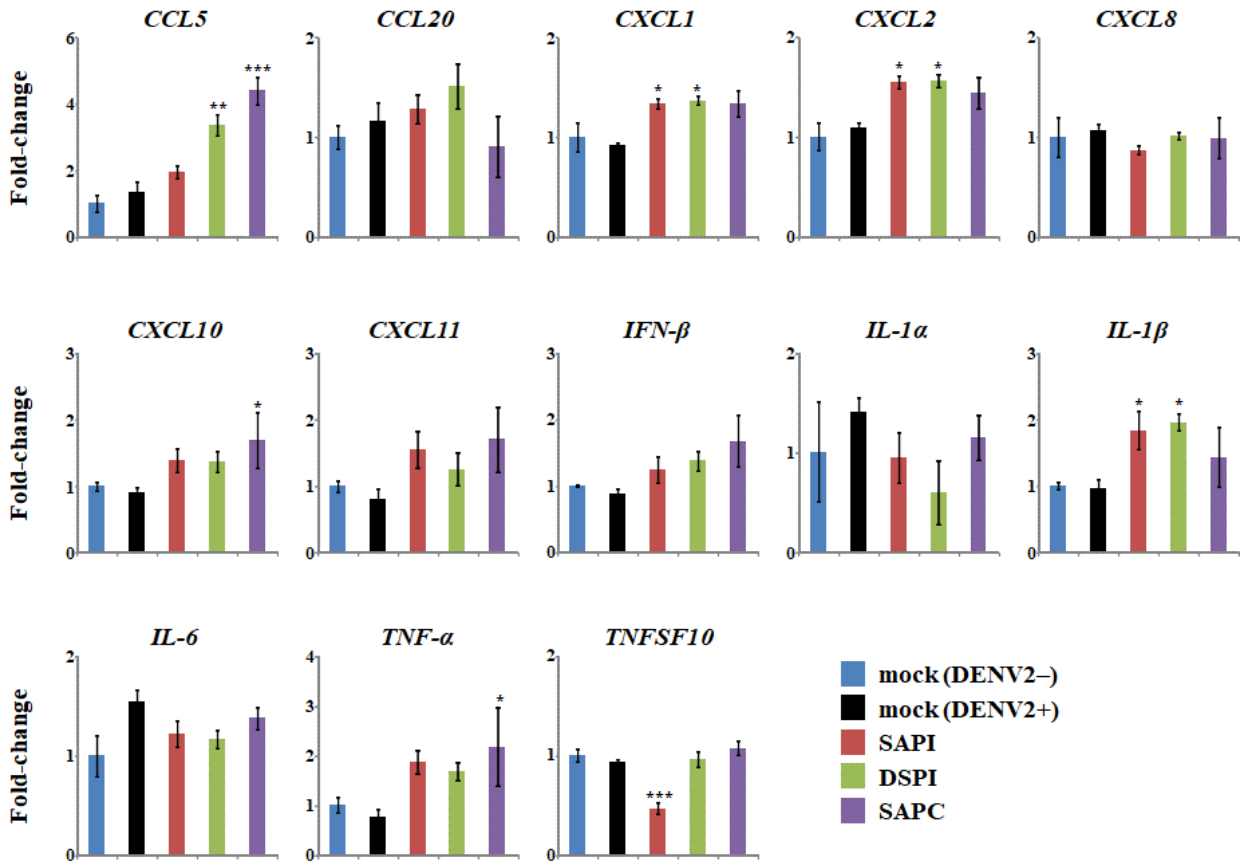

Figure 19. RT-qPCR analysis of cytokine and chemokine expression at 24 h after DENV2 infection. The expressions of cytokine and chemokine genes in A549 cells at 24 h after DENV2 infection were analyzed with RT-qPCR. The final concentrations of SAPI, DSPI, and SAPC were each 10 μM. *ACTB* was used as the internal control. Fold changes were calculated with the ΔΔCt method relative to the mock ($DENV2^+$) group. Values are means ± SEM (n = 4). Data were analyzed in comparison with the mock ($DENV2^+$) group using a one-way ANOVA followed by a *post hoc* Dunnett's test. *$p < 0.05$; **$p < 0.01$; ***$p < 0.001$.

SAPI suppresses inflammatory responses via TLR4 activation

To investigate whether SAPI suppresses inflammatory responses *via* the activation of TLR4, macrophage cells derived from THP-1 cells were stimulated with LPS. The THP-1 cells were treated with PMA for 3 days, rested for 5 days in medium without PMA, and then differentiated to macrophages (PMAr cells) (111). The PMAr cells were differentiated to M1-like macrophages by co-stimulation with LPS and IFN-γ for 24 h, and the TNF-α in the supernatant was then quantified as a proinflammatory marker with an ELISA. There were no significant differences among the amounts of TNF-α in the unstimulated groups (LPS^{-}, IFN-γ^{-}) and the IFN-γ-stimulated groups (LPS^{-}, IFN-γ^{+}) with or without lipid molecules (Figure 20A). The amount of TNF-α was markedly higher in the LPS- and IFN-γ-co-stimulated group (LPS^{+}, IFN-γ^{+}) than in the unstimulated group (LPS^{-}, IFN-γ^{-}) without lipid molecules, and SAPI treatment significantly suppressed this increase in TNF-α. In contrast, neither DSPI nor SAPC treatment suppressed the production of TNF-α. No cytotoxic effect was observed in this assay (Figure 20B).

In addition, A549 cells were co-stimulated with LPS and soluble CD14 (sCD14). The expression of the *CCL5* gene increased 3-fold after co-stimulation with LPS and sCD14 compared with that in the unstimulated group, and SAPI treatment significantly inhibited this increase in *CCL5* expression (Figure 21). However, neither DSPI nor SAPC suppressed this increase in the expression of *CCL5*. These data demonstrate that SAPI specifically suppresses the inflammatory responses *via* the activation of TLR4.

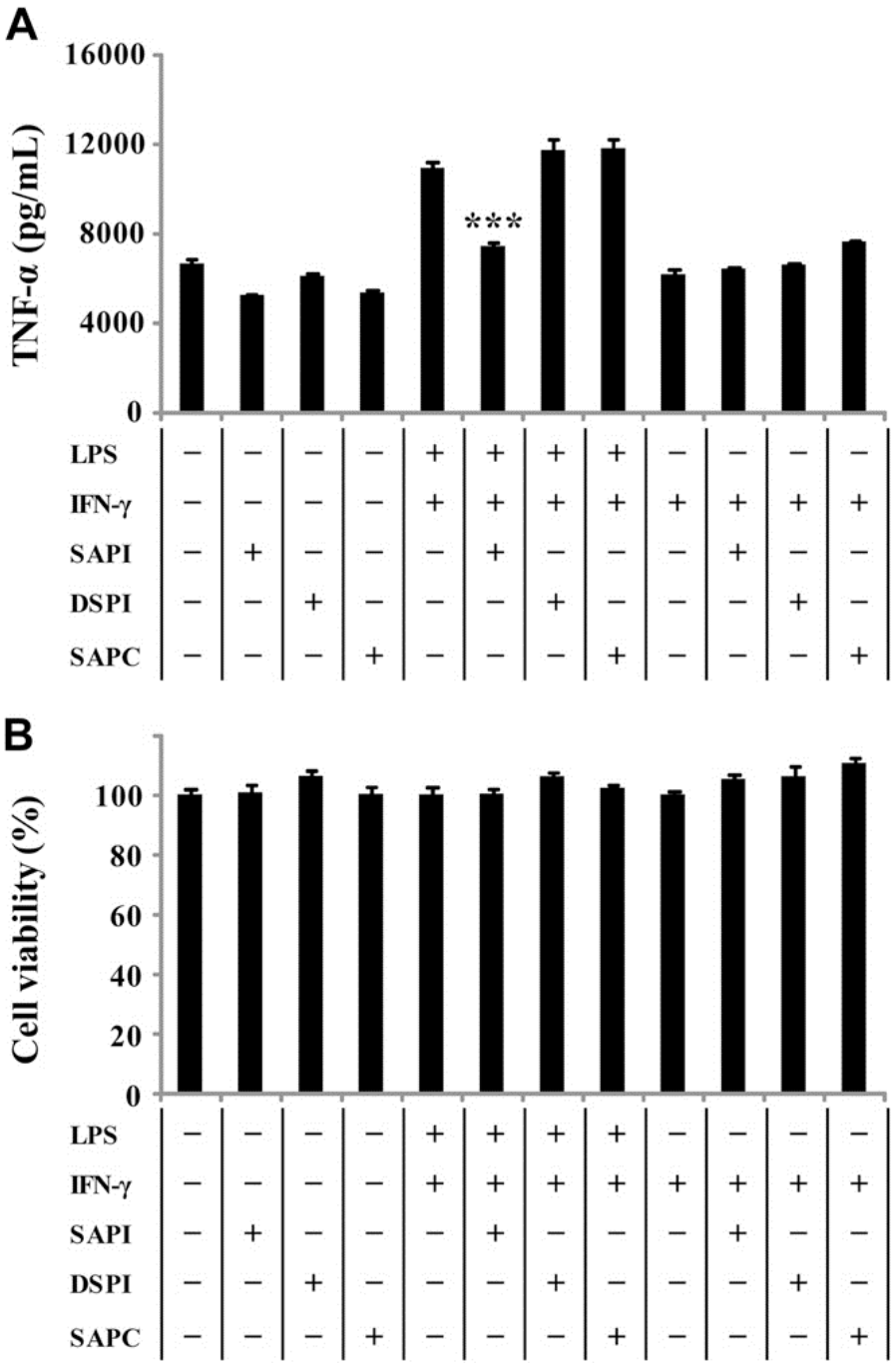

Figure 20. Effect of SAPI on the LPS and IFN-γ co-stimulation-induced production of TNF-α in PMAr cells. (A) The amount of TNF-α in the supernatant of PMAr cells at 24 h after their co-stimulation with LPS (100 ng/ml) and IFN-γ (20 ng/ml) was quantified with ELISA. (B) Cytotoxic effects were evaluated with a resazurin reduction assay. The final concentrations of SAPI, DSPI, and SAPC were each 10 μM. Values are means ± SEM (n = 4). Data were analyzed in comparison with the LPS- and IFN-γ-co-stimulated group (LPS^+, $IFN\text{-}\gamma^+$) using a one-way ANOVA followed by a *post hoc* Dunnett's test. ***$p < 0.001$.

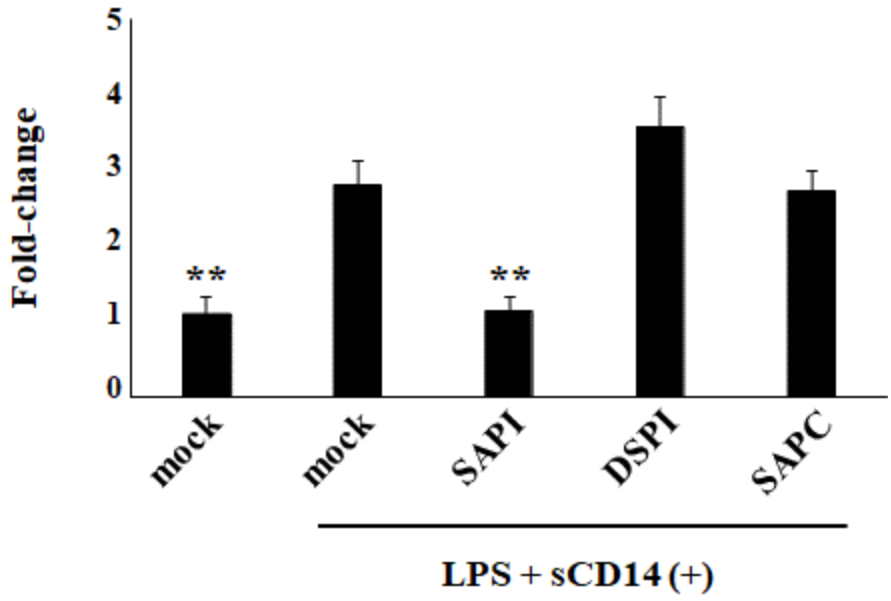

Figure 21. Effect of SAPI on the LPS and sCD14 co-stimulation-induced expression of *CCL5*. The expression of *CCL5* gene in A549 cells at 48 h after co-stimulation with LPS (100 ng/ml) and sCD14 (100 ng/ml) was analyzed with RT-qPCR. The final concentrations of SAPI, DSPI, and SAPC were each 10 μM. *ACTB* was used as the internal control. Fold changes were calculated with the ΔΔCt method relative to the mock (LPS^+, $sCD14^-$) group. Values are means ± SEM (n = 4). Data were analyzed in comparison with the mock (LPS^+, $sCD14^+$) group using a one-way ANOVA followed by a *post hoc* Dunnett's test. $^{**}p < 0.01$.

Discussion

DF is an acute self-limiting febrile infectious disease. Most patients recover completely without manifestations of severe clinical disorders, but a small proportion progress to severe dengue, characterized by plasma leakage with or without hemorrhage (92). Therefore, the host protective mechanisms and the existence of endogenous defensive factors against DENV infection are important. However, these protective mechanisms are poorly understood, and a better understanding of the host defensive machinery is important for the development of therapeutic strategies against DENV infection.

Here, the novel biological functions of SAPI *in vitro* were identified. SAPI inhibits the cytopathic effects induced by DENV2 infection as well as the replication of all DENV serotypes, without inhibiting viral entry into the host cells. Notably, anti-DENV2 activity was displayed by SAPI but not by any other PI molecular species or PI metabolites, including LPI and SA-PIPs. Furthermore, SA-phospholipids showed no anti-DENV2 activity. These data demonstrate that both the fatty acid components and the phosphoinositol group of SAPI are important for its anti-DENV2 activity. SAPI is the most abundant endogenous molecular species of PI, and the concentration of SAPI in human plasma is about 4.3–11.0 μM (1, 124). In preliminary studies, the concentrations of SAPI in pooled human plasma and pooled human sera were 21.3 μM and 23.3 μM, respectively. Because the anti-DENV2 activity of SAPI *in vitro* was 4.03 μM, the amount of SAPI in human blood should be adequate to display antiviral activity. These findings suggest that SAPI degradation or an abnormality in SAPI biosynthesis could exacerbate dengue infection. The activity of serum secretory phospholipase A2 (sPLA2) is significantly increased in

patients with dengue hemorrhagic fever within the first 120 h following onset, and sPLA2 activity is also associated with disease severity markers, including the level of PAF and the degree of viremia (125). PAF is a proinflammatory lipid mediator as well as an important mediator of vascular leakage in acute DF (126). Because proinflammatory lipid mediators, including PAF and AA metabolites, are generated by the activity of sPLA2 (127), and SAPI is a major source of AA, sPLA2 activity may accelerate not only the production of PAF but also the degradation of SAPI, triggering severe dengue. Mammalian membrane-bound O-acyltransferase 7 (MBOAT7) is a specific phospholipid acyltransferase that incorporates AA into the *sn*-2 position of PI (128, 129). The *MBOAT7* variant rs641738 is a risk factor for disease severity in nonalcoholic fatty liver disease (NAFLD) in humans *via* the alteration of hepatic PI acyl-chain remodeling (130, 131). NAFLD is also associated with the severity of DF, insofar as it is associated with hemoconcentration, thrombocytopenia, and longer hospital stay in dengue-infected patients with plasma leakage (132). These findings suggest that the perturbation of PI remodeling caused by sPLA2 activity and *MBOAT7* variants is associated with the severity of DF. Because the association between PI remodeling and dengue infection is poorly understood, further studies are required to determine whether SAPI suppresses severe dengue.

SAPI also suppresses the production of DENV2 sNS1 along with the inflammatory response induced by DENV2 infection. PI has anti-inflammatory activity against TLR activation (116–118). In contrast, DENV sNS1 accelerates the inflammatory response and DENV replication by activating TLR4, which disrupts the integrity of the endothelial cell monolayer (119–123). To investigate whether SAPI inhibits TLR4 activation, PMAr cells, which are macrophage cells derived from THP-1 cells, were stimulated with LPS. Macrophage cells are one of the major cell types infected by DENV *in vivo*, and DENV infection of PMAr cells has been previously

reported (133). Interestingly, SAPI suppressed the increase in TNF-α levels in the supernatants of PMAr cells co-stimulated with LPS and IFN-γ. In addition, I investigated whether A549 cells, which are known to produce inflammatory responses in response to DENV2 infection, respond to LPS stimulation. Because A549 cells do not express cell surface CD14 (134), and it is therefore difficult to stimulate A549 cells with LPS only, A549 cells were co-stimulated with LPS and sCD14. SAPI inhibited the expression of the *CCL5* gene induced by co-stimulation with LPS and sCD14. These data demonstrate that SAPI suppresses the inflammatory response *via* TLR4 stimulation. Additionally, TNF-α has been shown to induce endothelial dysfunction, which contributes to the development of severe dengue (135), and *Rhodobacter sphaeroides* LPS, which is an antagonist of TLR4 activation, protects endothelial function *in vitro* and *in vivo* (120). Together, these findings suggest that SAPI is a protective factor for endothelial function *in vivo*. Further studies are required to clarify the involvement SAPI in the protection of endothelial function *in vitro* and *in vivo*.

Previous studies have reported relationships between viral infection and lipid molecules. For example, protectin D1, which is a SPM derived from DHA, suppresses influenza virus infection by inhibiting the nuclear export of viral RNA (78). POPG suppresses influenza virus infection and respiratory syncytial virus infection by inhibiting viral entry into cells (107, 109, 110). PI-S also suppresses respiratory syncytial virus infection by inhibiting viral entry into cells (108). Additionally, SAPS suppresses the inflammatory responses induced by human rhinovirus (136) by disrupting the membrane microdomains (137), and GM3 ganglioside is an essential factor for DENV genome replication (138). Furthermore, sphingomyelin exacerbates West Nile virus infection by accelerating viral replication and viral particle biogenesis (139), and lysophosphatidylcholine is an important structural component of the West Nile virus replication

complex (140). In addition to SAPI, lipid screening identified several epoxides derived from AA, EPA, and DHA as having anti-DENV2 activity. Free epoxides are quickly incorporated into cell-membrane phospholipids (141, 142), and the remodeling of the membrane microdomain structure and corresponding changes in the phospholipid composition have been associated with effects on signaling (143). Therefore, the anti-DENV2 activities observed in screening could be exerted through morphological changes in the cell membrane, such as in the bilayer polarity and curvature, or through the altered localization of membrane proteins.

In contrast to SAPI, SAPC exacerbated DENV2 infection in terms of its cytopathic effects, viral replication, inflammatory responses, and production of DENV2 sNS1. Positive-strand RNA viruses, such as DENV, stimulate host cell PC synthesis at viral replication sites (99, 144). Cellular PC enhances the viral RNA-dependent RNA polymerase activity of tomato bushy stunt virus, a positive-sense single-stranded RNA virus, and the interaction between the viral RNA-dependent RNA polymerase and the viral positive-strand RNA (145). However, the analysis of SAPC localization using LC/ESI–MS/MS showed that extracellular SAPC is poorly incorporated into cells. Therefore, it seems more likely that SAPC accelerates DENV2 infection at the extracellular level. Further studies are required to better understand the effects of lipid molecules on DENV infection.

Lipid analysis with MS is a powerful tool for identifying and quantifying specific lipid molecular species from a myriad of lipids in various samples (23, 24, 42–45). LC/ESI–MS/MS system, equipped with a high-resolution Orbitrap MS, allows the accurate mass analysis of lipid molecular species and the acquisition of several characteristic fragment ions from which to determine the molecular structure (44). Using this system, SAPI, DSPI, and SAPC in samples were easily identified and quantified. Surprisingly, DSPI was dramatically incorporated into cells

in a time-dependent manner, whereas the amounts of SAPI and SAPC that were incorporated into the cells were small. These data suggest that the fatty acid components of phospholipids, particularly combinations of saturated fatty acids, are important for their incorporation into cells. Further studies are required to identify the fatty acid components of phospholipids that make them suitable for intracellular uptake and to analyze the cellular localization of the incorporated phospholipids. These studies should provide valuable information and increase understanding of the roles of cellular factors, particularly lipids, in DENV replication and may offer new therapeutic options.

In summary, my results demonstrate that extracellular SAPI is a novel endogenous inhibitor of DENV infection that modulates the inflammatory responses induced by DENV2. Although important roles of cellular PI metabolites as precursors of signaling molecules have been reported, the importance of PI in the blood is not yet fully understood. Further clarification of the precise mechanism(s) of action and target molecule(s) of SAPI will extend understanding of the host responses to DENV infection, and may facilitate library screening to discover novel anti-DENV compounds with more potent antiviral activity (nM range) than SAPI.

Summary

Several lipid molecules exhibited anti-DENV activities, especially, SAPI, which is the most abundant endogenous PI molecular species, exhibited the highest anti-DENV activity (EC_{50}: 4.03 μM). SAPI suppressed the cytopathic effects induced by DENV2 infection as well as the replication of all DENV serotypes. However, no other PI molecular species or PI metabolites, including LPI and SA-PIPs, displayed anti-DENV2 activity. A distribution analysis using LC/ESI–MS/MS suggests that SAPI exerts its anti-DENV2 activity extracellularly. A solid-phase binding assay, a preincubation assay and a viral entry assay demonstrate that SAPI does not bind directly to DENV2 particles and does not inhibit the entry of DENV2 into host cells. Furthermore, SAPI suppressed the production of DENV2 infection-induced cytokines and chemokines, including CCL5, CCL20, CXCL8, IL-6, and IFN-β. SAPI also suppressed the TNF-α production induced by LPS and IFN-γ co-stimulation in PMAr cells. These results demonstrated that SAPI is an endogenous inhibitor of DENV and modulated inflammatory responses in DENV2-infected cells, at least in part *via* TLR4.

Conclusion

Lipid molecules, which have essential roles in biological responses, are related to the pathogenesis of various diseases, such as obesity, hyperlipidemia, cardiovascular disease, infectious diseases, severe asthma, pain and Olmsted syndrome. To better understanding the relationship between lipid biology and diseases, it is important to develop the effective and precise analytical systems of diverse lipid molecules, and to elucidate the precise mechanisms of action and target molecules of lipid molecules.

In chapter I, for the purpose of discovery and identification of lipid molecules, including unknown molecules in biological samples, global lipidomics for analyzing oxidized fatty acids and the other lipid molecules was developed using RPLC coupled with Q Exactive Plus. Using global lipidomics, oxidized fatty acids in mouse lung tissue samples were widely analyzed by high-resolution accurate mass analysis, and multiple unknown lipid metabolites, such as 12-HETrE, 14-HDoPE and 21-HDoHE were identified by accurate mass analysis and high-resolution dd-MS^2. Using high-resolution MS and high-resolution dd-MS^2, the differences in molecular weight of <50 mDa, which cannot be distinguished by QqQ MS and QqLIT MS, could be discriminated unambiguously. Thousands of lipid molecules, including glycerolipids, glycerophospholipids and sphingolipids were also detected and identified in this system, and it is important to select the measurement mode for analyzing lipid molecules with different polarities. Furthermore, the sensitivity of my previous targeted lipidomics was improved by changing the composition of mobile phase. Compared with my previous method, the lower limit of

quantification of various molecules, such as LTB_4, PGD_2, PGE_2, 5,6-EET and 12-HETE was improved more than 10 times in new method.

In chapter II, lipid screening was carried out to screen for anti-DENV lipid molecules. The screening revealed that several lipid molecules exhibiting anti-DENV activities, and PI-L possessed the highest anti-DENV2 activity; whereas, PI-S did not exhibit any anti-DENV2 activity. These data suggest that the differences in anti-DENV2 activities between PI-L and PI-S were associated with the structural composition of the fatty acids in these lipid molecules. Next, the anti-DENV2 activities of five different PI molecular species were investigated. Among them, only SAPI, which is the most abundant endogenous PI molecular species, demonstrated anti-DENV2 activity and its EC_{50} was 4.03 μM. No other PI molecular species or PI metabolites, including LPI and SA-PIPs, displayed anti-DENV2 activity. DENV2 RNA in DENV2-infected BHK-21, A549, Huh-7 and HepG2 cells with or without treatment by SAPI was quantified by RT-qPCR. In the presence of SAPI, the amount of DENV2 RNA in all DENV2-infected cells was decreased more than 10-fold compared with that of non-treated DENV2-infected cells. Similar to DENV2, SAPI suppressed viral replication of all DENV serotypes. The distribution of SAPI was investigated using LC/ESI–MS/MS developed in the chapter I. Although SAPI incorporated into both DENV2-infected and non-infected cells in a time-dependent manner, the percentage of cellular SAPI was approximately 1% of total SAPI added, and approximately 95% of SAPI existed in supernatants. These findings suggest that SAPI may exert its antiviral activity extracellularly rather than intracellularly. Furthermore, a solid-phase binding assay, a preincubation assay and a viral entry assay revealed that SAPI does not bind directly to DENV2 particles and does not inhibit the entry of DENV2 into host cells. These results demonstrate that SAPI may not exert its effect by inhibiting the entry step of DENV2 into host cells. Finally, the

effects of SAPI on the inflammatory responses induced by DENV2 infection were investigated. Compared with non-infected cells, gene expression and protein expression of CCL5, CCL20, CXCL8, IL-6, and IFN-β were upregulated in DENV2-infected cells and this upregulation was significantly decreased following SAPI treatment. SAPI also suppressed the TNF-α production induced by LPS and IFN-γ co-stimulation in PMAr cells. These results demonstrated that SAPI is an endogenous inhibitor of DENV and modulated inflammatory responses in DENV2-infected cells, at least in part *via* TLR4.

The outcomes of these researches will contribute to elucidate the mechanism of diseases based on lipid biology and to discover the disease-specific biomarkers. The lipid analytical systems constructed in chapter I have already been applied to the analysis of the mechanisms of obesity, pain, Olmsted syndrome and DENV infection, and it is expected that the target diseases and the target lipid molecules will be expanded in the future. Further clarification of the precise mechanism(s) of action of SAPI based on the findings obtained in chapter II will contribute to better understand the host responses to DENV infection, and the identification of the target molecule(s) of SAPI may facilitate library screening to discover novel anti-DENV compounds with more potent antiviral activity (nM range) than SAPI.

Acknowledgements

I would like to express the deepest appreciation to Prof. H. Sawa, Division of Molecular Pathobiology, Research Center for Zoonosis Control, Hokkaido University, for his continuous support, valuable advice, suggestion, encouragement and detailed review of this thesis.

I am deeply grateful to Prof. Y. Sakoda, Laboratory of Microbiology, Faculty of Veterinary Medicine, Hokkaido University, for his valuable advice, suggestion, encouragement and detailed review of this thesis. I would like to express my gratitude to Dr. K. Matsuno, Laboratory of Microbiology, Faculty of Veterinary Medicine, Hokkaido University, and Dr. Y. Orba, Division of Molecular Pathobiology, Research Center for Zoonosis Control, Hokkaido University, for their valuable review and helpful suggestions on this thesis.

I thank Dr. T. Takasaki, Kanagawa Prefectural Institute of Public Health, for providing dengue virus.

I greatly appreciate all colleagues of SHIONOGI & CO., LTD., and Division of Molecular Pathobiology, Research Center for Zoonosis Control, Hokkaido University, especially Dr. A. Sato and Dr. T. Yoshioka, for their continuous support and helpful suggestions in this study.

Finally, I thank my family for their continuous support.

References

1. Quehenberger, O., Armando, A. M., Brown, A. H., Milne, S. B., Myers, D. S., Merrill, A. H., Bandyopadhyay, S., Jones, K. N., Kelly, S., Shaner, R. L., Sullards, C. M., Wang, E., Murphy, R. C., Barkley, R. M., Leiker, T. J., Raetz, C. R. H., Guan, Z., Laird, G. M., Six, D. A., Russell, D. W., McDonald, J. G., Subramaniam, S., Fahy, E., and Dennis, E. A. (2010) Lipidomics reveals a remarkable diversity of lipids in human plasma,. *J. Lipid Res.* **51**, 3299–3305
2. Fahy, E., Subramaniam, S., Brown, H. A., Glass, C. K., Merrill, A. H., Murphy, R. C., Raetz, C. R. H., Russell, D. W., Seyama, Y., Shaw, W., Shimizu, T., Spener, F., Meer, G. Van, Vannieuwenhze, M. S., White, S. H., Witztum, J. L., and Dennis, E. A. (2005) A comprehensive classification system for lipids. *J. Lipid Res.* **46**, 839–861
3. Harayama, T. and Riezman, H. (2018) Understanding the diversity of membrane lipid composition. *Nat. Rev. Mol. Cell Biol.* **19**, 281–296
4. Sezgin, E., Levental, I., Mayor, S., and Eggeling, C. (2017) The mystery of membrane organization : composition , regulation and roles of lipid rafts. *Nat. Rev. Mol. Cell Biol.* **18**, 361–374
5. Pralle, A., Keller, P., Florin, E., Simons, K., and Hörber, J. K. H. (2000) Sphingolipid–Cholesterol Rafts Diffuse as Small Entities in the Plasma Membrane of Mammalian Cells. *J. Cell Biol.* **148**, 997–1007
6. Lingwood, D. and Simons, K. (2010) Lipid Rafts As a Membrane-Organizing Principle. *Science* **327**, 46–51
7. Mollinedo, F. and Gajate, C. (2015) Advances in Biological Regulation Lipid rafts as major platforms for signaling regulation in cancer. *Adv. Biol. Regul.* **57**, 130–146
8. Kusumi, A., Fujiwara, T. K., Morone, N., Yoshida, K. J., Chadda, R., Xie, M., Kasai, R. S., and Suzuki, K. G. N. (2012) Seminars in Cell & Developmental Biology Membrane mechanisms for signal transduction : The coupling of the meso-scale raft domains to membrane-skeleton-induced compartments and dynamic protein complexes. *Semin. Cell Dev. Biol.* **23**, 126–144

9. Hromada-judycka, A. (2015) Co-operation of TLR4 and raft proteins in LPS-induced pro-inflammatory signaling. *Cell. Mol. Life Sci.* **72**, 557–581
10. Rajendran, L. and Simons, K. (2005) Lipid rafts and membrane dynamics. *J. Cell Sci.* **118**, 1099–1102
11. Pelkmans, L. (2005) Secrets of caveolae- and lipid raft-mediated endocytosis revealed by mammalian viruses. *Biochim. Biophys. Acta - Mol. Cell Biol. Lipids* **1746**, 295–304
12. Samanta, D., Mulye, M., Clemente, T. M., Justis, A. V, and Gilk, S. D. (2017) Manipulation of Host Cholesterol by Obligate Intracellular Bacteria. *Front. Cell. Infect. Microbiol.* **7**
13. Schönfeld, P. and Wojtczak, L. (2016) Short- and medium-chain fatty acids in energy metabolism : the cellular perspective. *J. Lipid Res.* **57**, 943–954
14. Dunning, K. R., Russell, D. L., and Robker, R. L. (2007) Lipids and oocyte developmental competence: the role of fatty acids and β-oxidation. *Reproduction* **148**, R15-27
15. Funk, C. D. (2001) Prostaglandins and Leukotrienes: Advances in Eicosanoid Biology. *Science* **294**, 1871–1875
16. Dennis, E. A. and Norris, P. C. (2015) Eicosanoid Storm in Infection and Inflammation. *Nat. Rev. Immunol.* **15**, 511–523
17. Serhan, C. N., Chiang, N., and Dyke, T. E. Van. (2008) Resolving Inflammation: Dual Anti-Inflammatory and Pro-Resolution Lipid Mediators. *Nat. Rev. Immunol.* **8**, 349–361
18. Serhan, C. N. (2014) Pro-resolving Lipid Mediators Are Leads for Resolution Physiology. *Nature* **510**, 92–101
19. Basil, M. C. and Levy, B. D. (2016) Specialized Pro-Resolving Mediators: Endogenous Regulators of Infection and Inflammation. *Nat. Rev. Immunol.* **16**, 51–67
20. Chiurchiù, V., Leuti, A., Dalli, J., Jacobsson, A., Battistini, L., Maccarrone, M., and Serhan, C. N. (2016) Proresolving Lipid Mediators Resolvin D1, Resolvin D2, and Maresin 1 Are Critical in Modulating T Cell Responses. *Sci. Transl. Med.* **8**, 353ra111
21. Cantalupo, A., Gargiulo, A., Dautaj, E., Liu, C., Zhang, Y., Hla, T., and Lorenzo, A. Di. (2017) S1PR1 (Sphingosine-1-Phosphate Receptor 1) Signaling Regulates Blood Flow and Pressure. *Hypertension* **70**, 426–434
22. Francois, H. and Coffman, T. M. (2004) Prostanoids and Blood Pressure: Which Way Is Up? *J. Clin. Invest.* **114**, 757–759

23. Hinata, M., Imai, S., Sanaki, T., Tsuchida, J., Yoshioka, T., Higashino, K., Yamamoto, M., Imai, M., Soga, M., Horita, N., Fukuda, I., Ikeda, M., Yamane, S., Morita, A., Kanemasa, T., Sakaguchi, G., Hasegawa, M., Minami, M., and Morioka, Y. (2018) Sensitization of transient receptor potential vanilloid 4 and increasing its endogenous ligand 5,6-epoxyeicosatrienoic acid in rats with monoiodoacetate-induced osteoarthritis. *Pain* **159**, 939–947
24. Sakurai, Y., Fujita, M., Kawasaki, S., Sanaki, T., Yoshioka, T., Higashino, K., Tofukuji, S., Yoneda, S., Takahashi, T., Koda, K., Asaki, T., Hasegawa, M., and Morioka, Y. (2019) Contribution of synovial macrophages to rat advanced osteoarthritis pain resistant to cyclooxygenase inhibitors. *Pain* **160**, 895–907
25. Dannhardt, G. and Kiefer, W. (2001) Cyclooxygenase inhibitors – current status and future prospects. *Eur. J. Med. Chem.* **36**, 109–126
26. Theron, A. J., Steel, H. C., Tintinger, G. R., Gravett, C. M., Anderson, R., and Feldman, C. (2014) Cysteinyl Leukotriene Receptor-1 Antagonists as Modulators of Innate Immune Cell Function. *J. Immunol. Res.* **2014**, 608930
27. Colazzo, F., Gelosa, P., Tremoli, E., Sironi, L., and Castiglioni, L. (2017) Role of the Cysteinyl Leukotrienes in the Pathogenesis and Progression of Cardiovascular Diseases. *Mediators Inflamm.* **2017**, 2432958
28. Oesterle, A., Laufs, U., and Liao, J. K. (2017) Pleiotropic Effects of Statins on the Cardiovascular System. *Circ. Res.* **120**, 229–243
29. Mubarak, K. K. (2010) A Review of Prostaglandin Analogs in the Management of Patients With Pulmonary Arterial Hypertension. *Respir. Med.* **104**, 9–21
30. White, C., Alshaker, H., Cooper, C., Winkler, M., and Pchejetski, D. (2016) The emerging role of FTY720 (Fingolimod) in cancer treatment. *Oncotarget* **7**, 23106–23127
31. Westcott, J. Y., Chang, S., Balazy, M., Stene, D. O., Pradelles, P., Maclouf, J., Voelkel, N. F., and Murphy, R. C. (1986) Analysis of 6-keto PGF1 Alpha, 5-HETE, and LTC4 in Rat Lung: Comparison of GM/MS, RIA, and EIA. *Prostaglandins* **32**, 857–873
32. Wang, Z., Ciabattoni, G., Créminon, C., Lawson, J., Fitzgerald, G. A., Patrono, C., and Maclouf, J. (1995) Immunological Characterization of Urinary 8-epi-prostaglandin F2 Alpha Excretion in Man. *J. Pharmacol. Exp. Ther.* **275**, 94–100

33. Walsh, S. W., Vaughan, J. E., Wang, Y., and Roberts, L. J. (2000) Placental isoprostane is significantly increased in preeclampsia. *FASEB J.* **14**, 1289–1296
34. Geraci, M. W., Gao, B., Shepherd, D. C., Moore, M. D., Westcott, J. Y., Fagan, K. A., Alger, L. A., Tuder, R. M., and Voelkel, N. F. (1999) Pulmonary Prostacyclin Synthase Overexpression in Transgenic Mice Protects Against Development of Hypoxic Pulmonary Hypertension. *J. Clin. Invest.* **103**, 1509–1515
35. Ecker, J., Scherer, M., Schmitz, G., and Liebisch, G. (2012) A rapid GC–MS method for quantification of positional and geometric isomers of fatty acid methyl esters. *J. Chromatogr. B* **897**, 98–104
36. Chiu, H., Tsai, S., Tseng, Y. J., Wu, M., Liao, W., Huang, C., and Kuo, C. (2015) An efficient and robust fatty acid profiling method for plasma metabolomic studies by gas chromatography–mass spectrometry. *Clin. Chim. Acta* **451**, 183–190
37. Schober, Y., Wahl, H. G., Renz, H., and Nockher, W. A. (2017) Determination of red blood cell fatty acid profiles : Rapid and high-confident analysis by chemical ionization-gas chromatography-tandem mass spectrometry. *J. Chromatogr. B* **1040**, 1–7
38. Han, X. and Gross, R. W. (1994) Electrospray ionization mass spectroscopic analysis of human erythrocyte plasma membrane phospholipids. *Proc. Natl. Acad. Sci.* **91**, 10635–10639
39. Kim, H., Wang, T. L., and Ma, Y. (1994) Liquid Chromatography/Mass Spectrometry of Phospholipids Using Electrospray Ionization. *Anal. Chem.* **66**, 3977–3982
40. Li, M., Yang, L., Bai, Y., and Liu, H. (2014) Analytical Methods in Lipidomics and Their Applications. *Anal. Chem.* **86**, 161–175
41. Wenk, M. R. (2010) Lipidomics : New Tools and Applications. *Cell* **143**, 888–895
42. Sanaki, T., Fujihara, T., Iwamoto, R., Yoshioka, T., Higashino, K., Nakano, T., and Numata, Y. (2015) Improvements in the High-Performance Liquid Chromatography and Extraction Conditions for the Analysis of Oxidized Fatty Acids Using a Mixed-Mode Spin Column. *Mod. Chem. Appl.* **3**, 1000161
43. Sanaki, T., Kasai-Yamamoto, E., Yoshioka, T., Sakai, S., Yuyama, K., Fujiwara, T., Numata, Y., and Igarashi, Y. (2017) Direct Involvement of Arachidonic Acid in the Development of Ear Edema via TRPV3. *J. Oleo Sci.* **66**, 591–599

44. Sanaki, T., Inaba, Y., Fujiwara, T., Yoshioka, T., Matsushima, K., Minagawa, K., Higashino, K., Nakano, T., and Numata, Y. (2016) A hybrid strategy using global analysis of oxidized fatty acids and bioconversion by *Bacillus circulans*. *Rapid Commun. Mass Spectrom.* **30**, 751–762
45. Sakamoto, H., Yoshida, T., Sanaki, T., Shigaki, S., Morita, H., Oyama, M., Mitsui, M., Tanaka, Y., Nakano, T., Mitsutake, S., Igarashi, Y., and Takemoto, H. (2017) Possible roles of long-chain sphingomyelines and sphingomyelin synthase 2 in mouse macrophage inflammatory response. *Biochem. Biophys. Res. Commun.* **482**, 202–207
46. Sanaki, T., Wakabayashi, M., Yoshioka, T., Yoshida, R., Shishido, T., Hall, W. W., Sawa, H., and Sato, A. (2019) Inhibition of dengue virus infection by 1-stearoyl-2-arachidonoyl-phosphatidylinositol in vitro. *FASEB J.* **33**, 13866–13881
47. Meer-janssen, Y. P. M. Van Der, Galen, J. Van, Batenburg, J. J., and Helms, J. B. (2010) Lipids in host–pathogen interactions: Pathogens exploit the complexity of the host cell lipidome. *Prog. Lipid Res.* **49**, 1–26
48. Heaton, N. S. and Randall, G. (2011) Multifaceted roles for lipids in viral infection. *Trends Microbiol.* **19**, 368–375
49. Schoggins, J. W. and Randall, G. (2013) Lipids in Innate Antiviral Defense. *Cell Host Microbe* **14**, 379–385
50. Heaton, N. S. and Randall, G. (2010) Dengue virus-induced autophagy regulates lipid metabolism. *Cell Host Microbe* **8**, 422–432
51. Choi, Y., Bowman, J. W., and Jung, J. U. (2018) Autophagy During Viral Infection — A Double-Edged Sword. *Nat. Rev. Microbiol.* **16**, 341–354
52. Zhang, J., Lan, Y., and Sanyal, S. (2017) Modulation of Lipid Droplet Metabolism—A Potential Target for Therapeutic Intervention in *Flaviviridae* Infections. *Front. Microbiol.* **8**, 2286
53. Martín-Acebes, M. A., Vázquez-Calvo, Á., and Saiz, J. C. (2016) Lipids and flaviviruses, present and future perspectives for the control of dengue, Zika, and West Nile viruses. *Prog. Lipid Res.* **64**, 123–137
54. Zhang, Z., He, G., Filipowicz, N. A., Randall, G., Belov, G. A., Kopek, B. G., and Wang, X. (2019) Host Lipids in Positive-Strand RNA Virus Genome Replication. *Front. Microbiol.* **10**, 286

55. Heaton, N. S., Perera, R., Berger, K. L., Khadka, S., LaCount, D. J., Kuhn, R. J., and Randall, G. (2010) Dengue virus nonstructural protein 3 redistributes fatty acid synthase to sites of viral replication and increases cellular fatty acid synthesis. *Proc. Natl. Acad. Sci.* **107**, 17345–17350

56. Ohol, Y. M., Wang, Z., Kemble, G., and Duke, G. (2015) Direct Inhibition of Cellular Fatty Acid Synthase Impairs Replication of Respiratory Syncytial Virus and Other Respiratory Viruses. *PLoS One* **10**, e0144648

57. Wang, L., Zhou, Y., Chen, Z., Sun, L., Wu, J., Li, H., Liu, F., Wang, F., Yang, C., Yang, J., Leng, Q., Zhang, Q., Xu, A., Shen, L., Sun, J., Wu, D., Fang, C., Lu, H., Yan, D., and Ge, B. (2019) PLCβ2 Negatively Regulates the Inflammatory Response to Virus Infection by Inhibiting Phosphoinositide-Mediated Activation of TAK1. *Nat. Commun.* **10**, 746

58. Yuan, S., Chu, H., Chan, J. F., Ye, Z., Wen, L., Yan, B., Lai, P., Tee, K., Huang, J., Chen, D., Li, C., Zhao, X., Yang, D., Chiu, M. C., Yip, C., Poon, V. K., Chan, C. C., Sze, K., Zhou, J., Chan, I. H., Kok, K., To, K. K., Kao, R. Y., Lau, J. Y., Jin, D., Perlman, S., and Yuen, K. (2019) SREBP-dependent lipidomic reprogramming as a broad-spectrum antiviral target. *Nat. Commun.* **10**, 120

59. Brouwers, J. F. (2011) Liquid Chromatographic-Mass Spectrometric Analysis of Phospholipids. Chromatography, Ionization and Quantification. *BBA - Mol. Cell Biol. Lipids* **1811**, 763–775

60. Houjou, T., Yamatani, K., Imagawa, M., Shimizu, T., and Taguchi, R. (2005) A Shotgun Tandem Mass Spectrometric Analysis of Phospholipids With Normal-Phase and/or Reverse-Phase Liquid Chromatography/Electrospray Ionization Mass Spectrometry. *Rapid Commun. Mass Spectrom.* **19**, 654–666

61. Pang, L., Liang, Q., Wang, Y., Ping, L., and Luo, G. (2008) Simultaneous Determination and Quantification of Seven Major Phospholipid Classes in Human Blood Using Normal-Phase Liquid Chromatography Coupled With Electrospray Mass Spectrometry and the Application in Diabetes Nephropathy. *J. Chromatogr. B* **869**, 118–125

62. Ikeda, K. and Taguchi, R. (2010) Highly Sensitive Localization Analysis of Gangliosides and Sulfatides Including Structural Isomers in Mouse Cerebellum Sections by Combination of Laser Microdissection and Hydrophilic Interaction Liquid

Chromatography/Electrospray Ionization Mass Spectrom. *Rapid Commun. Mass Spectrom.* **24**, 2957–2965

63. Wang, Y., Armando, A. M., Quehenberger, O., Yan, C., and Dennis, E. A. (2014) Comprehensive ultra-performance liquid chromatographic separation and mass spectrometric analysis of eicosanoid metabolites in human samples. *J. Chromatogr. A* **1359**, 60–69
64. Yamada, M., Kita, Y., Kohira, T., Yoshida, K., Hamano, F., Tokuoka, S. M., and Shimizu, T. (2015) A comprehensive quantification method for eicosanoids and related compounds by using liquid chromatography/mass spectrometry with high speed continuous ionization polarity switching. *J. Chromatogr. B* **995**–**996**, 74–84
65. Colas, R. A., Shinohara, M., Dalli, J., Chiang, N., and Serhan, C. N. (2019) Identification and signature profiles for pro-resolving and inflammatory lipid mediators in human tissue. *Am. J. Physiol. Cell Physiol.* **307**, 39–54
66. Shaner, R. L., Allegood, J. C., Park, H., Wang, E., Kelly, S., Haynes, C. A., Sullards, M. C., and Merrill, A. H. (2009) Quantitative analysis of sphingolipids for lipidomics using triple quadrupole and quadrupole linear ion trap mass spectrometers. *J. Lipid Res.* **50**, 1692–1707
67. Okudaira, M., Inoue, A., Shuto, A., Nakanaga, K., Kano, K., Makide, K., Saigusa, D., Tomioka, Y., and Aoki, J. (2014) Separation and quantifi cation of 2-acyl-1-lysophospholipids and 1-acyl-2-lysophospholipids in biological samples by LC-MS/MS. *J. Lipid Res.* **55**, 2178–2192
68. Kaufmann, A., Butcher, P., Maden, K., Walker, S., and Widmer, M. (2010) Comprehensive comparison of liquid chromatography selectivity as provided by two types of liquid chromatography detectors (high resolution mass spectrometry and tandem mass spectrometry): "Where is the crossover point?" *Anal. Chim. Acta* **673**, 60–72
69. Ogiso, H. and Taguchi, R. (2008) Reversed-Phase LC/MS Method for Polyphosphoinositide Analyses: Changes in Molecular Species Levels during Epidermal Growth Factor Activation in A431 Cells. *Anal. Chem.* **80**, 9226–9232
70. Yamada, T., Uchikata, T., Sakamoto, S., Yokoi, Y., Fukusaki, E., and Bamba, T. (2013) Development of a lipid profiling system using reverse-phase liquid chromatography

coupled to high-resolution mass spectrometry with rapid polarity switching and an automated lipid identification software. *J. Chromatogr. A* **1292**, 211–218

71. Taguchi, R. and Ishikawa, M. (2010) Precise and global identification of phospholipid molecular species by an Orbitrap mass spectrometer and automated search engine Lipid Search. *J. Chromatogr. A* **1217**, 4229–4239
72. Sandra, K., Pereira, S., Vanhoenacker, G., David, F., and Sandra, P. (2010) Comprehensive blood plasma lipidomics by liquid chromatography/quadrupole time-of-flight mass spectrometry. *J. Chromatogr. A* **1217**, 4087–4099
73. Pizarro, C., Arenzana-Rámila, I., Pérez-del-Notario, N., Pérez-Matute, P., and González-Sáiz, J.-M. (2013) Plasma Lipidomic Profiling Method Based on Ultrasound Extraction and Liquid Chromatography Mass Spectrometry. *Anal. Chem.* **85**, 12085–12092
74. Sara, M. H., Gaudin, M., Lewis, M. R., Martin, F., Holmes, E., Nicholson, J. K., and Dumas, M. (2014) Objective Set of Criteria for Optimization of Sample Preparation Procedures for Ultra-High Throughput Untargeted Blood Plasma Lipid Profiling by Ultra Performance Liquid Chromatography−Mass Spectrometry. *Anal. Chem.* **86**, 5766–5774
75. Ikeda, K., Oike, Y., Shimizu, T., and Taguchi, R. (2009) Global Analysis of Triacylglycerols Including Oxidized Molecular Species by Reverse-Phase High Resolution LC/ESI-QTOF MS/MS. *J. Chromatogr. B* **877**, 2639–2647
76. Endo, J., Sano, M., Isobe, Y., Fukuda, K., Kang, J. X., Arai, H., and Arita, M. (2014) 18-HEPE, an n-3 fatty acid metabolite released by macrophages, prevents pressure overload–induced maladaptive cardiac remodeling. *J. Exp. Med.* **211**, 1673–1687
77. Miyata, J., Fukunaga, K., Iwamoto, R., Isobe, Y., Niimi, K., Takamiya, R., Takihara, T., Tomomatsu, K., Suzuki, Y., Oguma, T., Sayama, K., Arai, H., Betsuyaku, T., Arita, M., and Asano, K. (2013) Dysregulated synthesis of protectin D1 in eosinophils from patients with severe asthma. *J. Allergy Clin. Immunol.* **131**, 353–360
78. Morita, M., Kuba, K., Ichikawa, A., Nakayama, M., Katahira, J., Iwamoto, R., Watanebe, T., Sakabe, S., Daidoji, T., Nakamura, S., Kadowaki, A., Ohto, T., Nakanishi, H., Taguchi, R., Nakaya, T., Murakami, M., Yoneda, Y., Arai, H., Kawaoka, Y., Penninger, J. M., Arita, M., and Imai, Y. (2013) The lipid mediator protectin D1 inhibits influenza virus replication and improves severe influenza. *Cell* **153**, 112–125

79. Tam, V. C., Quehenberger, O., Oshansky, C. M., Suen, R., Armando, A. M., Treuting, P. M., Thomas, P. G., Dennis, E. A., and Aderem, A. (2013) Lipidomic Profiling of Influenza Infection Identifies Mediators that Induce and Resolve Inflammation. *Cell* **154**, 213–227

80. Serhan, C. N., Spite, M., and Cla, J. (2014) Resolvins, Specialized Proresolving Lipid Mediators, and Their Potential Roles in Metabolic Diseases. *Cell Metab.* **19**, 21–36

81. Wenk, M. R. (2005) THE EMERGING FIELD OF LIPIDOMICS. *Nat. Rev. drug Discov.* **4**, 594–610

82. Sugimoto, M., Wakabayashi, M., Shimizu, Y., Yoshioka, T., Higashino, K., Numata, Y., Okuda, T., Zhao, S., Sakai, S., Igarashi, Y., and Kuge, Y. (2016) Imaging Mass Spectrometry Reveals Acyl-Chain- And Region-Specific Sphingolipid Metabolism in the Kidneys of Sphingomyelin Synthase 2-Deficient Mice. *PLoS One* **11**, e0152191

83. Sugimoto, M., Shimizu, Y., Yoshioka, T., Wakabayashi, M., Tanaka, Y., Higashino, K., Numata, Y., Sakai, S., Kihara, A., Igarashi, Y., and Kuge, Y. (2015) Histological Analyses by Matrix-Assisted Laser Desorption/Ionization-Imaging Mass Spectrometry Reveal Differential Localization of Sphingomyelin Molecular Species Regulated by Particular Ceramide Synthase in Mouse Brains. *BBA - Mol. Cell Biol. Lipids* **1851**, 1554–1565

84. Sugimoto, M., Shimizu, Y., Zhao, S., Ukon, N., Nishijima, K., Wakabayashi, M., Yoshioka, T., Higashino, K., Numata, Y., Okuda, T., Tamaki, N., Hanamatsu, H., Igarashi, Y., and Kuge, Y. (2016) Characterization of the Role of Sphingomyelin Synthase 2 in Glucose Metabolism in Whole-Body and Peripheral Tissues in Mice. *BBA - Mol. Cell Biol. Lipids* **1861**, 688–702

85. Wakabayashi, M., Yoshioka, T., Higashino, K., Numata, Y., Igarashi, Y., and Kihara, A. (2017) Decreases in 15-lipoxygenase metabolites in Olmsted syndrome model rats. *J. Dermatol. Sci.* **85**, 186–196

86. Bhatt, S., Gething, P. W., Brady, O. J., Messina, J. P., Farlow, A. W., Moyes, C. L., Drake, J. M., Brownstein, J. S., Hoen, A. G., Sankoh, O., Myers, M. F., George, D. B., Jaenisch, T., William Wint, G. R., Simmons, C. P., Scott, T. W., Farrar, J. J., and Hay, S. I. (2013) The global distribution and burden of dengue. *Nature* **496**, 504–507

87. Brady, O. J., Gething, P. W., Bhatt, S., Messina, J. P., Brownstein, J. S., Hoen, A. G., Moyes, C. L., Farlow, A. W., Scott, T. W., and Hay, S. I. (2012) Refining the Global Spatial Limits of Dengue Virus Transmission by Evidence-Based Consensus. *PLoS Negl. Trop. Dis.* **6**, e1760
88. Srikiatkhachorn, A., KrautrachuePond, A., Ratanaprakarn, W., Wongtapradit, L., Nithipanya, N., Kalayanarooj, S., Nisalak, A., Thomas, S. J., Gibbons, R. V., Mammen, M. P. J., Libraty, D. H., Ennis, F. A., Rothman, A. L., and Green, S. (2007) Natural History of Plasma Leakage in Dengue Hemorrhagic Fever. *Pediatr. Infect. Dis. J.* **26**, 283–290
89. Rigau-Perez, J. G., Clark, G. G., Gubler, D. J., Reiter, P., Sanders, E. J., and Vorndam, A. V. (1998) Dengue and dengue haemorrhagic fever. *Lancet* **352**, 971–977
90. Pan American Health Organization. (2016) Dengue: Guidelines for patient care in the Region of the Americas. 136
91. Pan American Health Organization. (2017) Tool for the diagnosis and care of patients with suspected arboviral diseases. *Pan Am. Heal. Organ.* 102
92. World Health Organization. (2009) Dengue: guidelines for diagnosis, treatment, prevention, and control. *Spec. Program. Res. Train. Trop. Dis.* 147
93. Meertens, L., Carnec, X., Lecoin, M. P., Ramdasi, R., Guivel-Benhassine, F., Lew, E., Lemke, G., Schwartz, O., and Amara, A. (2012) The TIM and TAM families of phosphatidylserine receptors mediate dengue virus entry. *Cell Host Microbe* **12**, 544–557
94. Cruz-Oliveira, C., Freire, J. M., Conceição, T. M., Higa, L. M., Castanho, M. A. R. B., and Da Poian, A. T. (2015) Receptors and routes of dengue virus entry into the host cells. *FEMS Microbiol. Rev.* **39**, 155–170
95. Carnec, X., Meertens, L., Dejarnac, O., Perera-Lecoin, M., Hafirassou, M. L., Kitaura, J., Ramdasi, R., Schwartz, O., and Amara, A. (2016) The Phosphatidylserine and Phosphatidylethanolamine Receptor CD300a Binds Dengue Virus and Enhances Infection. *J. Virol.* **90**, 92–102
96. Richard, A. S., Zhang, A., Park, S.-J., Farzan, M., Zong, M., and Choe, H. (2015) Virion-associated phosphatidylethanolamine promotes TIM1-mediated infection by Ebola, dengue, and West Nile viruses. *Proc. Natl. Acad. Sci.* **112**, 14682–14687

97. Mukhopadhyay, S., Kuhn, R. J., and Rossmann, M. G. (2005) A structural perspective of the Flavivirus life cycle. *Nat. Rev. Microbiol.* **3**, 13–22
98. Villareal, V. A., Rodgers, M. A., Costello, D. A., and Yang, P. L. (2015) Targeting host lipid synthesis and metabolism to inhibit dengue and hepatitis C viruses. *Antiviral Res.* **124**, 110–121
99. Perera, R., Riley, C., Isaac, G., Hopf-Jannasch, A. S., Moore, R. J., Weitz, K. W., Pasa-Tolic, L., Metz, T. O., Adamec, J., and Kuhn, R. J. (2012) Dengue virus infection perturbs lipid homeostasis in infected mosquito cells. *PLoS Pathog.* **8**, e1002584
100. Tang, W.-C., Lin, R.-J., Liao, C.-L., and Lin, Y.-L. (2014) Rab18 Facilitates Dengue Virus Infection by Targeting Fatty Acid Synthase to Sites of Viral Replication. *J. Virol.* **88**, 6793–6804
101. Cui, L., Lee, Y. H., Kumar, Y., Xu, F., Lu, K., Ooi, E. E., Tannenbaum, S. R., and Ong, C. N. (2013) Serum Metabolome and Lipidome Changes in Adult Patients with Primary Dengue Infection. *PLoS Negl. Trop. Dis.* **7**, e2373
102. Voge, N. V., Perera, R., Mahapatra, S., Gresh, L., Balmaseda, A., Loroño-Pino, M. A., Hopf-Jannasch, A. S., Belisle, J. T., Harris, E., Blair, C. D., and Beaty, B. J. (2016) Metabolomics-Based Discovery of Small Molecule Biomarkers in Serum Associated with Dengue Virus Infections and Disease Outcomes. *PLoS Negl. Trop. Dis.* **10**, e0004449
103. Cui, L., Pang, J., Lee, Y. H., Ooi, E. E., Ong, C. N., Leo, Y. S., and Tannenbaum, S. R. (2018) Serum metabolome changes in adult patients with severe dengue in the critical and recovery phases of dengue infection. *PLoS Negl. Trop. Dis.* **12**, e0006217
104. Cui, L., Lee, Y. H., Thein, T. L., Fang, J., Pang, J., Ooi, E. E., Leo, Y. S., Ong, C. N., and Tannenbaum, S. R. (2016) Serum Metabolomics Reveals Serotonin as a Predictor of Severe Dengue in the Early Phase of Dengue Fever. *PLoS Negl. Trop. Dis.* **10**, e0004607
105. Nobori, H., Toba, S., Yoshida, R., Hall, W. W., Orba, Y., Sawa, H., and Sato, A. (2018) Identification of Compound-B, a novel anti-dengue virus agent targeting the non-structural protein 4A. *Antiviral Res.* **155**, 60–66
106. Fernandez-Garcia, M.-D., Meertens, L., Bonazzi, M., Cossart, P., Arenzana-Seisdedos, F., and Amara, A. (2011) Appraising the Roles of CBLL1 and the Ubiquitin/Proteasome System for Flavivirus Entry and Replication. *J. Virol.* **85**, 2980–2989

107. Numata, M., Chu, H. W., Dakhama, A., and Voelker, D. R. (2010) Pulmonary surfactant phosphatidylglycerol inhibits respiratory syncytial virus-induced inflammation and infection. *Proc. Natl. Acad. Sci.* **107**, 320–325

108. Numata, M., Kandasamy, P., Nagashima, Y., Fickes, R., Murphy, R. C., and Voelker, D. R. (2015) Phosphatidylinositol inhibits respiratory syncytial virus infection. *J. Lipid Res.* **56**, 578–587

109. Numata, M., Kandasamy, P., Nagashima, Y., Posey, J., Hartshorn, K., Woodland, D., and Voelker, D. R. (2012) Phosphatidylglycerol suppresses influenza A virus infection. *Am. J. Respir. Cell Mol. Biol.* **46**, 479–487

110. Numata, M., Nagashima, Y., Moore, M. L., Berry, K. Z., Chan, M., Kandasamy, P., Peebles, R. S., Murphy, R. C., and Voelker, D. R. (2013) Phosphatidylglycerol provides short-term prophylaxis against respiratory syncytial virus infection. *J. Lipid Res.* **54**, 2133–2143

111. Daigneault, M., Preston, J. A., Marriott, H. M., Whyte, M. K. B., and Dockrell, D. H. (2010) The identification of markers of macrophage differentiation in PMA-stimulated THP-1 cells and monocyte-derived macrophages. *PLoS One* **5**, e8668

112. Saksono, B., Dewi, B. E., Nainggolan, L., and Suda, Y. (2015) A highly sensitive diagnostic system for detecting dengue viruses using the interaction between a sulfated sugar chain and a virion. *PLoS One* **10**, e012398

113. Rimkunas, R., Fox, J. M., Fremont, D. H., Kim, A. S., Zhang, R., Basore, K., Doranz, B. J., Crowe, J. E., Klimstra, W. B., Lin, H., Nair, S., Poddar, S., Fong, R. H., and Diamond, M. S. (2018) Mxra8 is a receptor for multiple arthritogenic alphaviruses. *Nature* **557**, 570–574

114. Bernard, E., Solignat, M., Gay, B., Chazal, N., Higgs, S., Devaux, C., and Briant, L. (2010) Endocytosis of chikungunya virus into mammalian cells: Role of clathrin and early endosomal compartments. *PLoS One* **5**, e11479

115. Hackett, B. A. and Cherry, S. (2018) Flavivirus internalization is regulated by a size-dependent endocytic pathway. *Proc. Natl. Acad. Sci.* **115**, 4246–4251

116. Mueller, M., Brandenburg, K., Dedrick, R., Schromm, A. B., and Seydel, U. (2005) Phospholipids Inhibit Lipopolysaccharide (LPS)-Induced Cell Activation: A Role for LPS-Binding Protein. *J. Immunol.* **174**, 1091–1096

117. Kuronuma, K., Mitsuzawa, H., Takeda, K., Nishitani, C., Chan, E. D., Kuroki, Y., Nakamura, M., and Voelker, D. R. (2009) Anionic pulmonary surfactant phospholipids inhibit inflammatory responses from alveolar macrophages and U937 cells by binding the lipopolysaccharide-interacting proteins CD14 and MD-2. *J. Biol. Chem.* **284**, 25488–25500
118. Wang, P. Y., Kitchens, R. L., and Munford, R. S. (1998) Phosphatidylinositides bind to plasma membrane CD14 and can prevent monocyte activation by bacterial lipopolysaccharide. *J. Biol. Chem.* **273**, 24309–24313
119. Alayli, F. and Scholle, F. (2016) Dengue virus NS1 enhances viral replication and pro-inflammatory cytokine production in human dendritic cells. *Virology* **496**, 227–236
120. Modhiran, N., Watterson, D., Muller, D. A., Panetta, A. K., Sester, D. P., Liu, L., Hume, D. A., Stacey, K. J., and Young, P. R. (2015) Dengue virus NS1 protein activates cells via Toll-like receptor 4 and disrupts endothelial cell monolayer integrity. *Sci. Transl. Med.* **7**, 304ra142
121. Beatty, P. R., Puerta-Guardo, H., Killingbeck, S. S., Glasner, D. R., Hopkins, K., and Harris, E. (2015) Dengue virus NS1 triggers endothelial permeability and vascular leak that is prevented by NS1 vaccination. *Sci. Transl. Med.* **7**, 304ra141
122. Glasner, D. R., Ratnasiri, K., Puerta-Guardo, H., Espinosa, D. A., Beatty, P. R., and Harris, E. (2017) Dengue virus NS1 cytokine-independent vascular leak is dependent on endothelial glycocalyx components. *PLoS Pathog.* **13**, e1006673
123. Puerta-Guardo, H., Glasner, D. R., and Harris, E. (2016) Dengue Virus NS1 Disrupts the Endothelial Glycocalyx, Leading to Hyperpermeability. *PLoS Pathog.* **12**, e1005738
124. Reichel, M., Hönig, S., Liebisch, G., Lüth, A., Kleuser, B., Gulbins, E., Schmitz, G., and Kornhuber, J. (2015) Alterations of plasma glycerophospholipid and sphingolipid species in male alcohol-dependent patients. *Biochim. Biophys. Acta - Mol. Cell Biol. Lipids* **1851**, 1501–1510
125. Jeewandara, C., Gomes, L., Udari, S., Paranavitane, S. A., Shyamali, N. L. A., Ogg, G. S., and Malavige, G. N. (2017) Secretory phospholipase A2 in the pathogenesis of acute dengue infection: *Immunity, Inflamm. Dis.* **5**, 7–15
126. Jeewandara, C., Gomes, L., Wickramasinghe, N., Gutowska-Owsiak, D., Waithe, D., Paranavitane, S. A., Shyamali, N. L. A., Ogg, G. S., and Malavige, G. N. (2015) Platelet

Activating Factor Contributes to Vascular Leak in Acute Dengue Infection. *PLoS Negl. Trop. Dis.* **9**, e0003459

127. Murakami, M., Sato, H., Miki, Y., Yamamoto, K., and Taketomi, Y. (2016) A new era of secreted phospholipase A2. *J. Lipid Res.* **56**, 1248–1261
128. Gijón, M. A., Riekhof, W. R., Zarini, S., Murphy, R. C., and Voelker, D. R. (2008) Lysophospholipid acyltransferases and arachidonate recycling in human neutrophils. *J. Biol. Chem.* **283**, 30235–30245
129. Lee, H.-C., Inoue, T., Sasaki, J., Kubo, T., Matsuda, S., Nakasaki, Y., Hattori, M., Tanaka, F., Udagawa, O., Kono, N., Itoh, T., Ogiso, H., Taguchi, R., Arita, M., Sasaki, T., and Arai, H. (2012) LPIAT1 regulates arachidonic acid content in phosphatidylinositol and is required for cortical lamination in mice. *Mol. Biol. Cell* **23**, 4689–4700
130. Mancina, R. M., Dongiovanni, P., Petta, S., Pingitore, P., Meroni, M., Rametta, R., Borén, J., Montalcini, T., Pujia, A., Wiklund, O., Hindy, G., Spagnuolo, R., Motta, B. M., Pipitone, R. M., Craxì, A., Fargion, S., Nobili, V., Käkelä, P., Kärjä, V., Männistö, V., Pihlajamäki, J., Reilly, D. F., Castro-Perez, J., Kozlitina, J., Valenti, L., and Romeo, S. (2016) The MBOAT7-TMC4 Variant rs641738 Increases Risk of Nonalcoholic Fatty Liver Disease in Individuals of European Descent. *Gastroenterology* **150**, 1219–1230.e6
131. Luukkonen, P. K., Zhou, Y., Hyötyläinen, T., Leivonen, M., Arola, J., Orho-Melander, M., Orešič, M., and Yki-Järvinen, H. (2016) The MBOAT7 variant rs641738 alters hepatic phosphatidylinositols and increases severity of non-alcoholic fatty liver disease in humans. *J. Hepatol.* **65**, 1263–1265
132. Suwarto, S., Diahtantri, R. A., Hidayat, M. J., and Widjaya, B. (2018) Nonalcoholic fatty liver disease is associated with increased hemoconcentration, thrombocytopenia, and longer hospital stay in dengue-infected patients with plasma leakage. *PLoS One* **13**, e0205965
133. Castañeda-Sánchez, J. I., Domínguez-Martínez, D. A., Olivar-Espinosa, N., García-Pérez, B. E., Loroño-Pino, M. A., Luna-Herrera, J., and Salazar, M. I. (2016) Expression of Antimicrobial Peptides in Human Monocytic Cells and Neutrophils in Response to Dengue Virus Type 2. *Intervirology* **59**, 8–19

134. Thorley, A. J., Grandolfo, D., Lim, E., Goldstraw, P., Young, A., and Tetley, T. D. (2011) Innate immune responses to bacterial ligands in the peripheral human Lung – Role of alveolar epithelial TLR expression and signalling. *PLoS One* **6**, e21827
135. Chen, H.-C., Hofman, F. M., Kung, J. T., Lin, Y.-D., and Wu-Hsieh, B. A. (2007) Both Virus and Tumor Necrosis Factor Alpha Are Critical for Endothelium Damage in a Mouse Model of Dengue Virus-Induced Hemorrhage. *J. Virol.* **81**, 5518–5526
136. Stokes, C. A., Kaur, R., Edwards, M. R., Mondhe, M., Robinson, D., Prestwich, E. C., Hume, R. D., Marshall, C. A., Perrie, Y., O'Donnell, V. B., Harwood, J. L., Sabroe, I., and Parker, L. C. (2016) Human rhinovirus-induced inflammatory responses are inhibited by phosphatidylserine containing liposomes. *Mucosal Immunol.* **9**, 1303–1316
137. Parker, L. C., Prestwich, E. C., Ward, J. R., Smythe, E., Berry, A., Triantafilou, M., Triantafilou, K., and Sabroe, I. (2008) A phosphatidylserine species inhibits a range of TLR- but not IL-1beta-induced inflammatory responses by disruption of membrane microdomains. *J. Immunol.* **181**, 5606–5617
138. Wang, K., Wang, J., Sun, T., Bian, G., Pan, W., Feng, T., Wang, P., Li, Y., and Dai, J. (2016) Glycosphingolipid GM3 is indispensable for dengue virus genome replication. *Int. J. Biol. Sci.* **12**, 872–883
139. Martín-Acebes, M. A., Gabandé-Rodríguez, E., García-Cabrero, A. M., Sánchez, M. P., Ledesma, M. D., Sobrino, F., and Saiz, J.-C. (2016) Host sphingomyelin increases West Nile virus infection in vivo. *J. Lipid Res.* **57**, 422–432
140. Liebscher, S., Ambrose, R. L., Aktepe, T. E., Mikulasova, A., Prier, J. E., Gillespie, L. K., Lopez-Denman, A. J., Rupasinghe, T. W. T., Tull, D., McConville, M. J., and Mackenzie, J. M. (2018) Phospholipase A2 activity during the replication cycle of the flavivirus West Nile virus. *PLOS Pathog.* **14**, e1007029
141. Karara, A., Dishman, E., Falck, J. R., and Capdevila, J. H. (1991) Endogenous epoxyeicosatrienoyl-phospholipids: A novel class of cellular glycerolipids containing epoxidized arachidonate moieties. *J. Biol. Chem.* **266**, 7561–7569
142. Spector, A. A., Fang, X., Snyder, G. D., and Weintraub, N. L. (2004) Epoxyeicosatrienoic acids (EETs): Metabolism and biochemical function. *Prog. Lipid Res.* **43**, 55–90

143. Abate, W., Alghaithy, A. A., Parton, J., Jones, K. P., and Jackson, S. K. (2010) Surfactant lipids regulate LPS-induced interleukin-8 production in A549 lung epithelial cells by inhibiting translocation of TLR4 into lipid raft domains. *J. Lipid Res.* **51**, 334–344
144. Zhang, J., Zhang, Z., Chukkapalli, V., Nchoutmboube, J. A., Li, J., Randall, G., Belov, G. A., and Wang, X. (2016) Positive-strand RNA viruses stimulate host phosphatidylcholine synthesis at viral replication sites. *Proc. Natl. Acad. Sci.* **113**, E1064–E1073
145. Pogany, J. and Nagy, P. D. (2015) Activation of Tomato Bushy Stunt Virus RNA-Dependent RNA Polymerase by Cellular Heat Shock Protein 70 Is Enhanced by Phospholipids In Vitro. *J. Virol.* **89**, 5714–5723

Summary in Japanese（和文要旨）

生体内において細胞膜の構成成分、エネルギー源、生理活性物質として機能する脂質は肥満症、糖尿病、高血圧、気管支喘息、疼痛、ウイルス感染症等の病原性の発現に関連する。これまでに、脂質代謝関連酵素や脂質受容体をターゲット分子とした治療薬や脂質分子自体をリード化合物とした脂質アナログが開発され、実際に複数の医薬品が臨床活用されている。

構造や生体内濃度の異なる多様な脂質分子の測定には、高感度かつ高選択的な分析法が求められる。脂質分子の分析法は、抗体法とクロマトグラフィー法の2 つに大別されるが、多成分のプロファイル分析にはクロマトグラフィー法が適する。ガスクロマトグラフィーの場合、誘導体化が必須であるため、脂質分子の分離には液体クロマトグラフィー (LC) が適する。LC用の検出器には構造情報の得られる質量分析 (MS) の利用が最適である。MSを用いた脂質測定系は、不特定の分子を網羅的に測定するglobal lipidomicsと特定の分子を選択的に測定するtargeted lipidomicsの2 つに大別される。これまでに、グリセロ脂質、グリセロリン脂質、スフィンゴ脂質に関するglobal lipidomicsの適用例は多数報告されているが、酸化脂肪酸に関する報告例はほとんど無い。Targeted lipidomicsは生理活性脂質メディエーターの分析に汎用される。私は以前に、酸化脂肪酸を対象としたtargeted lipidomicsを構築しているが、生体試料中の極微量な酸化脂肪酸を効果的に分析するためには、更なる高感度化が必要である。

第 I 章では、global lipidomicsの構築およびtargeted lipidomicsの高感度化を実施した。高分解能MSを用いて、マウス肺ホモジネート中の酸化脂肪酸を測定した結果、精密質量測定により12-ヒドロキシエイコサテトラエン酸や14-ヒドロキシドコサヘキサエン酸 (HDoHE) 等の12-リポキシゲナーゼ (LOX) 代謝物が主代謝物として検出された。さらに、複数の未知分子イオンピークも検出され、高分解能データ依存型タンデム質量分析法 (dd-MS^2) により、12-ヒドロキシエイコサトリエン酸や14-ヒドロキシドコサペンタエン酸等の12-LOX代謝物、21-HDoHEや22-HDoHE等のドコサヘキサエン酸代謝物が同定された。特に、21-HDoHEの構造解析では、50 mDa未満の分子量の違いをdd-MS^2 により明確に識別することができた。次いで、マウス肺ホモジネート中のグリセロ脂質、グリセロリン脂質、スフィンゴ脂質を測定した結果、正イオンモードでは2,467 個の分子、負イオンモードでは1,070 個の分子が同定された。興味深いことに、トリアシルグリセロールやセラミド等は正イオンモードで、ホスファチジン酸 (PA) や血小板活性化因子 (PAF) 等は負イオンモードで主に検出され、極性の異なる脂質分子種の分析において、測定モードの選択が重要であることが示された。次に、targeted lipidomicsの高感度化を実施した。従来法では、分析物の保持を安定させるために酢酸アンモニウムを移動相に添加していたが、大量の塩は感度低下の要因であるため除外した。また、酸化脂肪酸のイオン化効率を改善するために、ギ酸をより高い酸解離定数を持つ酢酸に変更した。移動相条件の変更により、従来法と比較してロイコトリエンB_4、プロスタグランジンE_2、5,6-エポキシエイコサトリエン酸等の定量下限は10 倍以上改善された。

デング熱は蚊媒介性ウイルスであるデングウイルス (DENV) の感染により惹起される急性熱性感染症である。全世界で年間約1 億人がデング熱を発症し、この内約50 万人

が重症化すると推定されている。現在、効果的な抗DENV薬は存在せず、抗DENV薬の創製には宿主におけるDENV感染機構のより良い理解が必要である。これまでに、DENV感染細胞における脂質合成・代謝経路の活性化が報告されているが、抗DENV活性を有する脂質分子の報告はない。第 II 章では、抗DENV活性を有する脂質分子を探索した。始めに、134 種類の脂質分子を対象としてスクリーニングした結果、ウシ肝臓由来ホスファチジルイノシトール (PI) が抗DENV2 型 (DENV2) 活性を示した。一方、大豆由来PIは抗DENV2 活性を示さず、これらの活性の違いは、分子内の脂肪酸組成の違いに起因することが示唆された。次に、脂肪酸組成の異なる5 つのPI分子種の抗DENV2 活性を評価した結果、1-ステアロイル-2-アラキドノイル-PI (SAPI) のみが抗DENV2 活性を示し、50% 有効濃度は4.03 μMであった。DENV感染細胞を用いて細胞内ウイルスRNA量をリアルタイムRT-PCRにより測定した結果、SAPI未処置群と比較して、全ての血清型においてSAPI処置による10 倍以上のウイルスRNA量の減少が認められた。次に、第 I 章で構築した脂質測定系を用いてSAPIの局在を解析した結果、添加したSAPIの約95% が細胞上清中に存在することが明らかとなった。この事から、SAPIの抗DENV活性は細胞外からの効果であると考えられた。DENV2 粒子に対するSAPIの結合能およびDENVの細胞への侵入効率に対するSAPIの効果を検討した結果、SAPIとDENV2 との直接的な結合およびDENVの細胞への侵入効率に対するSAPIの阻害効果は認められなかった。最後に、DENV2 感染誘発炎症応答に対するSAPIの効果を検討した。非感染群と比較し、DENV2 感染によるCCL5、CCL20、IL-6、IL-8 およびIFN-β等のサイトカイン・ケモカイン類の遺伝子およびタンパク質発現の亢進が認められた。一方、DENV2 感染群と比較し、SAPI処置群では、DENV2 感染による前述の遺伝子およ

びタンパク質発現の亢進に対する抑制効果が認められた。以上より、SAPIはDENV感染に対する宿主防御因子の機能を持つことが示唆された。

以上より、第 I 章ではglobal lipidomicsの構築およびtargeted lipidomicsの高感度化を実施し、第 II 章では抗DENV活性を有する脂質分子としてSAPIを見出した。本論文に記載した研究成果は、脂質生化学を起点とした疾患メカニズム解析や疾患特異的なバイオマーカーの探索に貢献するものと思われる。第 I 章で構築した脂質測定系は肥満、疼痛、遺伝性掌蹠角化症であるオルムステット症候群およびDENV感染症のメカニズム解析にすでに適用されおり、今後、解析対象となる疾患や脂質分子の拡大が期待される。また、第 II 章で得られた知見を基にしたSAPIの更なる作用メカニズムの解明は、DENV感染に対する宿主防御機構についての新たな側面を明らかにすると共に、SAPIの標的分子の同定により新たな抗DENV薬開発の発展に寄与することが期待される。